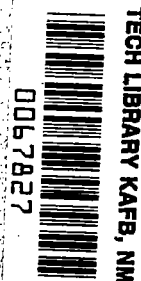


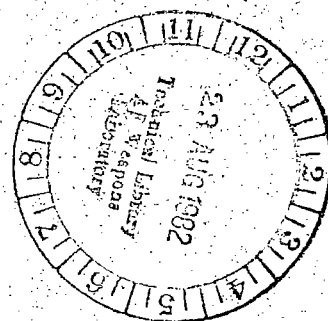
August 1982

**Aeropropulsive Characteristics
at Mach Numbers up to 2.2 of
Axisymmetric and Nonaxisymmetric
Nozzles Installed on an F-18 Model**

Francis J. Capone



LOAN COPY: RETURN TO
AFWL TECHNICAL LIBRARY
WRIGHT-PATTERSON AFB, OH





0067827

**NASA
Technical
Paper
2044**

1982

**Aeropropulsive Characteristics
at Mach Numbers up to 2.2 of
Axisymmetric and Nonaxisymmetric
Nozzles Installed on an F-18 Model**

Francis J. Capone
Langley Research Center
Hampton, Virginia

SUMMARY

An investigation to determine the aeropropulsive characteristics of nonaxisymmetric nozzles on an F-18 jet effects model has been conducted in the Langley 16-Foot Transonic Tunnel and the AEDC 16-Foot Supersonic Wind Tunnel. The performance of a two-dimensional convergent-divergent nozzle, a single expansion ramp nozzle, and a wedge nozzle was compared with that of the baseline axisymmetric nozzle. Test data were obtained at static conditions and at Mach numbers from 0.60 to 2.20 at an angle of attack of 0° . Nozzle pressure ratio was varied from jet-off to about 20.

Afterbody aeropropulsive performance of the F-18 with the two-dimensional convergent-divergent nozzles (2-D C-D) is equal to or higher than the configuration with axisymmetric nozzles. At dry power, the single expansion ramp nozzle (SERN) and the wedge nozzle configurations (at supersonic speeds) also had higher performance than the F-18 with axisymmetric nozzles. The afterburner power SERN configuration had lower performance than the axisymmetric nozzle configuration because of the non-optimum alignment of the resultant gross thrust vector and probable adverse flow effects.

INTRODUCTION

Studies on twin-engine fighter airplanes (refs. 1 to 3) have identified potential benefits for installation of nonaxisymmetric or two-dimensional (2-D) nozzles. This nozzle concept is geometrically amenable to improvements in nozzle/airframe integration to achieve installed drag reduction; thrust vectoring for maneuver enhancement and short-field take-off and landing; and thrust reversing for increased agility, ground handling, and reduced landing ground roll. Development of the non-axisymmetric nozzle has concentrated primarily on three nozzle types: the single expansion ramp (refs. 4 to 8), the convergent-divergent (refs. 4 and 6), and the wedge (refs. 4 and 9 to 11).

As part of a coordinated technology program (ref. 2), three nonaxisymmetric nozzles and a baseline axisymmetric nozzle were tested on a 0.10-scale F-18 prototype airplane model in the Langley 16-Foot Transonic Tunnel. These nonaxisymmetric nozzles included a single expansion ramp nozzle (SERN), a two-dimensional convergent-divergent (2-D C-D) nozzle, and a wedge nozzle. The F-18 airplane is a lightweight, highly maneuverable, twin-engine fighter with a relatively clean afterbody for nozzle installation. No control surface support structure (such as booms and fairings) is located adjacent to or ahead of the nozzles, and the vertical tails are located well forward of the nozzle/airframe juncture. The results of that investigation have been reported in reference 12 and summarized in references 13 and 14.

This paper presents the results from a recent investigation conducted in the 16-Foot Supersonic Wind Tunnel at the Arnold Engineering and Development Center with the same F-18 propulsion model. The purpose of the present investigation was to extend the data base of the relative performance of nonaxisymmetric to axisymmetric nozzles to higher Mach numbers (1.60, 2.00, and 2.20). Nozzle pressure ratio was varied up to 20 and angle of attack was held constant at 0° . Afterbody drag data measured during the investigation for reference 12 but not reported therein are presented herein. Some afterbody aeropropulsive characteristics at Mach numbers from

0.60 to 1.20 from reference 12 are also included to show Mach number effects over the entire Mach number range.

SYMBOLS

All forces and moments, except gross thrust F_g , are referenced to the stability axis system. The moment reference center was located at fuselage station 116.47.

A_e	nozzle exit area, cm^2
A_t	nozzle throat area, cm^2
$C_{D,\text{aft}}$	aft-end drag coefficient, $\frac{D}{q_\infty S}$
\bar{c}	mean geometric chord, 35.12 cm
D	aft-end drag, N
F	thrust along stability axis, N
F_g	gross thrust, N
F_i	ideal isentropic thrust, $\dot{m} \sqrt{RT_{t,j} \frac{2\gamma}{\gamma-1} \left[1 - \left(\frac{p_\infty}{p_{t,j}} \right)^{(\gamma-1)/\gamma} \right]}$, N
M	free-stream Mach number
\dot{m}	measured mass-flow rate, kg/sec
N_{Re}	Reynolds number per meter
p_a	ambient pressure, Pa
$p_{t,j}$	average jet total pressure, Pa
$p_{t,\infty}$	free-stream total pressure, Pa
p_∞	free-stream static pressure, Pa
q_∞	free-stream dynamic pressure, Pa
R	gas constant (for $\gamma = 1.3997$), 287.3 J/kg-K
r	vertical distance from nozzle SERN reference line to nozzle flap internal surface, positive up (fig. 10), cm
S	wing reference area, 3716.2 cm^2
$T_{t,j}$	jet total temperature, K
$T_{t,\infty}$	free-stream total temperature, K

x axial distance along SERN reference line from nozzle connect station,
positive downstream (fig. 10), cm

y_1, y_2 vertical distances from wedge center line (fig. 12), cm

γ ratio of specific heats, 1.3997 for air

δ_v geometric thrust vector angle, deg

Abbreviations:

A/B afterburning

AEDC Arnold Engineering and Development Center

ASME American Society of Mechanical Engineers

axi axisymmetric

BL butt line, cm

C-D convergent-divergent

DPR design pressure ratio

FRP fuselage reference plane

FS fuselage station

NPR nozzle pressure ratio

SERN single expansion ramp nozzle

2-D two-dimensional (nonaxisymmetric)

16FTT Langley 16-Foot Transonic Tunnel

16S AEDC 16-Foot Supersonic Wind Tunnel

APPARATUS AND PROCEDURE

Wind Tunnels

This investigation was conducted in the Langley 16-Foot Transonic Tunnel (16FTT) and the AEDC 16-Foot Supersonic Wind Tunnel (16S). The 16FTT is a single-return, atmospheric tunnel with a slotted, octagonal test section and continuous air exchange. The wind tunnel has a variable airspeed up to a Mach number of 1.30. Test-section plenum suction is used for speeds above a Mach number of 1.10. A complete description of this facility and operating characteristics can be found in reference 15.

The 16S is a single-return variable-pressure tunnel with a square test section. The contour of the nozzle sidewalls are remotely adjustable and can provide a Mach number range from 1.50 to 4.75. The maximum Reynolds number in this facility for

this investigation was restricted because one of the main drive motors failed. A complete description of this facility and operating characteristics can be found in reference 16.

Model and Support System

A 0.10-scale F-18 afterbody jet-effects model was employed for this investigation and is shown in the sketch of figure 1 and the photographs of figure 2. The F-18 airplane is a lightweight, highly maneuverable fighter with a relatively clean afterbody for nozzle installation. As shown in figures 1 and 2, the configuration is characterized by nose strakes, a straight wing, inlet diverter bleed slots through the wing, twin vertical tails located well forward on the afterbody, and closely spaced twin engines. The 0.10-scale model reproduced F-18 airplane lines except for the faired-over inlets (required for power model tests) located on the forebody well forward of the afterbody and the wind alterations required for the model support system. The term afterbody, as used in this paper, refers to the metric portion of the model on which forces and moments are measured. The metric break, or seal station, begins at FS 144.78. The afterbody includes the aft fuselage, nozzles (including internal thrust hardware), and empennage surfaces. The model forebody and wing were nonmetric. A 0.064-cm gap in the external skin at the metric-break station prevented fouling between the nonmetric forebody/wing and metric afterbody. A flexible rubber strip located in the metric-break gap was used as a seal to prevent internal flow in the model. The metric afterbody was attached to a six-component strain-gage balance which was grounded to the nonmetric forebody.

16FTT support system.- As shown in figures 1 and 2, the model was supported at the wing tips in the tunnel. The model FRP was located 7.13 cm below the tunnel center line. The outer wing panels, from 65 percent of the semispan to the tip, were modified from airplane lines to accommodate the wing-tip support system and air supply system. The two wing-tip booms were attached to the normal tunnel support system with V-struts as shown in figure 2(a). High-pressure air and instrumentation lines were routed through the V-struts and wing-tip booms entering the model fuselage through gun-drilled passages in both wings.

16S support system.- A stronger wing-tip support system than the one used in the 16FTT was used in the 16S and is shown in the photograph of figure 2(b). The change of support systems was necessitated by unstart loads associated with the 16S. The booms had a semispan of 47.41 cm and were supported in the 16S with straight struts.

Propulsion Simulation System

External high-pressure air systems at both facilities provided a continuous flow of clean, dry air to simulate jet exhaust flow. Jet stagnation temperature was maintained at 294 K in 16FTT and 310 K in 16S. This high-pressure air is transferred from a common high-pressure plenum in the model center section into the metric portion of the model by means of two internal flow transfer assemblies. A sketch showing details of one of these assemblies is presented in figure 3. These flow transfer devices have been used in several previous investigations (refs. 4, 10, and 17). Flexible metal bellows are located in each end of the flow transfer assemblies and act to minimize pressurization tares and provide a tare-free assembly.

Flow transition and instrumentation sections (fig. 3), including 17.9-percent-open choke plates, were attached to each of the flow transfer assemblies and terminated at FS 169.32, which was the common connect station for all nozzles.

Nozzle Designs

The baseline F-18 axisymmetric nozzle and three nonaxisymmetric or 2-D nozzles were tested. The nonaxisymmetric nozzles represent three generically different types: (1) two-dimensional convergent-divergent (2-D C-D), (2) single expansion ramp nozzle (SERN), and (3) wedge.

Two power settings were investigated for each nozzle type and represented a dry or cruise power setting with a model throat area of 16.13 cm^2 and an afterburning (A/B) power setting with a throat area of 25.81 cm^2 . The three nonaxisymmetric nozzles had an exhaust-duct aspect ratio of 1.00 upstream of the nozzle throat. The SERN and the 2-D C-D nozzle had throat aspect ratios (ratio of throat width to height) of 3.71 and 2.32 for dry and A/B power settings, respectively. The wedge nozzle had an exhaust-duct aspect ratio (includes wedge thickness) at the throat of 1.00 for both power settings. Based on an effective throat height (sum of upper and lower throat heights), the wedge nozzle had a throat aspect ratio of 3.26 at dry power setting and 2.03 at A/B power setting. Thrust vectoring was investigated for all 2-D nozzle types and thrust reversing was investigated for the 2-D C-D and wedge nozzles only; these results are reported in reference 12 at Mach numbers up to 1.20. Nozzle configurations tested during this investigation are summarized in table I for both wind-tunnel facilities.

Baseline axisymmetric nozzle.— The baseline axisymmetric nozzles installed on the F-18 model are shown in the photographs of figure 4. A sketch of the nozzle showing both the dry and A/B power configurations is given in figure 5. This axisymmetric exhaust nozzle represents a hinged-flap, variable-position, convergent-divergent nozzle. Both the convergent and divergent portions of the nozzle are conical. On full-scale hardware, a single actuation system controls the nozzle throat and exit area. The nozzle exit area A_e is set by an adjustable linkage rod and becomes a unique function of throat area. Thus, for a set linkage rod length/hinge location, the nozzle expansion ratio A_e/A_t is determined by A_t . Nozzle expansion ratios of 1.28 and 1.56 that represented dry and A/B power settings, respectively, were used.

Two-dimensional convergent-divergent nozzle.— The 2-D C-D nozzles installed on the F-18 model are shown in the photographs of figures 6 and 7. Sketches of the nozzle representing configurations with both power settings are shown in figure 8.

The 2-D C-D nozzle is a variable-area internal-expansion exhaust system which has a three-flap design between fixed sidewalls. The 2-D convergent flap controls nozzle throat area. The 2-D variable-position divergent flap and external boattail flap assembly controls both nozzle exit area and thrust vector angle independently of throat area. The model was tested with a nozzle expansion ratio A_e/A_t of 1.15 and 1.65 for both power settings.

Single expansion ramp nozzles.— The SERN installed on the F-18 model is shown in the photograph of figure 9. Sketches showing the geometry of the nozzle with both power settings are presented in figure 10.

The SERN is a 2-D, variable-area, internal/external expansion exhaust system. Basic components consist of a transition section from a round cross section at the tail-pipe connect flange to a 2-D cross section at the nozzle throat, a 2-D variable-geometry convergent-divergent upper flap assembly used to vary power setting (throat area), a 2-D variable ventral flap used to vary nozzle expansion ratio A_e/A_t , and a 2-D external expansion ramp which can be varied for vectoring applications. Since the throat is forward of the ventral flap, the power setting (A_t) is independent of the ventral flap position or expansion ratio A_e/A_t . The model was tested with nozzle expansion ratios of 1.06 and 1.15 for the dry power setting and with nozzle expansion ratios of 1.19 and 1.36 for the A/B power setting. Although figure 10 shows vectoring configurations for the SERN, no vectoring results are presented herein but can be found in reference 12.

The SERN shape blends well with airframe contours. In addition, during full-scale nozzle design, sidewall thickness was minimized by locating actuation hardware in the available area on top of the exhaust duct. The result is a nozzle installation that minimizes drag-producing base regions.

Wedge nozzle.— A photograph of the wedge nozzle installed on the F-18 model is presented as figure 11, and sketches of the nozzle showing representations of both power settings and all nozzle expansion ratios are given in figure 12. The wedge nozzle is a 2-D, variable-area, internal/external expansion exhaust system. The nozzle has a collapsing wedge centerbody and a fixed external nozzle flap or boat-tail. The wedge geometry for a flight nozzle can be varied by unique scissor-type linkages and hinges that allow nozzle exit area and expansion ratio to be varied independently of the throat area. For A/B power, the wedge is collapsed to obtain the desired throat area. Nozzle expansion ratios of 1.10, 1.30, and 1.50 were tested with the dry power setting, and nozzle expansion ratios of 1.20 and 1.40 were tested with the A/B power setting.

Nozzle Installations

Each nonaxisymmetric nozzle type was integrated into the F-18 model so that realistic external lines were established, which were expected to minimize the potential for external flow separation in the transonic speed range. Internal clearance between the engine and airframe skin needed for structural frames, engine installation and removal, engine-bay cooling air, nozzle actuation equipment, and other required accessories within the airplane afterbody were considered in establishing these realistic external lines.

For installation of the nonaxisymmetric nozzles, modifications were made to the model afterbody starting at about FS 152.40. This modification consisted of filling in the engine/nozzle interfairing that began at this fuselage station and adding filler at the fuselage corners for smooth transition to the rectangular nonaxisymmetric nozzles. A sketch showing both a profile view of all nozzles and typical afterbody cross sections is presented in figure 13 to illustrate afterbody modification. All nozzles were attached to the model at FS 169.32.

Each afterbody/nozzle combination was then tested in the Northrop diagnostic water tunnel in order to determine and fix regions of external separated flow. The configuration with the baseline axisymmetric nozzles was used as a calibration standard to adjust test-section velocity. Test-section velocity was adjusted to give the same nozzle flow separation at the angle of attack known from tests previously con-

ducted in transonic wind tunnels. A further discussion of the rationale for operating this tunnel can be found in reference 18.

Initially, the exit of the 2-D C-D nozzle was fixed at the same fuselage station as the axisymmetric nozzle. However, tests conducted in the Northrop water tunnel indicated a problem of flow separation at about FS 169.32 because of locally higher afterbody slopes. This flow separation was eliminated in the water tunnel tests by extending the nozzle exit 2.94 cm aft.

Instrumentation

External afterbody aerodynamic and internal nozzle thrust forces and moments were measured with an internal six-component strain-gage balance. Ten pressure orifices in the metric-break gap at FS 144.78 were used to measure pressures for tare corrections. Internal cavity pressure, also used for pressure-area force tares, was measured at 10 locations in the afterbody cavity. The angle of attack of the nonmetric wing and forebody was determined from a calibrated attitude indicator located in the model nose.

Mass-flow rate in each nozzle was determined from total pressure and temperature measurements in the flow transfer assemblies (fig. 3) and by constants determined from calibrations with ASME standard nozzles in the 16FTT. Total mass-flow rate (both nozzles) was measured by a venturi external to the tunnel in 16S. Flow conditions in each nozzle were determined from two total-pressure rakes and one total-temperature probe located in the instrumentation section aft of the transition section and choke plate (fig. 3). Each rake, one from the top and one from the side of both instrumentation sections, contained three total-pressure probes.

Data Reduction

All data for both the model and the wind-tunnel facilities were recorded simultaneously on magnetic tape. The recorded data were used to compute standard force and moment coefficients with wing area and mean geometric chord being used for reference area and length, respectively.

Because the center line of the balance was located below the flow transfer assembly (bellows) center line, a force and moment interaction (tare) between the bellows and balance existed. In addition, although the bellows were designed to minimize momentum and pressurization tares, small bellows tares still existed with the jet on. These tares result from small pressure differences between the ends of the bellows when internal velocities are high and also from small differences in the forward and aft bellows spring constants when the bellows are pressurized. The bellows/balance interaction tares were determined by single and combined calibration loadings on the balance, with and without the jet operating with the ASME calibration nozzles installed. These tare forces and moments were then removed from the appropriate balance component data. A more detailed description of this procedure can be found in references 4 and 10. These calibration loadings were conducted at 101.4 kPa (atmospheric pressure) in the 16FTT and at 24 kPa in the 16S. The calibrations in 16S were done at reduced pressure in order to approximate wind-on conditions more closely. In addition, balance corrections were also made to account for metric-break gap and internal cavity pressure/area tares.

Angle of attack α , which is the angle between the afterbody center line and the relative wind, was determined by applying deflection terms caused by model and balance bending under aerodynamic load and a flow angularity term to the angle measured by the attitude indicator. A flow angularity adjustment of 0.1° was applied, which is the average angle measured in the 16FTT. No flow angularity adjustment was made for the 16S.

Since the choke plate and nozzle flow instrumentation were downstream of the round-to-rectangular duct transition section (fig. 3), nozzle performance parameters were independent of duct transition effects. Total-pressure profiles were determined for the ASME calibration nozzles and for the 2-D C-D nozzle at A/B power with the divergent flaps removed. Thus, total-pressure measurements were taken at the throat of a convergent 2-D nozzle. Each internal total-pressure probe was then corrected to the integrated value of jet total pressure at the nozzle throat.

Thrust-removed coefficients are obtained by determining the components of thrust in the axial and normal direction and subtracting these values from the measured afterbody forces. These thrust components at forward speeds are determined from measured static data and are a function of the free-stream static and dynamic pressures. As such, thrust-removed coefficients at nozzle pressure ratios greater than that measured at static conditions are calculated by extrapolating the static data.

Tests

Data were obtained in the 16FTT at Mach numbers from 0.60 to 1.20 and in the 16S at Mach numbers from 1.60 to 2.20. Nozzle pressure ratio was varied up to about 20 depending upon the facility. Angle of attack and horizontal-tail incidence were both 0° . Nominal values of free-stream test conditions for each facility are presented in the following table:

M	Facility	$P_{t,\infty}$ kPa	P_∞ kPa	q_∞ kPa	$T_{t,\infty}$ K	N_{Re}
0.60	16FTT	101.4	81.8	20.6	320	10.43×10^6
.80		↓	68.4	30.7	325	12.30
.90			61.7	35.0	330	12.63
1.20			43.0	43.4	338	13.12
1.30			37.7	45.6	340	13.20
1.60	16S	36.5	8.6	15.4	322	4.66×10^6
2.00		42.6	5.5	15.2	↓	4.72
2.20		48.3	4.5	15.3		4.86

PRESENTATION OF RESULTS

The results of this investigation are presented in plotted ratio and coefficient form in the following figures:

	Figure
Static nozzle performance	14
Afterbody performance (thrust minus drag):	
Axisymmetric nozzle	15
2-D C-D nozzle	16
SERN	17
Wedge nozzle	18
Afterbody drag:	
Axisymmetric nozzle	19
2-D C-D nozzle	20
SERN	21
Wedge nozzle	22
Nozzle comparisons:	
Subsonic afterbody aeropropulsive performance for dry power	23
Supersonic afterbody aeropropulsive performance for A/B power	24
Subsonic afterbody drag for dry power	25
Supersonic afterbody drag for A/B power	26
NPR schedule	27
Nozzle comparisons at schedule NPR:	
Afterbody aeropropulsive performance for dry power	28
Afterbody aeropropulsive performance for A/B power	29
Incremental afterbody aeropropulsive performance	30
Afterbody drag for dry and A/B power	31
Incremental afterbody drag	32

RESULTS AND DISCUSSION

Static Performance

A comparison of the static performance of the nozzles is presented in figure 14 for both dry and A/B power settings at selected expansion ratios. The performance levels shown are typical for these type nozzles (refs. 4, 6, and 10). Nozzle types with all internal exhaust flow expansion - namely, the axisymmetric and the 2-D C-D nozzles - are characterized by a single performance peak which occurs near the nozzle pressure ratio required for fully expanded exhaust flow. (See DPR in table I.) Peak internal performance can be shifted to higher nozzle pressure ratios by increasing nozzle expansion ratio A_e/A_t . (See ref. 12.) Nozzle types with both internal and external exhaust flow expansion - namely, the SERN and the wedge nozzle - are characterized by two performance peaks. The nozzle pressure ratio at which each of these peaks occurs is a function of the nozzle expansion ratio at the exit (values given in this paper) and also of the expansion ratio at the end of the external flap or wedge expansion surface. (See ref. 6.) Internal performance of nozzles with external expansion surfaces will be sensitive to external flow effects during forward flight.

Static internal performance of the 2-D C-D nozzle throughout the range of nozzle pressure ratio and of the SERN at $p_{t,j}/p_a > 6$ is competitive with the axisymmetric convergent-divergent nozzle at dry power setting. (See fig. 14.) Performance of the wedge nozzle and of the SERN at $p_{t,j}/p_a < 6$ generally is 2 to 4 percent below the

axisymmetric nozzle at dry power setting. Both the SERN and the wedge nozzle, however, have external expansion surfaces; thus, internal performance will be altered by external flow effects at forward speeds. At A/B power, all three nonaxisymmetric nozzles have higher performance than the axisymmetric nozzle, with the 2-D C-D nozzle exhibiting the highest performance. However, the axisymmetric nozzle expansion ratio at A/B power is much higher than the nozzle expansion ratios for the nonaxisymmetric nozzles. A lower expansion ratio for the axisymmetric nozzle should produce internal performance levels similar to that obtained for the 2-D C-D nozzle.

Basic Aeropropulsive Performance

The variation of the aeropropulsive performance parameter $(F - D)/F_i$ with nozzle pressure ratio $p_{t,j}/p_\infty$ is presented in figures 15 to 18 for each nozzle type and expansion ratio A_e/A_t at Mach numbers from 0.60 to 2.20.

As expected, because of increased drag, the aeropropulsive performance of all configurations decreased with increasing Mach number. Consistent trends with nozzle expansion ratio are not evident from the data obtained with SERN and wedge nozzle installations. Both these nozzles have external expansion surfaces which would be affected by external flow effects and, thus, have internal performance which depends on Mach number, angle of attack, nozzle pressure ratio, and configuration external geometry. On the other hand, the 2-D C-D nozzle, which has no external expansion surfaces, has internal performance independent of external flow effects as long as the nozzle exhaust flow does not separate from the nozzle divergent flaps. Thus, the variation of wind-on 2-D C-D nozzle performance with nozzle expansion ratio shown in figure 16 follows trends indicated at static conditions. (See ref. 12.) That is, low nozzle expansion ratios generally produce higher performance at low nozzle pressure ratios, and high nozzle expansion ratios generally produce higher performance at high nozzle pressure ratios. Since actual flight hardware would be continuously variable within mechanical constraints, nozzle expansion ratio would be programmed, as closely as possible, for optimum performance over the operating range of nozzle pressure ratio.

Typical comparisons of F-18 aeropropulsive performance between the various nozzles are shown at subsonic and supersonic speeds in figures 23 and 24, respectively. A summary of this performance at the scheduled NPR of figure 27 for the various nozzle installations is presented in figures 28 and 29. Nozzle expansion ratios are also given in figures 28 and 29.

The variation of nozzle pressure ratio with Mach number shown in figure 27 is typical for the F-18 airplane for both nozzle power settings. Although discussion of the results at this particular schedule of nozzle pressure ratio would generally be applicable for other schedules, the relative difference between comparisons may vary.

An incremental afterbody performance parameter is summarized in figure 30 for both nozzle power settings over the range of Mach numbers. This incremental afterbody performance is the difference between performance for the F-18 with nonaxisymmetric nozzles and that for the baseline axisymmetric nozzles. A positive increment indicates higher performance for the F-18 with nonaxisymmetric nozzles.

Dry Power Performance

2-D C-D nozzle.- Afterbody aeropropulsive performance is equal to or higher for the F-18 with the 2-D C-D nozzle ($A_e/A_t = 1.65$) than for the configuration with the axisymmetric nozzle ($A_e/A_t = 1.28$). This higher performance occurs over the NPR range (fig. 23) and over the Mach number range (fig. 30). Subsonic and transonic performance characteristics are presented for the 2-D C-D nozzle with the 1.65 expansion ratio because this was the nozzle configuration tested at the 16S. However, the F-18 with the 2-D C-D nozzle at an expansion ratio of 1.15 also has higher performance than the axisymmetric nozzle with an expansion ratio of 1.28 over the NPR range at Mach numbers from 0.60 to 1.20. (Compare figs. 15 and 16 or see refs. 12 and 13.)

The performance of the dry power 2-D C-D nozzle at $M \leq 1.2$ can be estimated for the same expansion ratio as the axisymmetric nozzle by using the results of figure 16. This would result in an increase of $\Delta(F - D)/F_i$ of about 0.005 at $M = 0.60$ and a decrease of this parameter of 0.004 and 0.008 at $M = 0.90$ and 1.20. At $M = 1.60$ to 2.20, the axisymmetric nozzle has larger underexpansion losses than the 2-D C-D nozzle because the axisymmetric nozzle is operating at too low an expansion ratio for the operating NPR associated with these higher Mach numbers.

SERN.- Afterbody aeropropulsive performance at $M = 0.90$ of the F-18 with the SERN ($A_e/A_t = 1.15$) at the dry power setting (fig. 23), is nearly the same as with the axisymmetric nozzle for $NPR < 6$; for $NPR > 6$, SERN performance is slightly higher than the axisymmetric nozzle. Although the SERN static performance (fig. 14) at $NPR = 4$ is about 4 percent less than either the axisymmetric or 2-D C-D nozzles, favorable external flow recompression effects on the free expansion surface are enough to make its performance at forward speeds comparable. At $NPR > 7$, the SERN has the highest static performance of the nozzles tested (fig. 14) since internal performance at the higher NPR is primarily influenced by the external expansion ratio. Consequently, at the scheduled NPR, the dry power SERN configuration has higher performance over the Mach number range (fig. 30) than the axisymmetric nozzle even though its internal expansion ratio is less than the axisymmetric nozzle. These results illustrate that comparisons of performance between internal and internal/external expansion nozzles cannot necessarily be made for nozzles at the same expansion ratio. It may also be possible to operate a nozzle of the SERN type at a fixed internal expansion ratio with a resulting savings in both nozzle weight and complexity by not having to actuate the lower nozzle ventral flap.

Wedge nozzle.- At the scheduled NPR, the dry power wedge nozzle has higher performance than the axisymmetric or other nonaxisymmetric nozzles at supersonic Mach numbers (fig. 30). As with the SERN, external flow recompression effects on wedge are beneficial enough to overcome the lower static performance (fig. 14) of this nozzle.

Afterburner Performance

2-D C-D nozzle.- As shown previously for dry power settings, aeropropulsive performance at A/B power for the F-18 with the 2-D C-D nozzle ($A_e/A_t = 1.65$) is also equal to or higher than the configuration with the axisymmetric nozzle (fig. 24). Figure 30 indicates that the 2-D C-D nozzle configuration has the highest A/B power performance of all the configurations over the entire Mach number range. At $M = 0.60$ to 1.20, this higher performance can be attributed to the fact that this nozzle is at a lower expansion ratio (1.15 compared with 1.56) than the axisymmetric nozzles (1.65 expansion ratio not tested in 16FTT). At $M = 1.60$ to 2.20, the effect

of the small difference in expansion ratio (1.65 compared with 1.56) should have little effect on performance.

SERN.- The configuration with the A/B power SERN generally has lower performance than that with the axisymmetric nozzle over either the NPR range (fig. 24) or Mach number range (fig. 30). This lower performance may result from two factors. First, contrary to dry power results, there may be an adverse instead of beneficial effect of the external flow interacting with the external expansion ramp. In addition, there is a thrust loss due to a nonoptimum alignment of the resultant gross thrust vector relative to the airplane body axis for the nozzle in the nonvectored mode. Reference 12 indicates that the resultant thrust angle for the A/B power SERN varies linearly from about 0° at $\text{NPR} = 4$ to about 6.5° at $\text{NPR} = 6$. For the dry power nozzle, this angle varies from -4° at $\text{NPR} = 4$ to 4° at $\text{NPR} = 10$. References 6 to 8 indicate that this flow angle usually increases in a linear fashion from about $\text{NPR} = 4$ to 20. For the SERN at A/B power, the resultant thrust angle at $\text{NPR} > 8$ is 12° to 16° . The magnitude of the reduction in $(F - D)/F_j$ for a 12° misalignment of the thrust vector is 0.022, which is significant but not enough to account for all the differences seen in figure 30 at $M > 1.60$. The remaining difference is probably due to nonefficient turning of the exhaust flow along the ramp (refs. 3, 7, and 12). Nonetheless, optimum alignment of the SERN resultant thrust vector angle to minimize this thrust loss would result in higher performance. (See refs. 4, 7, 8, and 17.) This could be accomplished by varying the external expansion ramp flap that is normally used for thrust vectoring. Control of the external expansion ramp flap angle through an integrated flight/propulsion control system could maximize SERN aeropropulsive performance and also eliminate either nose-up or nose-down pitching moments that would occur from the nonaligned gross thrust vector.

Wedge nozzle.- In general, the A/B power wedge nozzle has somewhat higher performance than the axisymmetric nozzle at $\text{NPR} < 6$ (fig. 24). This nozzle, however, has lower performance than the axisymmetric nozzle at the scheduled NPR over the Mach number range (fig. 30). As with the SERN, the performance of this nozzle is also a function of the external expansion ratio and it may be that the internal expansion ratio of this nozzle is too high. Research has not been conducted to date to optimize the performance of these types of nozzles at supersonic speeds.

The results shown in figure 30 for dry and A/B power over a wide Mach number range are significant because they demonstrate that 2-D C-D nozzles can be installed on a twin-engine fighter and generate higher installed thrust-minus-drag characteristics than the baseline airplane axisymmetric nozzles which have been refined through a complete development program. The SERN and the wedge nozzle also show advantages under some conditions and may be capable of considerable further improvement.

Afterbody Drag Characteristics

The variation of afterbody drag $C_{D,\text{aft}}$ with nozzle pressure ratio $p_{t,j}/p_{t,\infty}$ is presented in figures 19 to 22 for each nozzle type and expansion ratio A_e/A_t at Mach numbers from 0.60 to 2.20. Afterbody drag coefficients were obtained by determining the components of thrust in the axial and normal directions and subtracting these values from the measured afterbody forces. The thrust components at forward speeds are determined from measured static data ($M = 0$) and are a function of the free-stream static and dynamic pressure. Because of this, any effects of the external flow on the internal performance of either the SERN or the wedge nozzle are reflected as a change in afterbody drag.

Typical comparisons of F-18 afterbody drag between the various nozzles are shown at subsonic and supersonic speeds in figures 25 and 26, respectively. A summary of afterbody drag coefficient at scheduled pressure ratio is given in figure 31. Incremental afterbody drag is presented in figure 32. A negative increment indicates lower afterbody drag for the F-18 with nonaxisymmetric nozzles installed.

An examination of the basic data of figures 25 and 26 shows no consistent trends of afterbody drag variation for the F-18 with the nonaxisymmetric nozzles. Afterbody drag for the nonaxisymmetric nozzle configurations can be greater or less than the F-18 with the axisymmetric nozzle depending upon power setting, Mach number, and pressure ratio. Nonetheless, the nonaxisymmetric nozzle drag characteristics are generally quite favorable relative to those of the axisymmetric nozzles, particularly at the lowest and highest Mach numbers. Also, overall, the configuration with the wedge nozzle has the lowest afterbody drag. This result is probably because of the low boattail angle of the wedge nozzle cowl.

This result is further illustrated in the summary data of figure 32 where incremental afterbody drag is shown over the Mach number range at the scheduled nozzle pressure ratios (fig. 27) shown in figure 31. For both the dry and A/B power settings, the wedge nozzle always has lower afterbody drag than the axisymmetric nozzle. The 2-D C-D configuration also has lower drag than the axisymmetric nozzle except in the A/B power at subsonic and transonic speeds. The SERN drag characteristics are generally similar to those of the 2-D C-D nozzle except that the axisymmetric nozzle drag values are also exceeded at $M = 0.90$ and $M = 1.60$ in dry power (fig. 32). However, in general, the data shown in figure 32 indicate that nonaxisymmetric nozzles have lower afterbody drag than the axisymmetric nozzle at dry power setting.

CONCLUSIONS

An investigation to determine the aeropropulsive characteristics of nonaxisymmetric nozzles on an F-18 jet effects model has been conducted in the Langley 16-Foot Transonic Tunnel and the AEDC 16-Foot Supersonic Wind Tunnel. The performance of a two-dimensional convergent-divergent nozzle (2-D C-D), a single expansion ramp nozzle (SERN), and a wedge nozzle was compared with that of the baseline axisymmetric nozzle. Test data were obtained at static conditions and at Mach numbers from 0.60 to 2.20 at an angle of attack of 0° . Nozzle pressure ratio was varied from jet-off to about 20. Results of this study indicate the following conclusions:

1. Afterbody aeropropulsive performance is equal to or higher for the F-18 with 2-D C-D nozzles than for the configuration with the axisymmetric nozzles.
2. At dry power, the SERN and the wedge nozzle configurations (at supersonic speeds) also had higher performance than the F-18 with the axisymmetric nozzles.
3. The afterburner power SERN had poorer performance than the axisymmetric nozzle because of the nonoptimum alignment of the resultant gross thrust vector and probable adverse external flow effects.

4. The F-18 with the nonaxisymmetric nozzles generally had lower afterbody drag than the axisymmetric nozzle configuration at dry power.

Langley Research Center
National Aeronautics and Space Administration
Hampton, VA 23665
June 29, 1982

REFERENCES

1. Hiley, P. E.; Wallace, H. W.; and Booz, D. E.: Nonaxisymmetric Nozzles Installed in Advanced Fighter Aircraft. J. Aircr., vol. 13, no. 12, Dec. 1976, pp. 1000-1006.
2. Berrier, Bobby L.; Palcza, J. Lawrence; and Richey, G. Keith: Nonaxisymmetric Nozzle Technology Program - An Overview. AIAA Paper 77-1225, Aug. 1977.
3. Capone, Francis J.: The Nonaxisymmetric Nozzle - It Is for Real. AIAA Paper 79-1810, Aug. 1979.
4. Capone, Francis J.: Static Performance of Five Twin-Engine Nonaxisymmetric Nozzles With Vectoring and Reversing Capability. NASA TP-1224, 1978.
5. Lander, J. A.; Nash, D. O.; and Palcza, J. Lawrence: Augmented Deflector Exhaust Nozzle (ADEN) Design for Future Fighters. AIAA Paper No. 75-1318, Sept.-Oct. 1975.
6. Berrier, Bobby L.; and Re, Richard J.: Effect of Several Geometric Parameters on the Static Internal Performance of Three Nonaxisymmetric Nozzle Concepts. NASA TP-1468, 1979.
7. Re, Richard J.; and Berrier, Bobby L.: Static Internal Performance of Single Expansion-Ramp Nozzles With Thrust Vectoring and Reversing. NASA TP-1962, 1982.
8. Speir, Donald W.; and Blozy, Jack T.: Development of Exhaust Nozzle Internal Performance Prediction Techniques for Advanced Aircraft Applications. AIAA-81-1490, July 1981.
9. Maiden, Donald L.: Performance of an Isolated Two-Dimensional Wedge Nozzle With Fixed Cowl and Variable Wedge Centerbody at Mach Numbers up to 2.01. NASA TN D-8218, 1976.
10. Capone, Francis J.; and Maiden, Donald L.: Performance of Twin Two-Dimensional Wedge Nozzles Including Thrust Vectoring and Reversing Effects at Speeds up to Mach 2.20. NASA TN D-8449, 1977.
11. Goetz, Gerald F.; Young, John H.; and Palcza, J. Lawrence: A Two-Dimensional Airframe Integrated Nozzle Design With Inflight Thrust Vectoring and Reversing Capabilities for Advanced Fighter Aircraft. AIAA Paper No. 76-626, July 1976.
12. Capone, Francis J.; and Berrier, Bobby L.: Investigation of Axisymmetric and Nonaxisymmetric Nozzles Installed on a 0.10-Scale F-18 Prototype Airplane Model. NASA TP-1638, 1980.
13. Capone, Francis J.; Gowadia, Noshir S.; and Wooten, W. H.: Performance Characteristics of Nonaxisymmetric Nozzles Installed on an F-18 Propulsion Model. J. Aircr., vol. 17, no. 6, June 1980, pp. 387-392.
14. Petit, John E.; and Capone, Francis J.: Performance Characteristics of a Wedge Nozzle Installed on an F-18 Propulsion Wind Tunnel Model. AIAA Paper 79-1164, June 1979.

15. Peddrew, Kathryn H., compiler: A User's Guide to the Langley 16-Foot Transonic Tunnel. NASA TM-83186, 1981.
16. Test Facilities Handbook, Eleventh ed. Arnold Eng. & Develop. Center, June 1979.
17. Capone, Francis J.: Aeropropulsive Characteristics of Twin Nonaxisymmetric Vectoring Nozzles Installed With Forward-Swept and Aft-Swept Wings. NASA TP-1778, 1981.
18. Lorincz, Dale J.: A Water Tunnel Flow Visualization Study of the F-15. NASA CR-144878, 1978.

TABLE I.- NOZZLE PARAMETERS

Nozzle	A_e/A_t	DPR	Facility	
			16FTT	16S
Axisymmetric:				
Dry power	1.28	4.48	X	X
A/B power	1.56	6.74	X	X
2-D C-D:				
Dry power	1.15	3.46	X	
Dry power	1.65	7.50	X	X
A/B power	1.15	3.46	X	
A/B power	1.65	7.50		X
SERN:				
Dry power	1.06	2.72	X	
Dry power	1.15	3.46	X	X
A/B power	1.19	3.78	X	
A/B power	1.36	5.16	X	X
Wedge:				
Dry power	1.10	3.05	X	
Dry power	1.30	4.65	X	
Dry power	1.50	6.24	X	X
A/B power	1.20	3.86	X	
A/B power	1.40	5.43	X	X

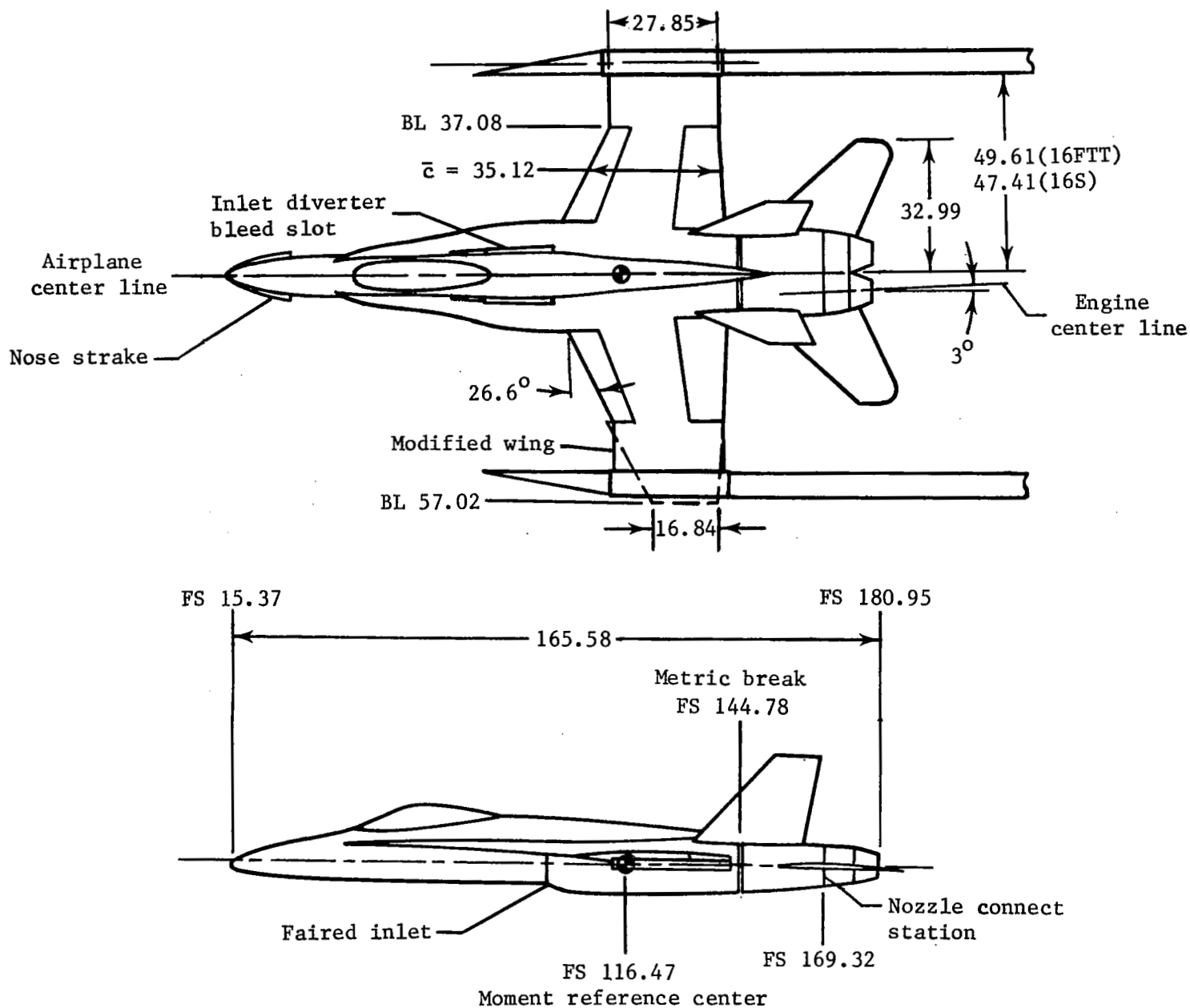
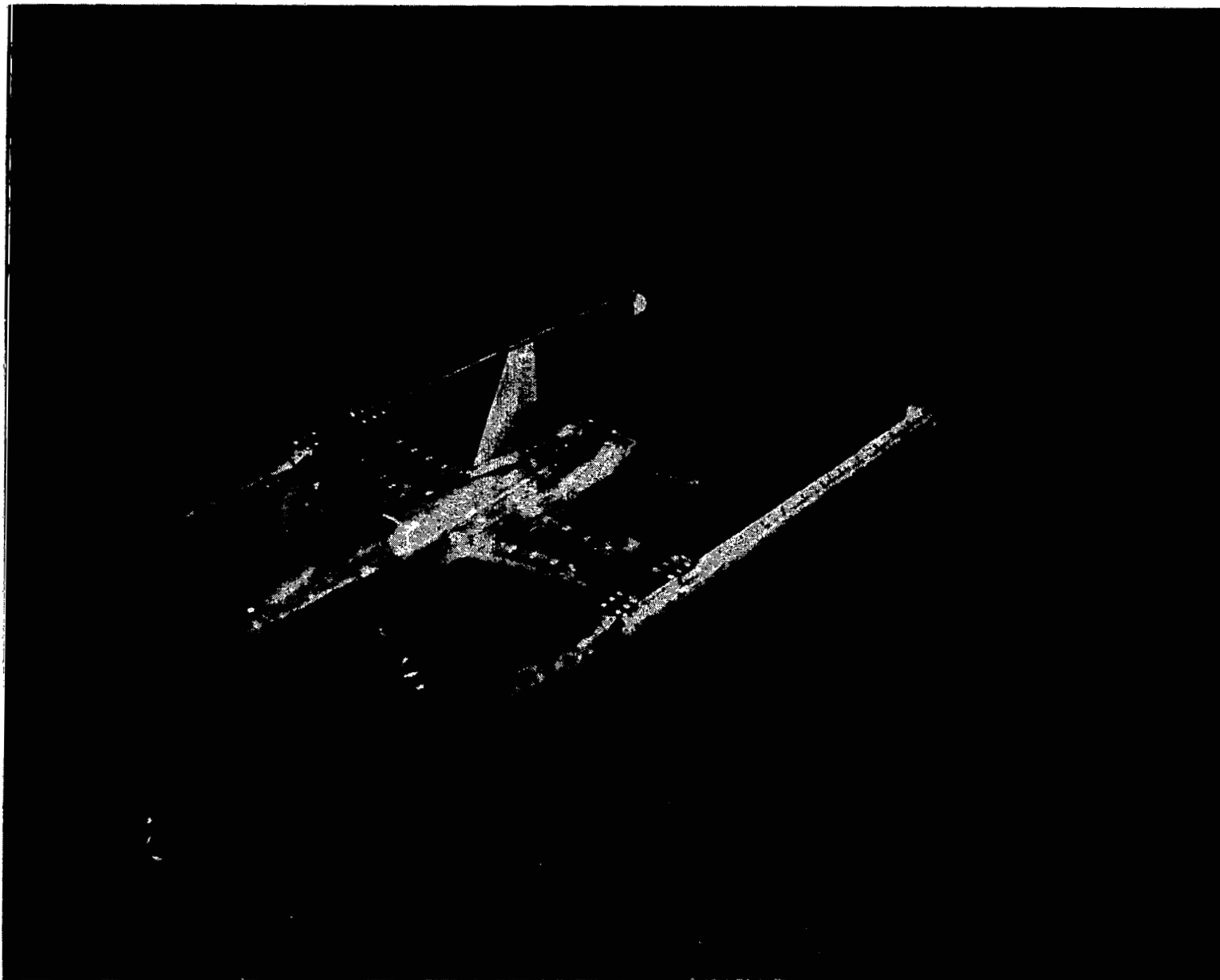


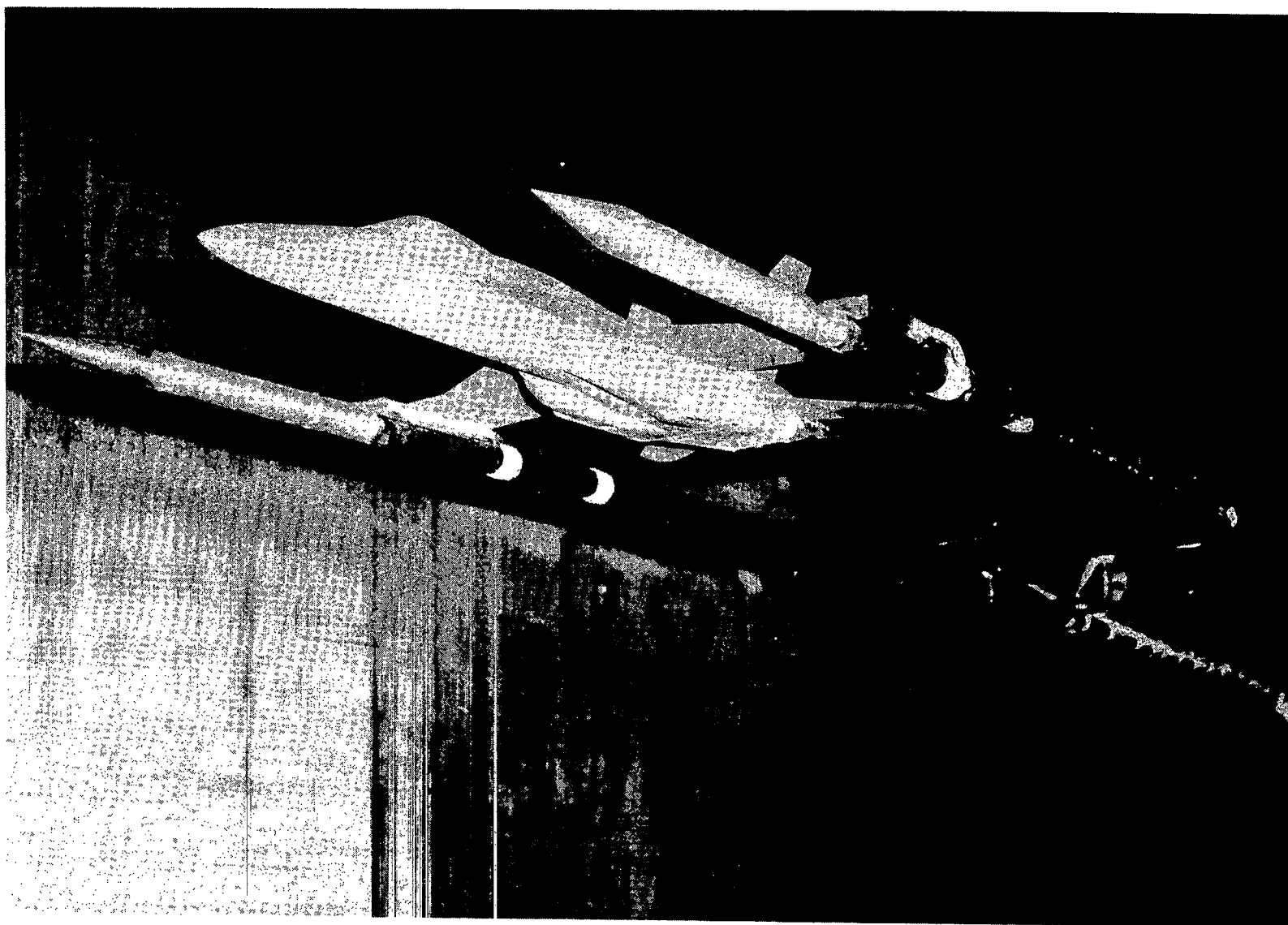
Figure 1.- F-18 model. Linear dimensions are in centimeters.



L-78-1908

(a) Langley 16-Foot Transonic Tunnel.

Figure 2.- F-18 model installed in tunnels.



L-82-159

(b) AEDC 16-Foot Supersonic Wind Tunnel.

Figure 2.- Concluded.

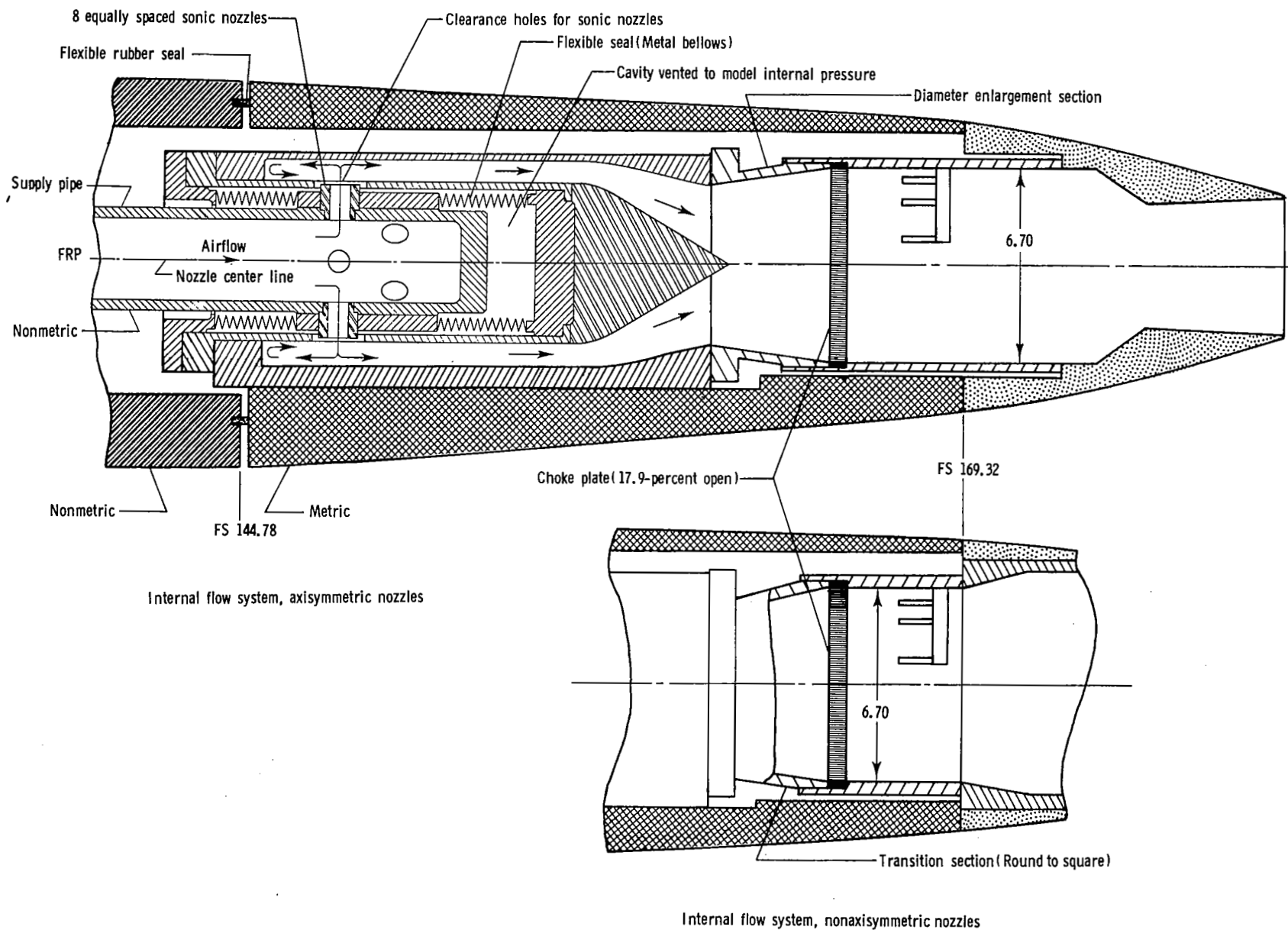
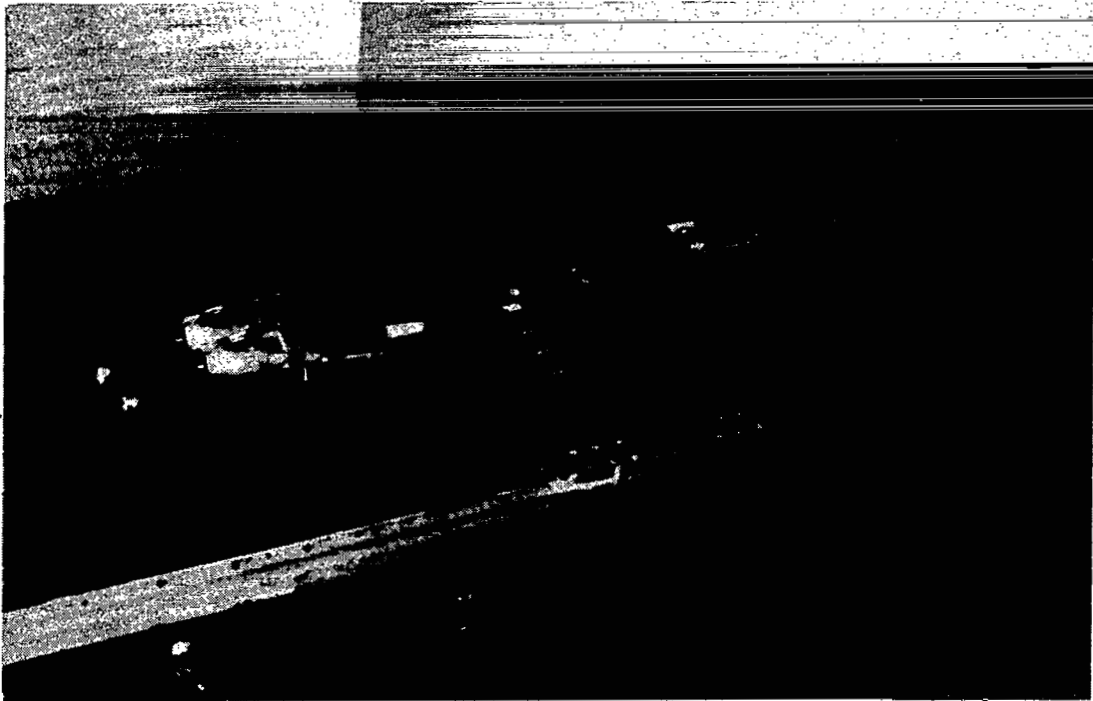
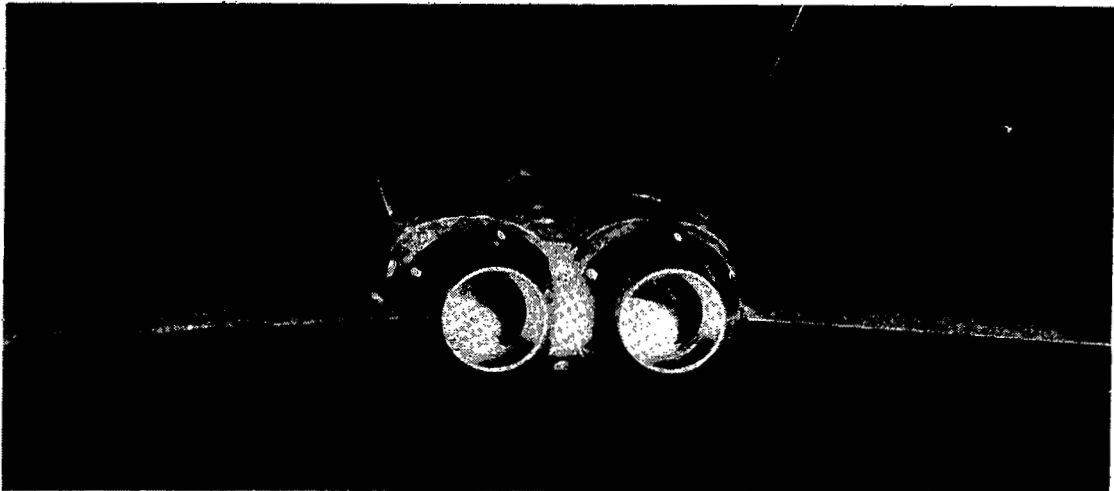


Figure 3.- Internal flow systems showing flow transfer assemblies.
Linear dimensions are in centimeters.



L-78-1648



L-78-1646

Figure 4.- Baseline axisymmetric nozzles, dry power, installed on F-18 model.

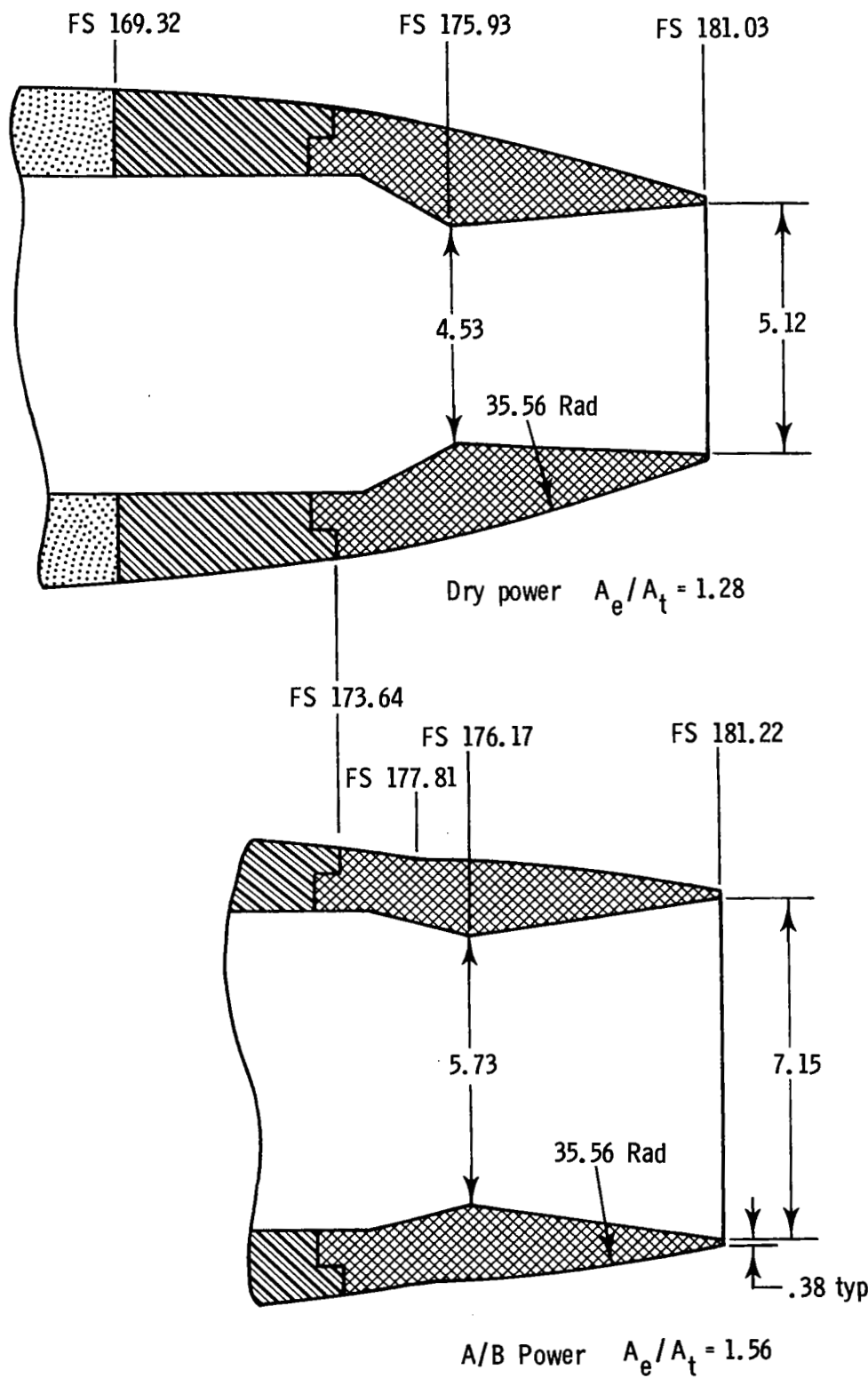
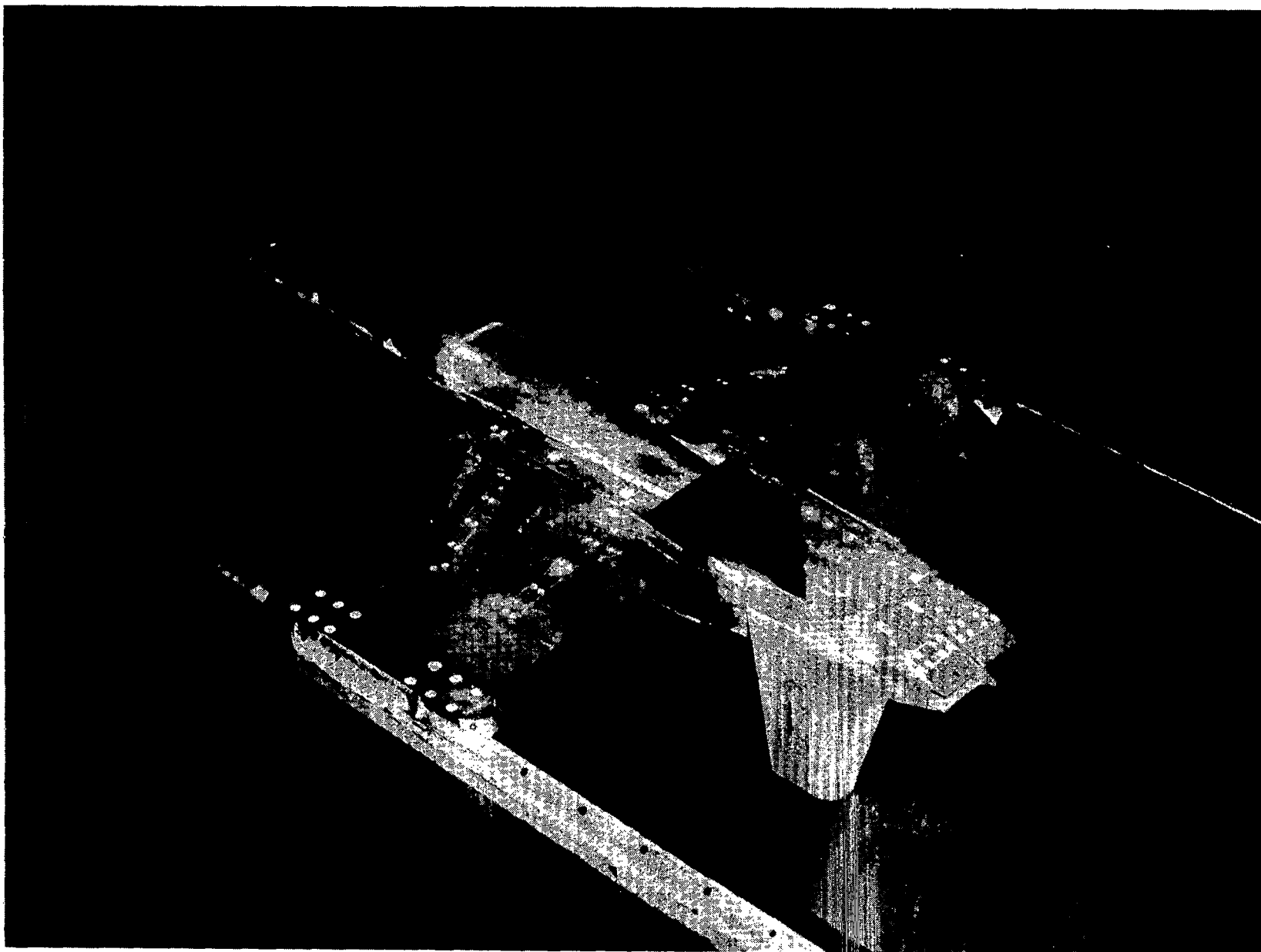
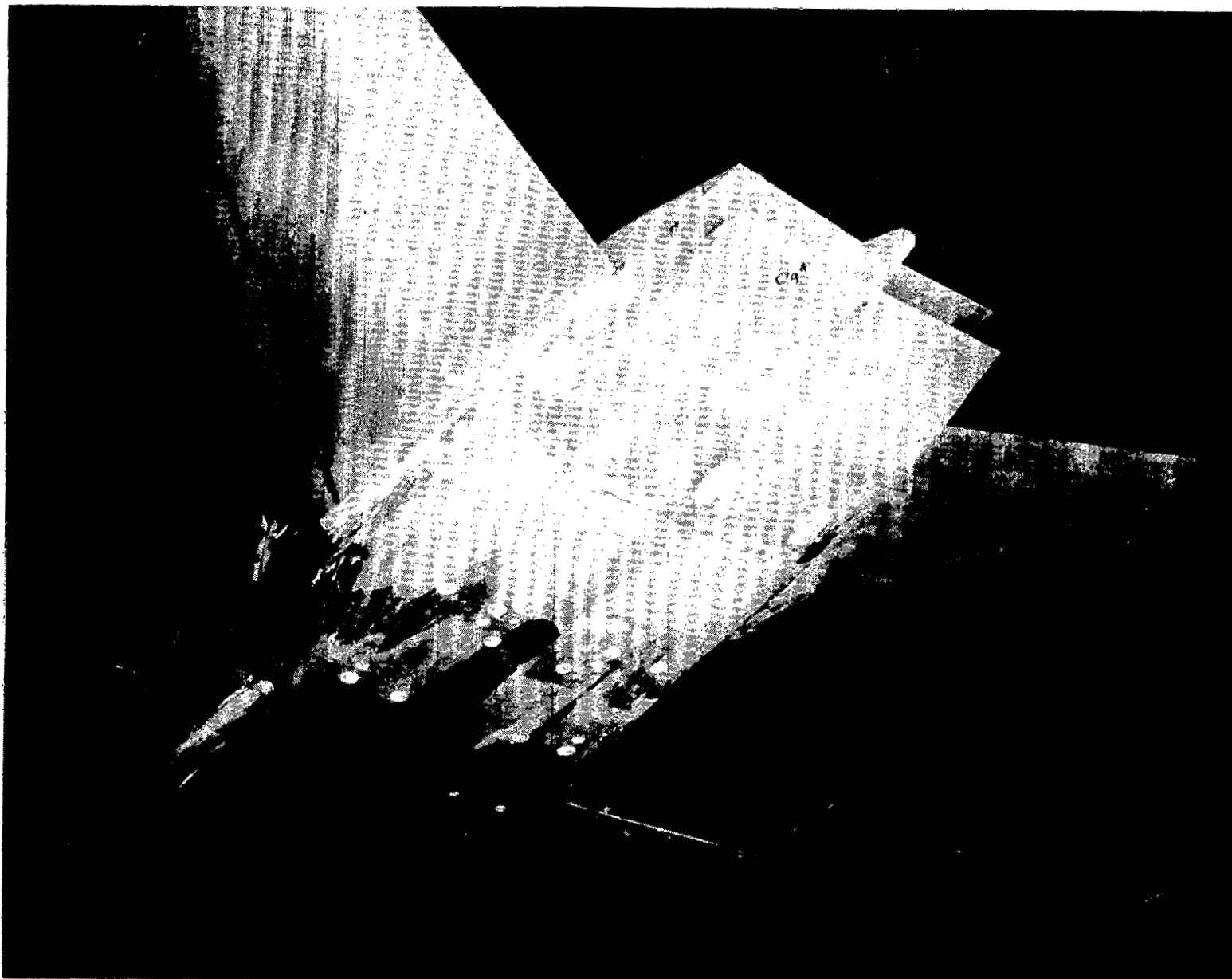


Figure 5.-, Axisymmetric nozzle. Linear dimensions are in centimeters.



L-78-2105

Figure 6.- Overall view of 2-D C-D nozzle installed on F-18 model.



L-78-4817

Figure 7.- 2-D C-D nozzle, dry power, installed on F-18 model.

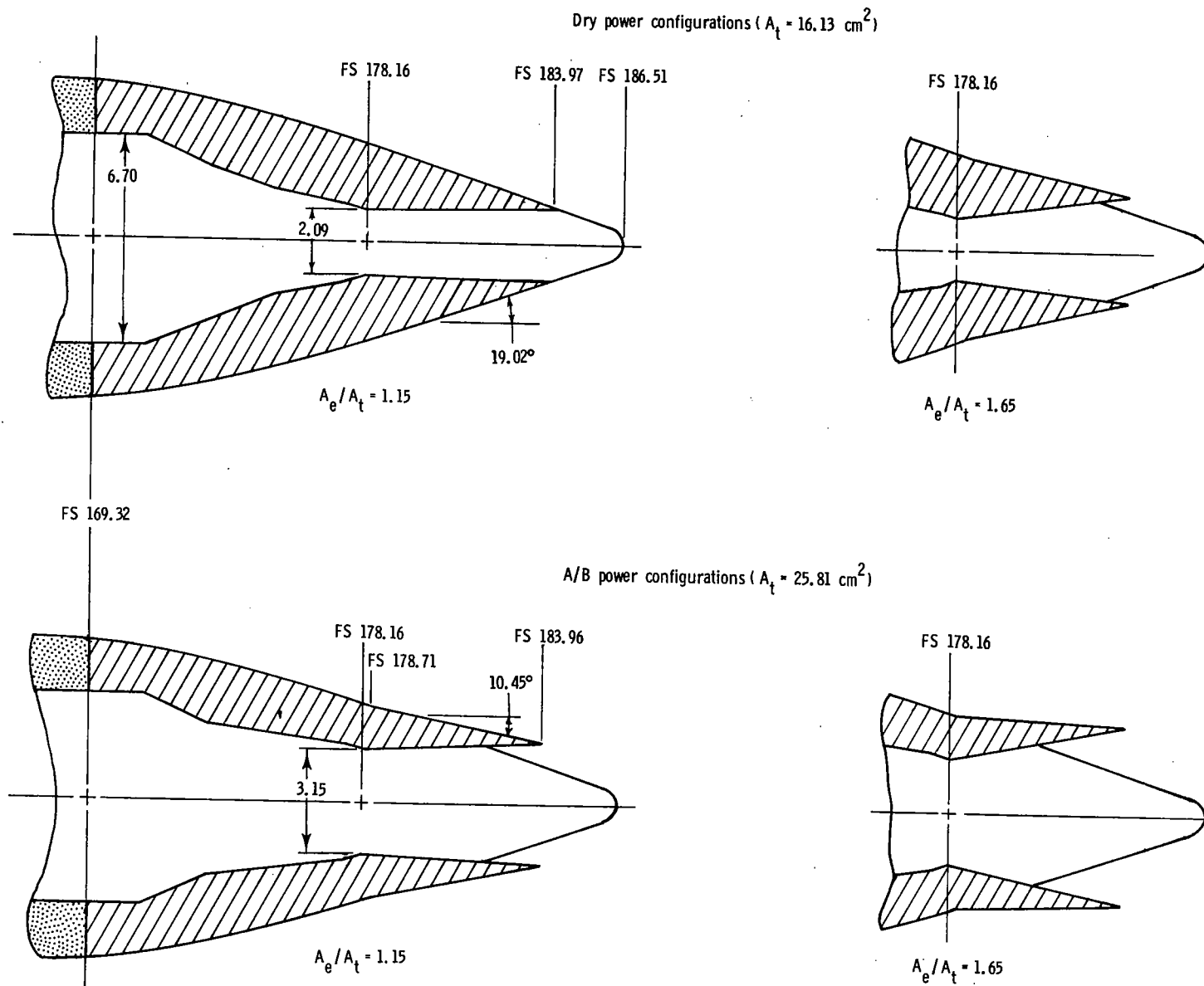


Figure 8.- 2-D C-D nozzle. Nozzle has diverging sidewalls from FS 171.09 to FS 173.09; nozzle width from FS 173.09 to exit is 7.74 cm. Linear dimensions are in centimeters.

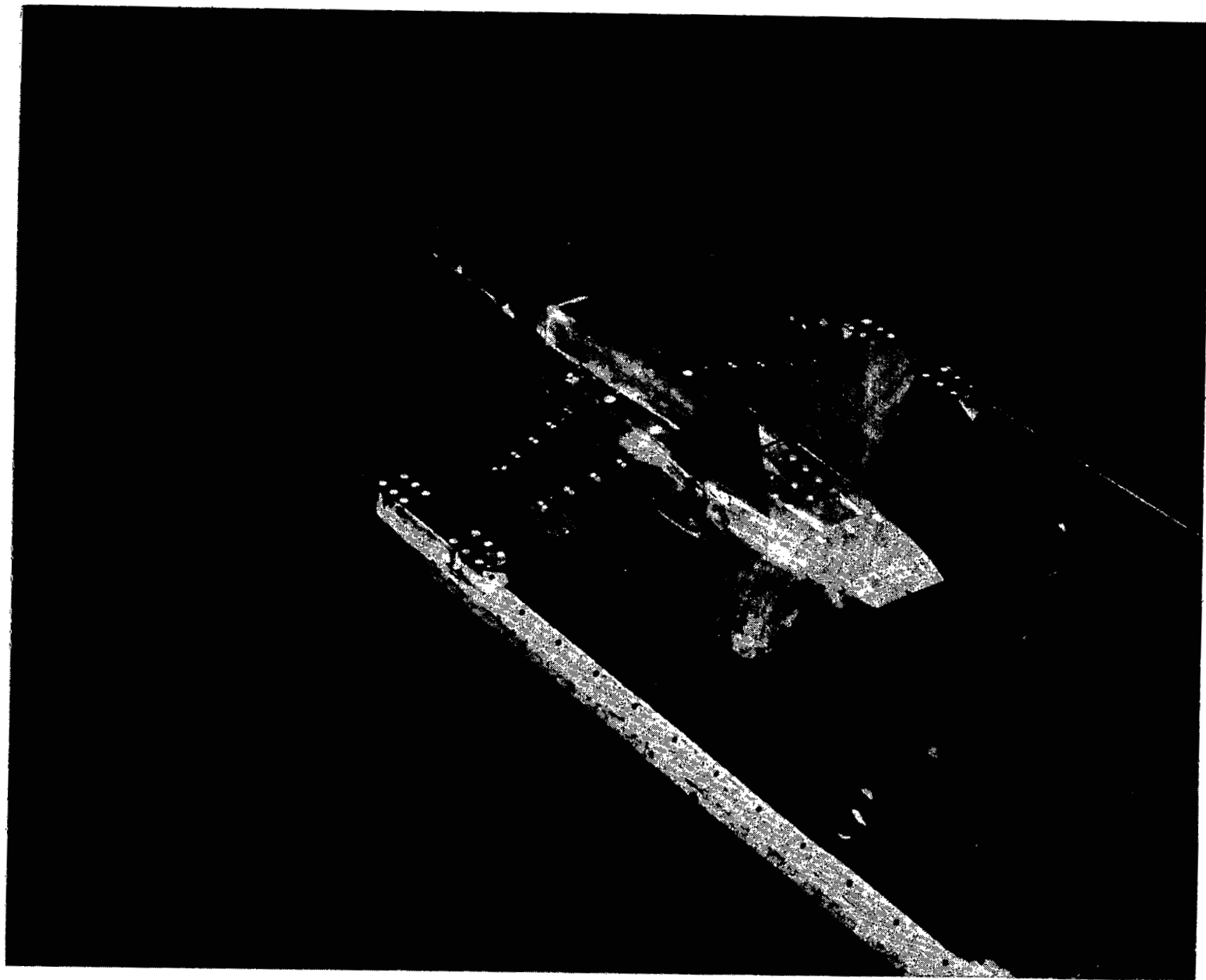
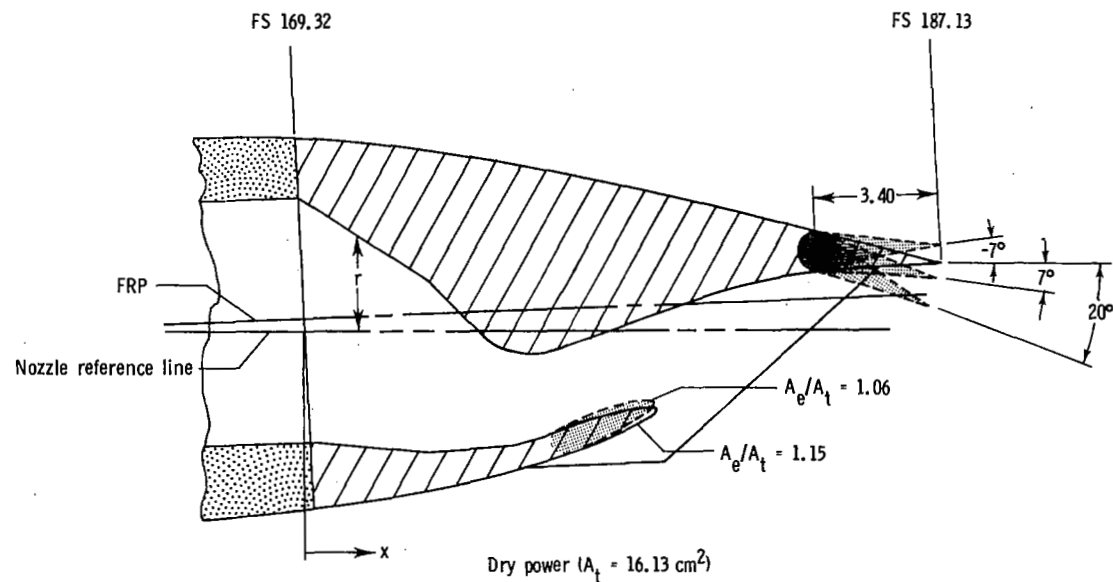
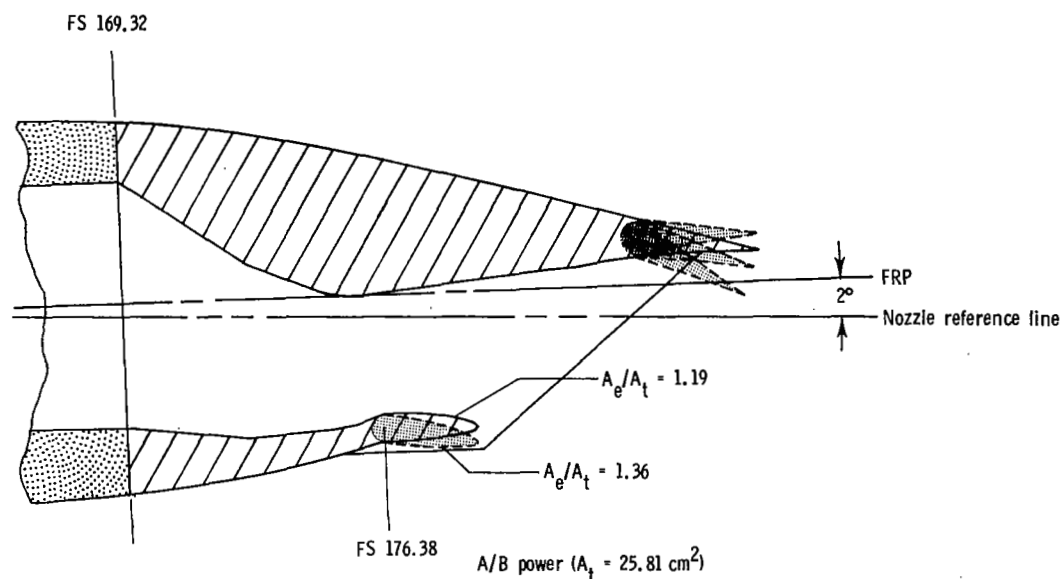


Figure 9.- Overall view of SERN installed on F-18 model.

L-78-2024



Upper flap geometry ($\delta_v = 0^\circ$)		
x	Dry power r	A/B power r
3.48	1.41	1.41
5.04	-0.18	st. line
5.44	-0.44	
5.73	-0.53	0.64
5.99	-0.60	0.59
6.62		0.57
6.84	-0.55	
7.12	-0.48	st. line
10.79	st. line	1.16
11.36	0.97	1.22
11.92	1.14	1.26
12.20	1.22	1.27
12.48	1.26	1.26
12.77	1.35	1.35
13.05	1.41	1.41
13.61	1.52	1.52
14.18	1.60	1.60
14.75	1.67	1.67
15.32	1.71	1.71
17.81	1.82	1.82



Lower flap geometry ($A_e/A_t = 1.15$)	
x	r
3.48	-3.32
5.85	-3.12
6.66	-2.92
6.92	-2.80
7.40	-2.61
7.68	-2.52
8.25	-2.35
8.81	-2.23
9.38	-2.14
9.78	-2.11

Figure 10.- SERN. Nozzle has diverging sidewalls from FS 169.32 to FS 171.86; nozzle width from FS 171.86 to exit is 7.73 cm. Linear dimensions are in centimeters.

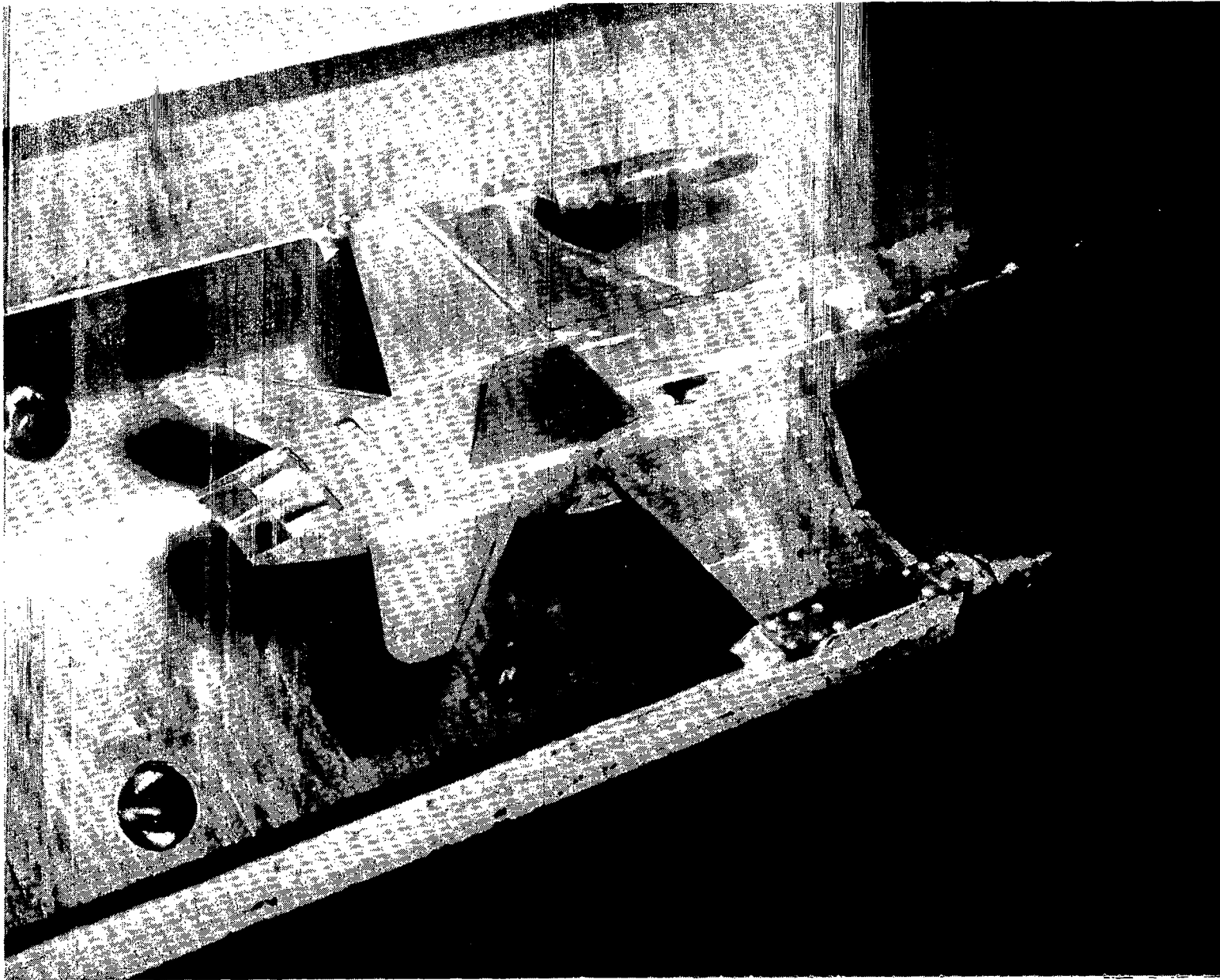


Figure 11.- Overall view of wedge nozzle installed on F-18 model.

L-78-2555

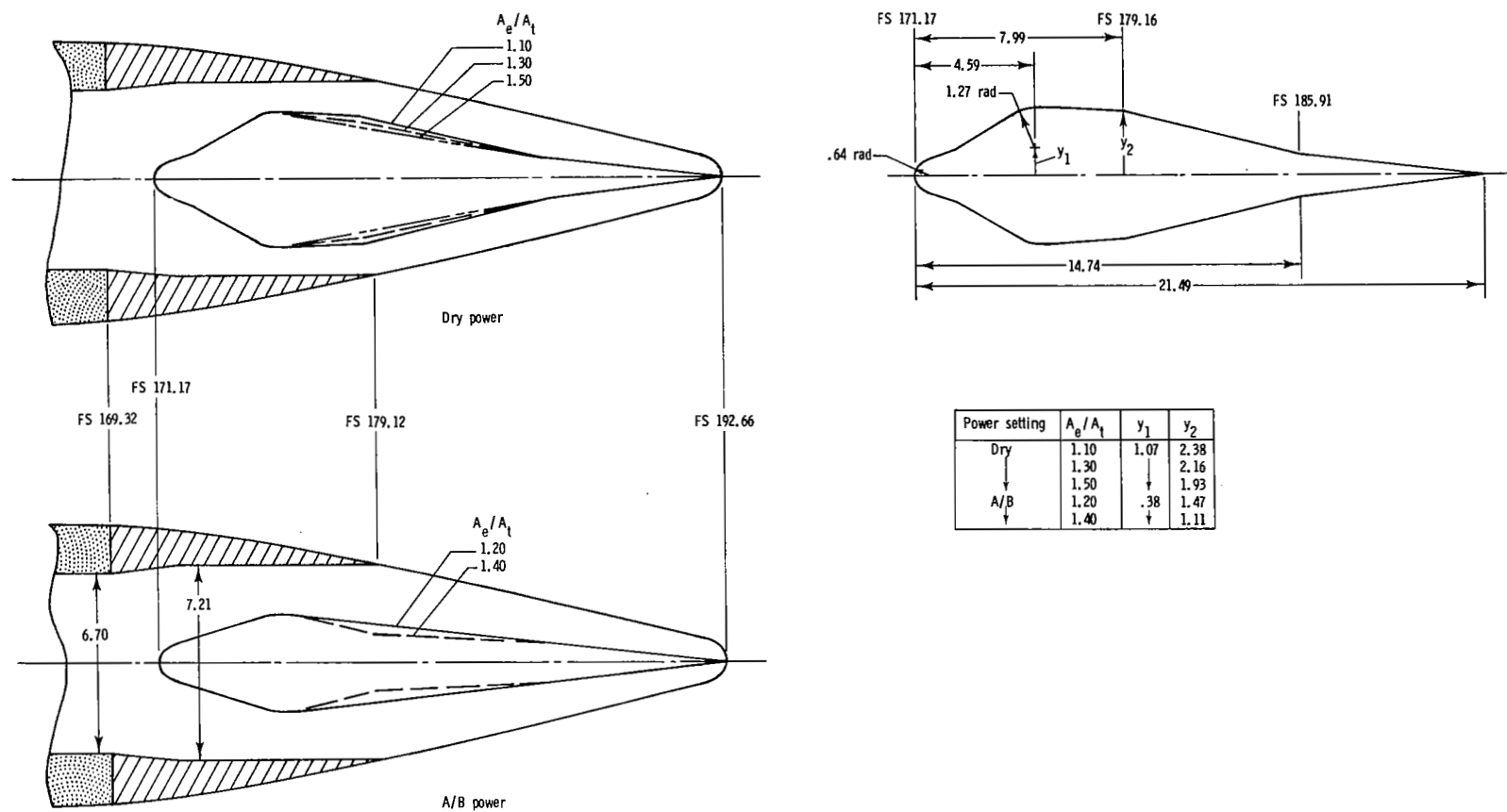
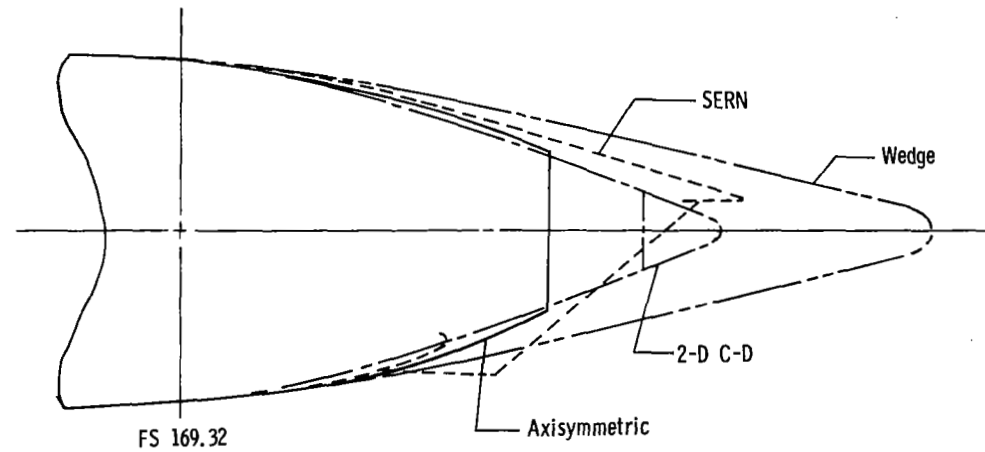
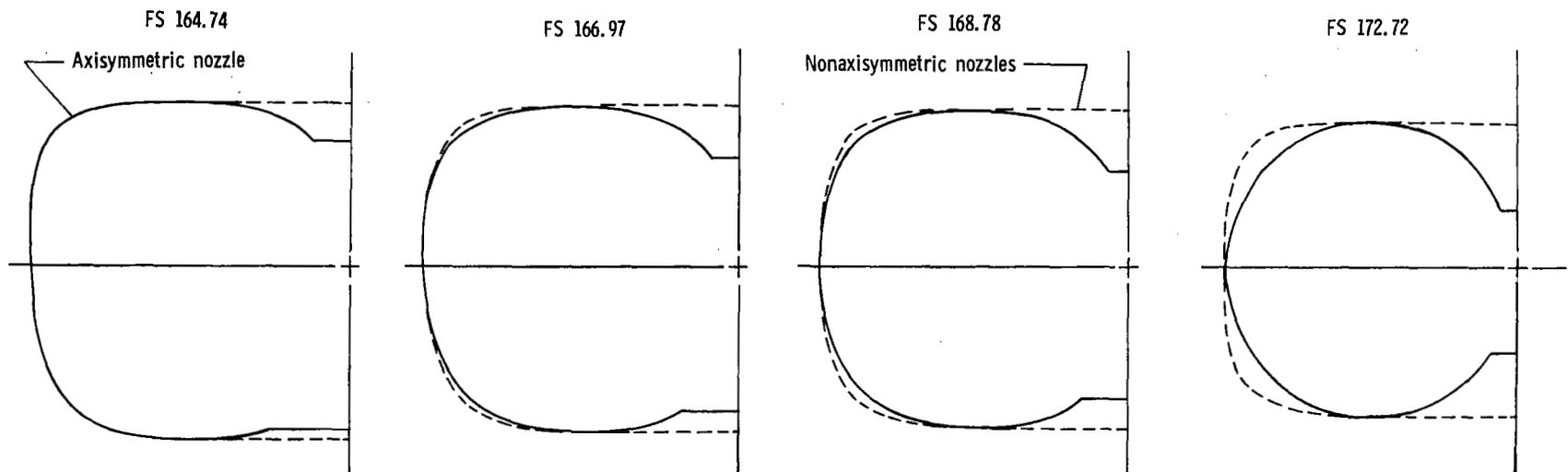


Figure 12.- Wedge nozzle. Nozzle has diverging sidewalls from FS 169.32 to FS 171.86; nozzle width from FS 171.86 to exit is 7.21 cm. Linear dimensions are in centimeters.



Composite external profile view of nozzles tested



Typical afterbody cross sections

Figure 13.- Composite view of external lines of nozzles and some afterbody cross sections.

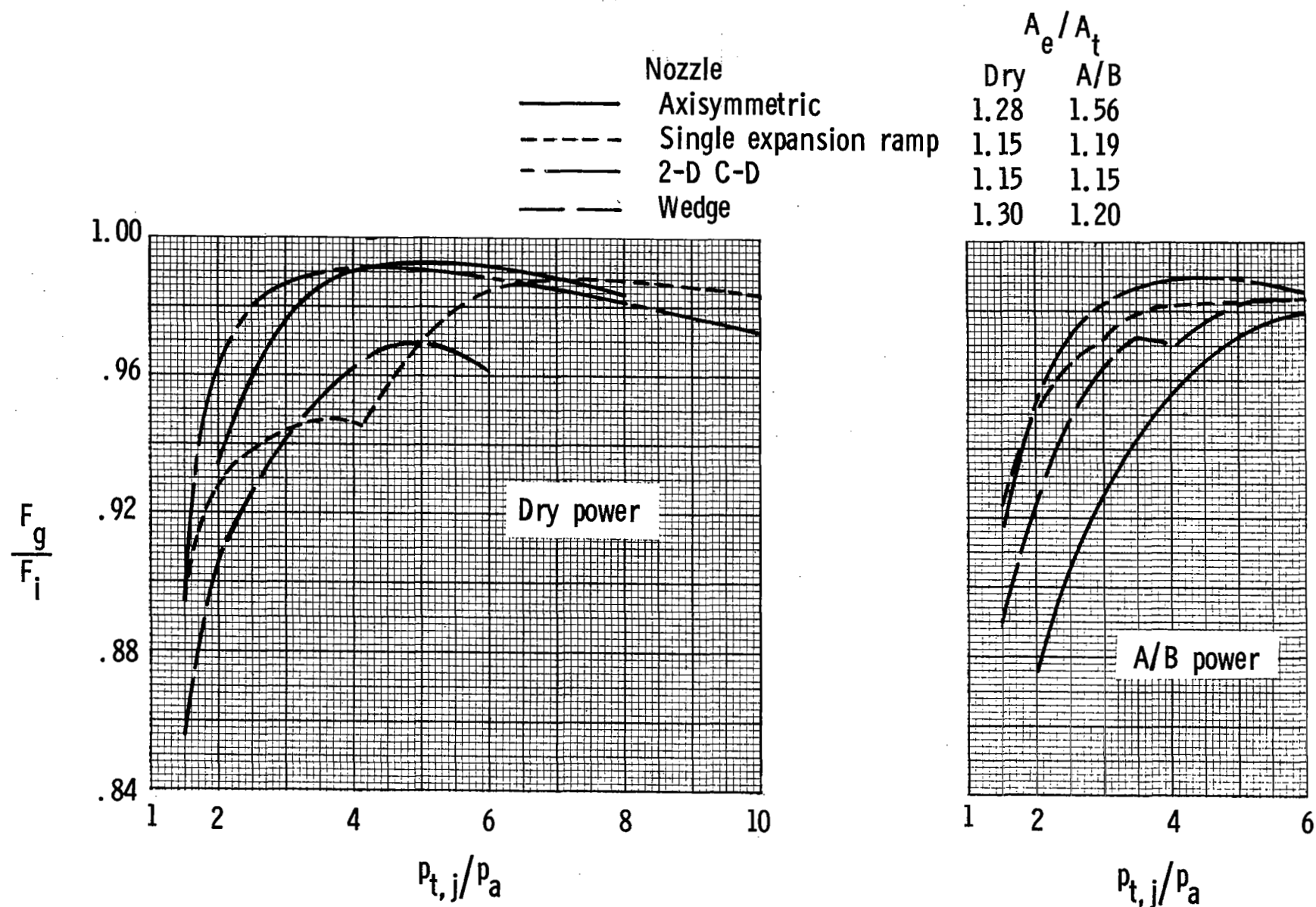


Figure 14.- Comparison of unvectored static nozzle performance.

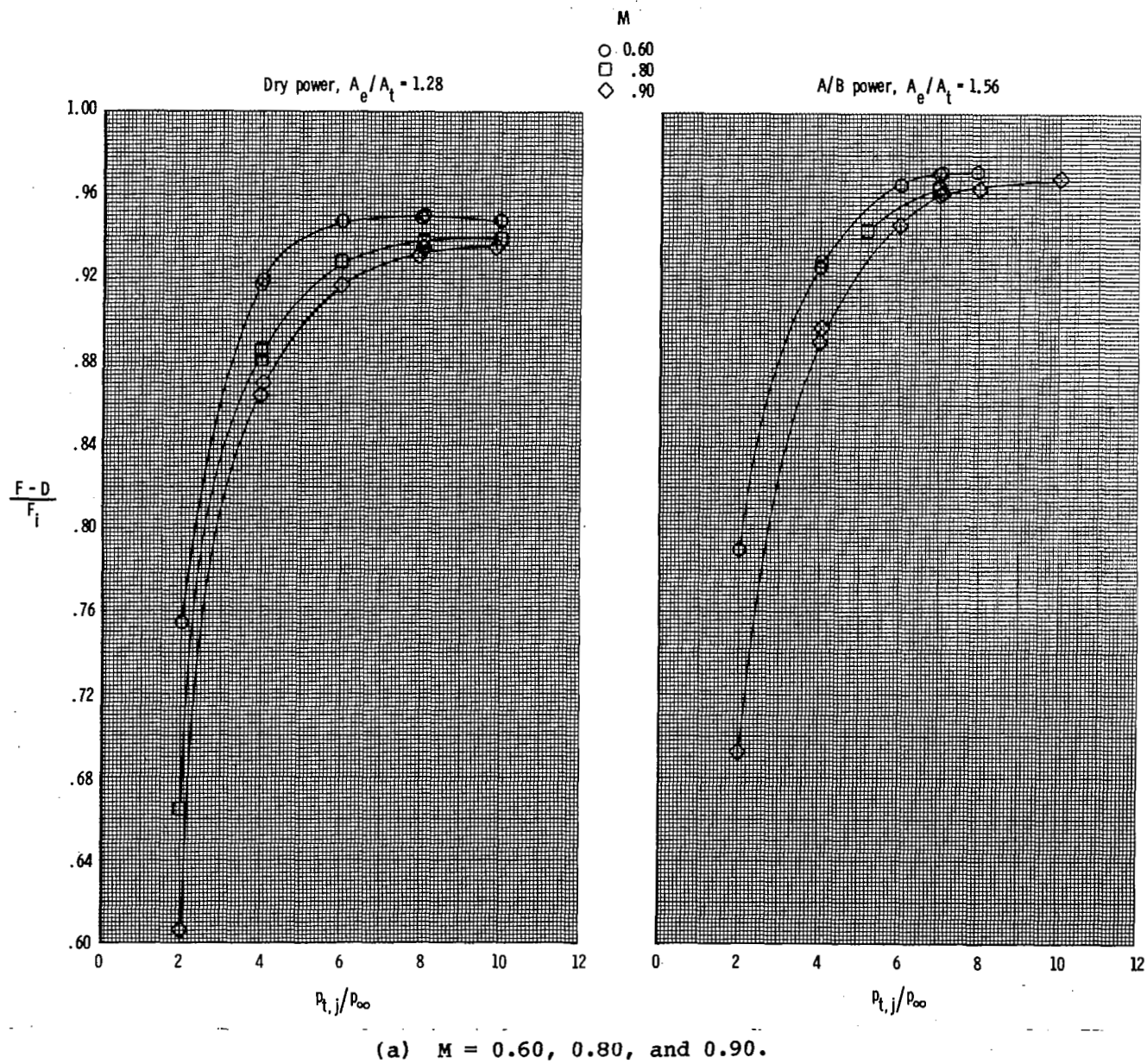
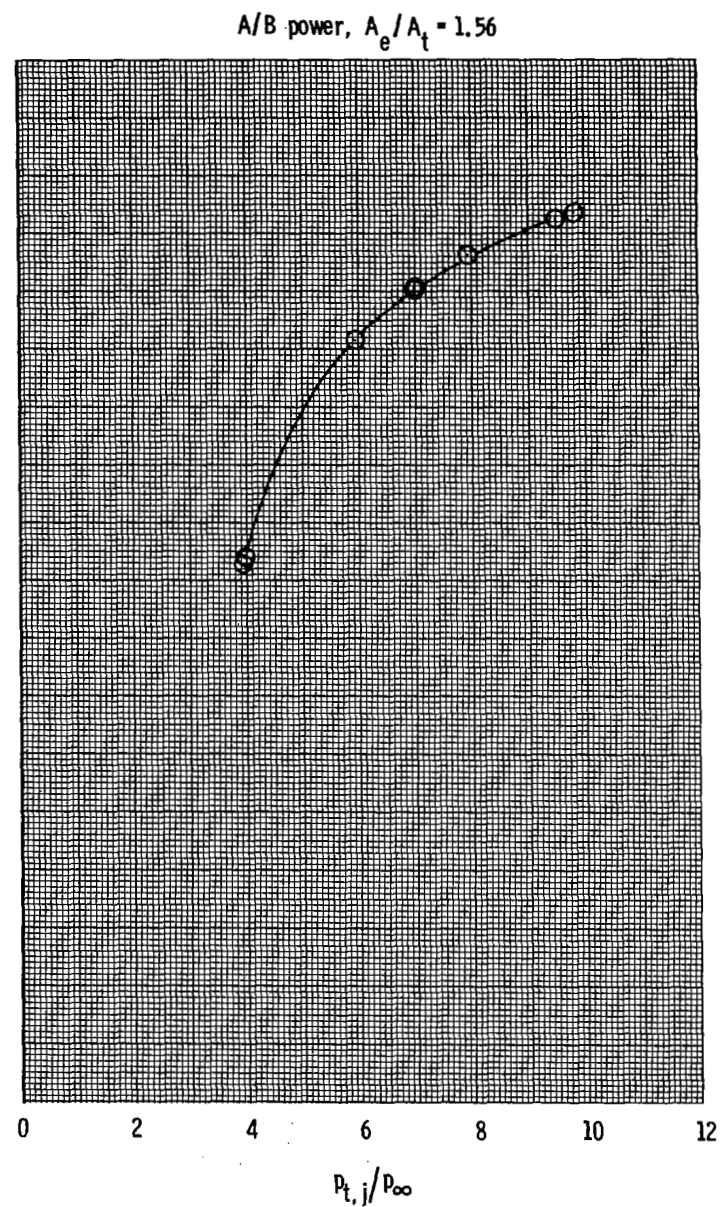
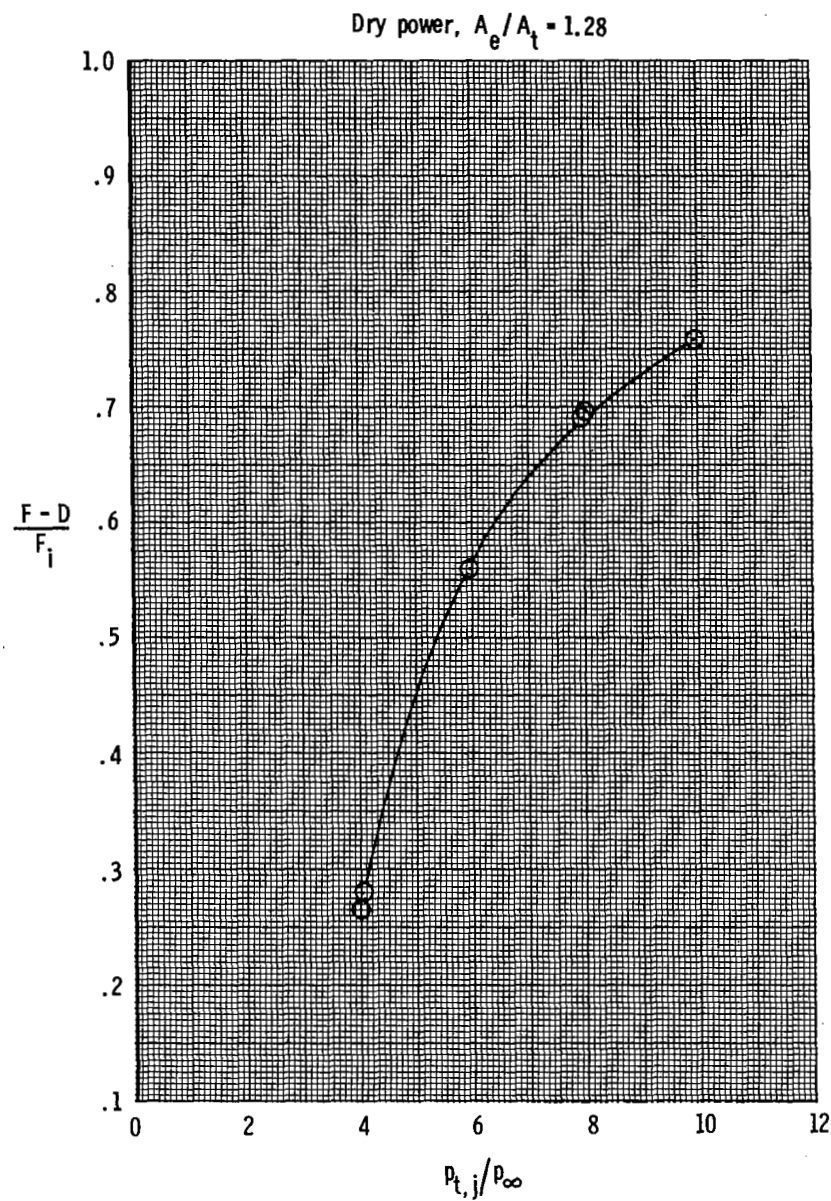


Figure 15.- Effect of Mach number on afterbody performance for axisymmetric nozzle.
Symbols with ticks indicate repeat points.



(b) $M = 1.20$.

Figure 15.- Continued.

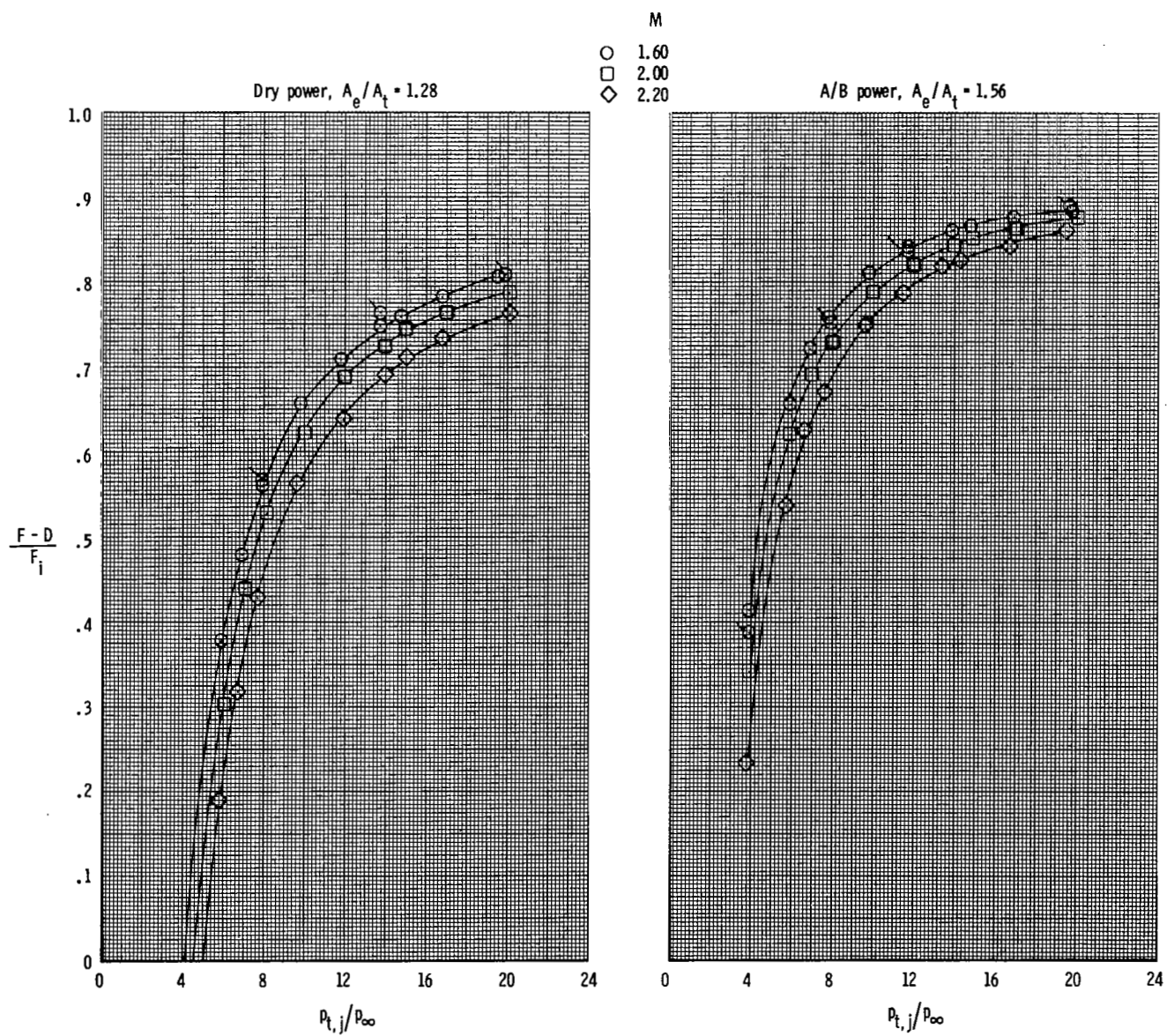


Figure 15.- Concluded.

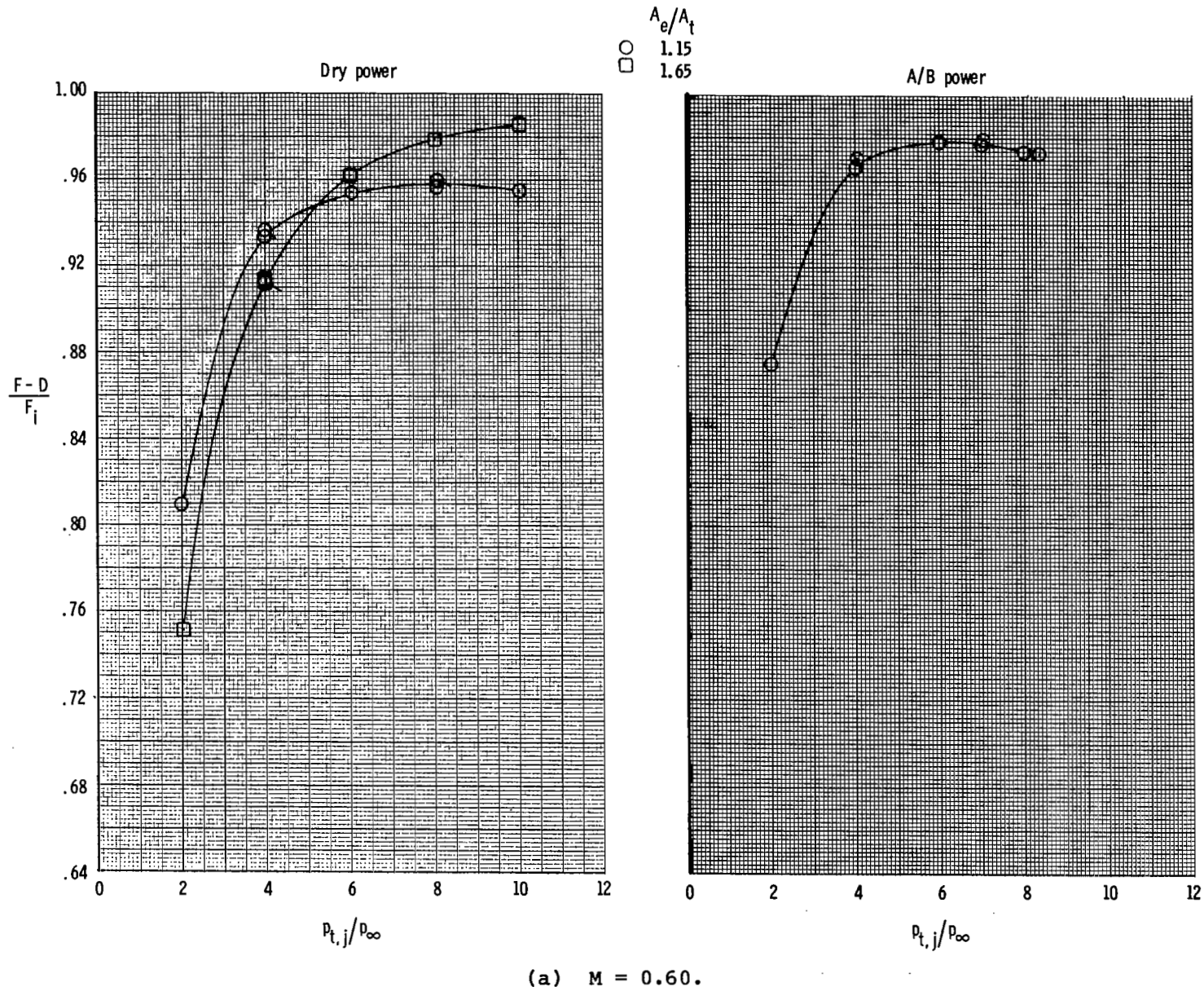
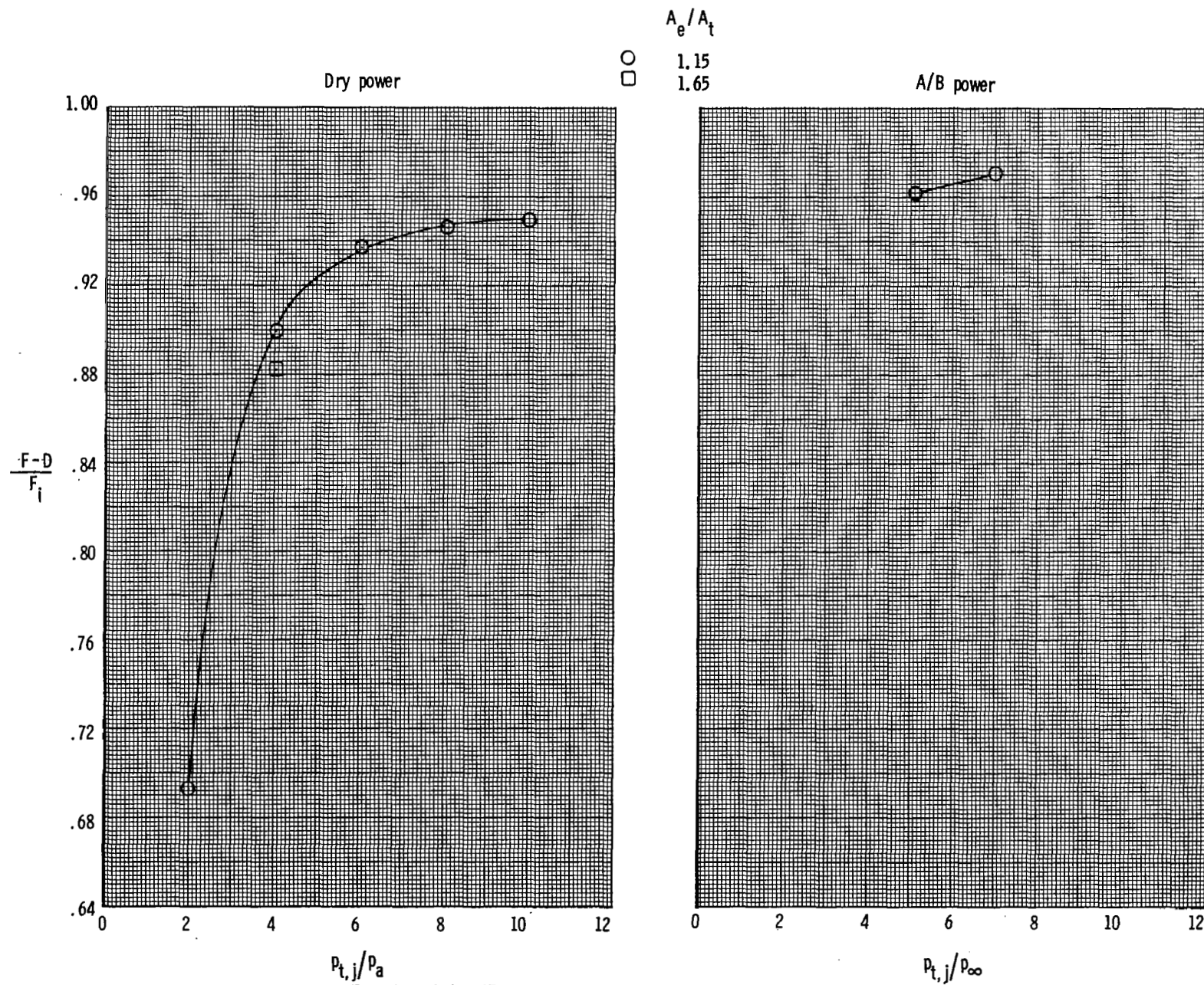


Figure 16.- Effect of expansion ratio and Mach number on afterbody performance for 2-D C-D nozzle. Symbols with ticks indicate repeat points.



(b) $M = 0.80$.

Figure 16.- Continued.

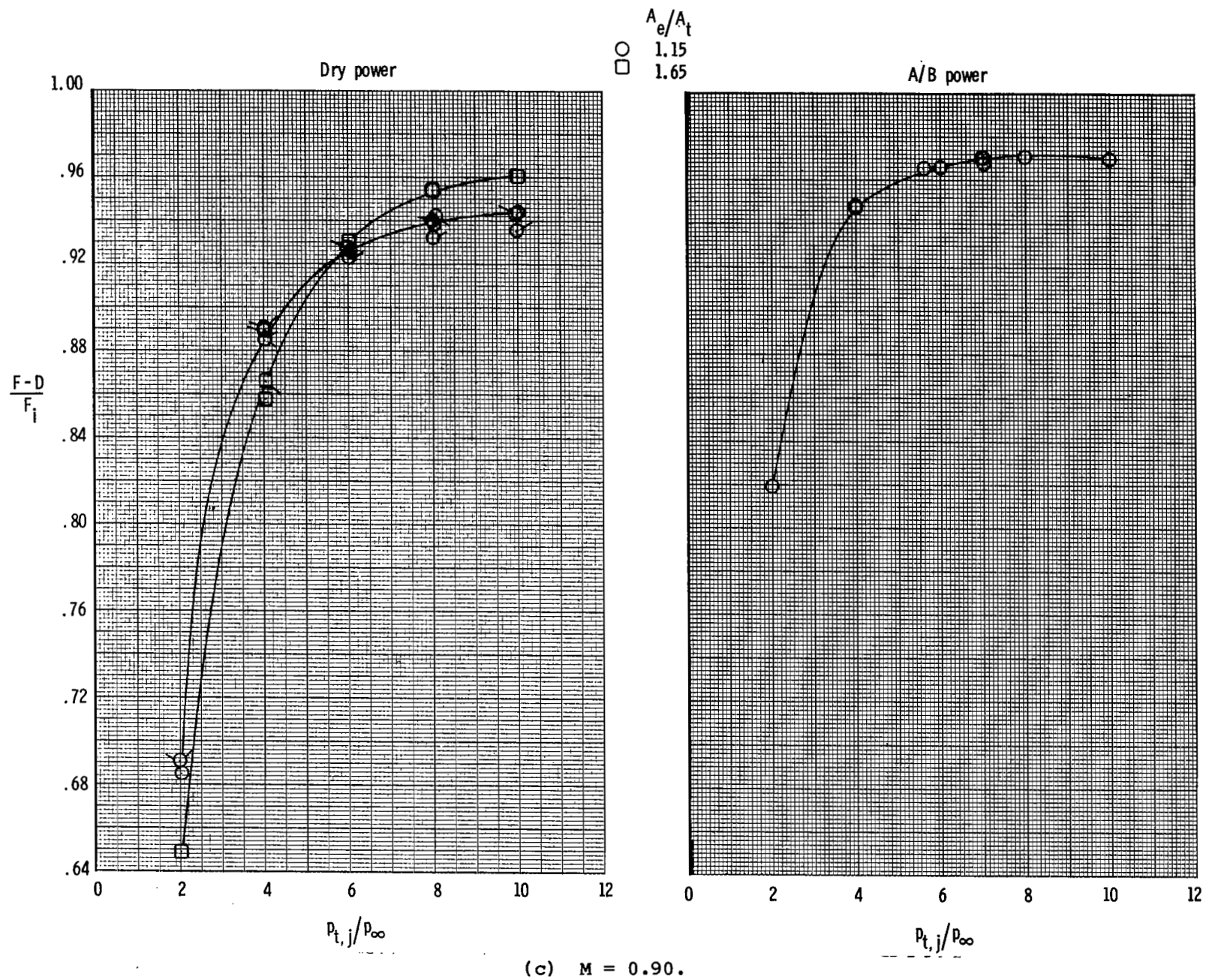
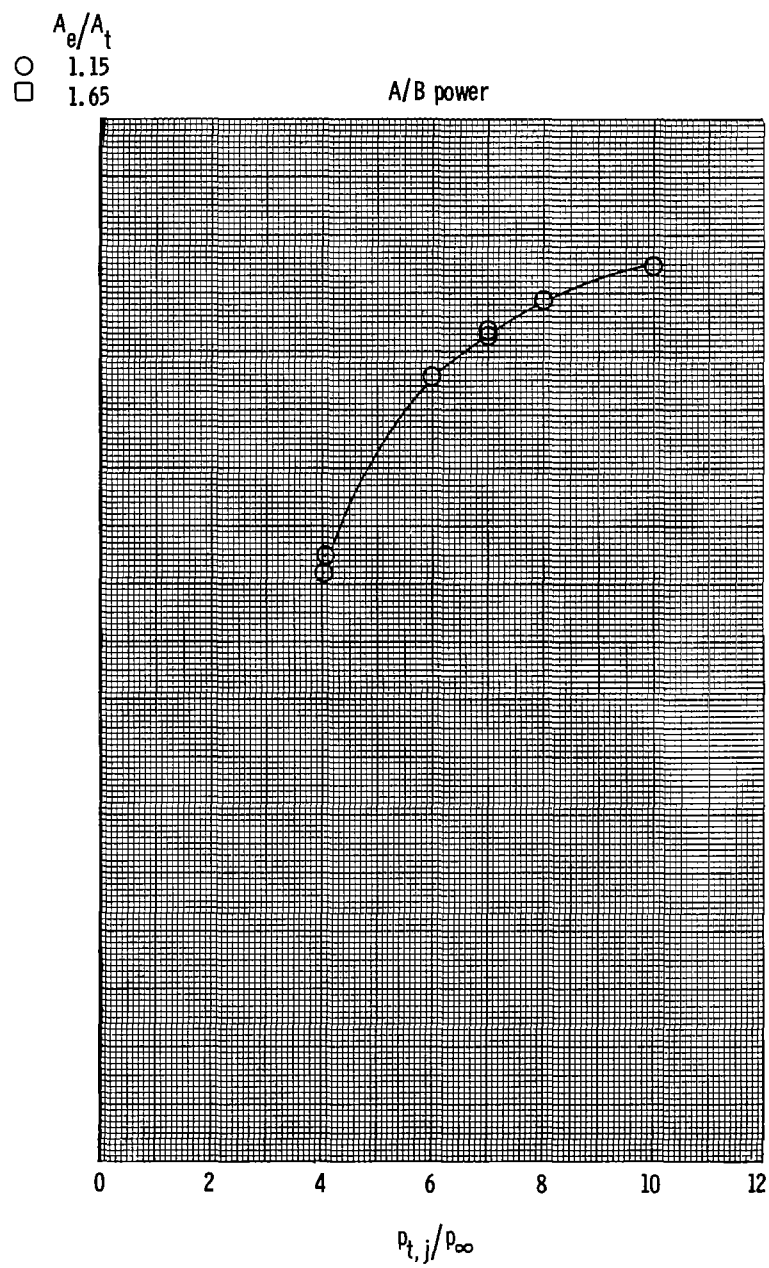
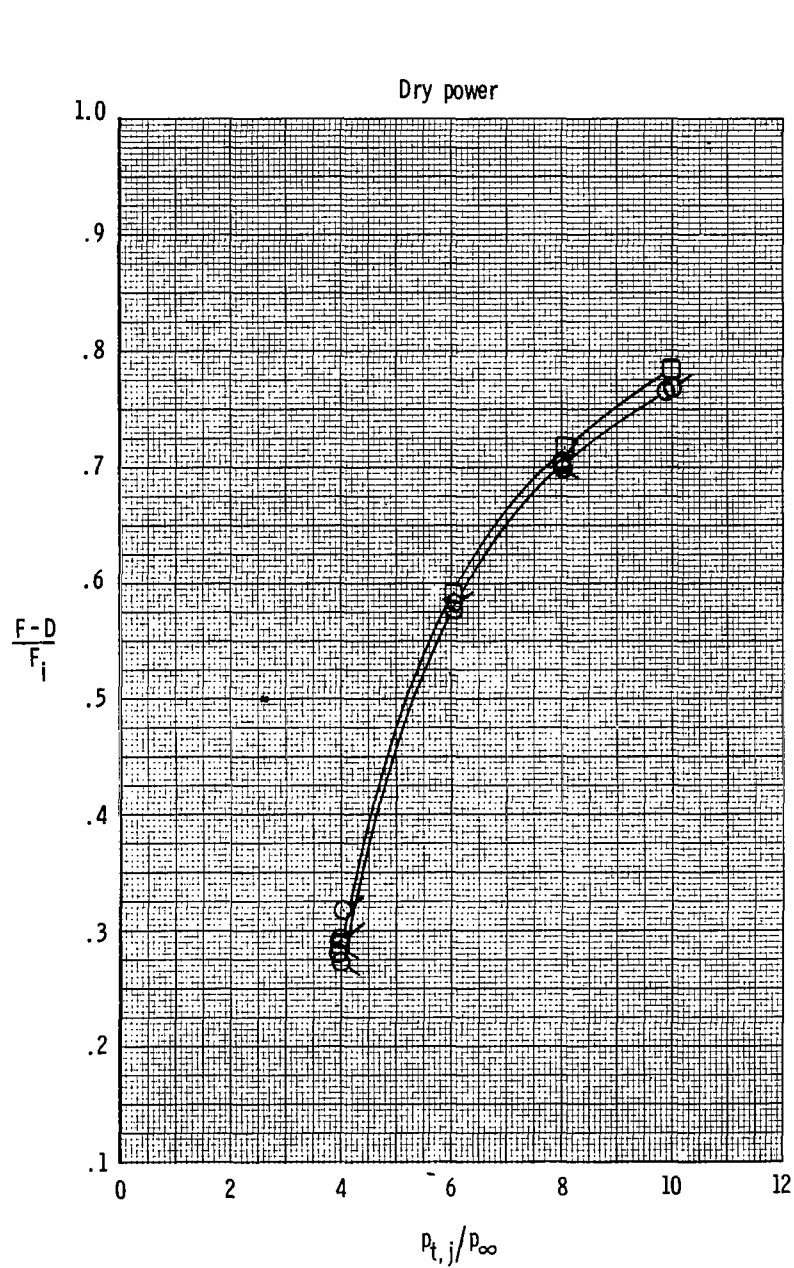
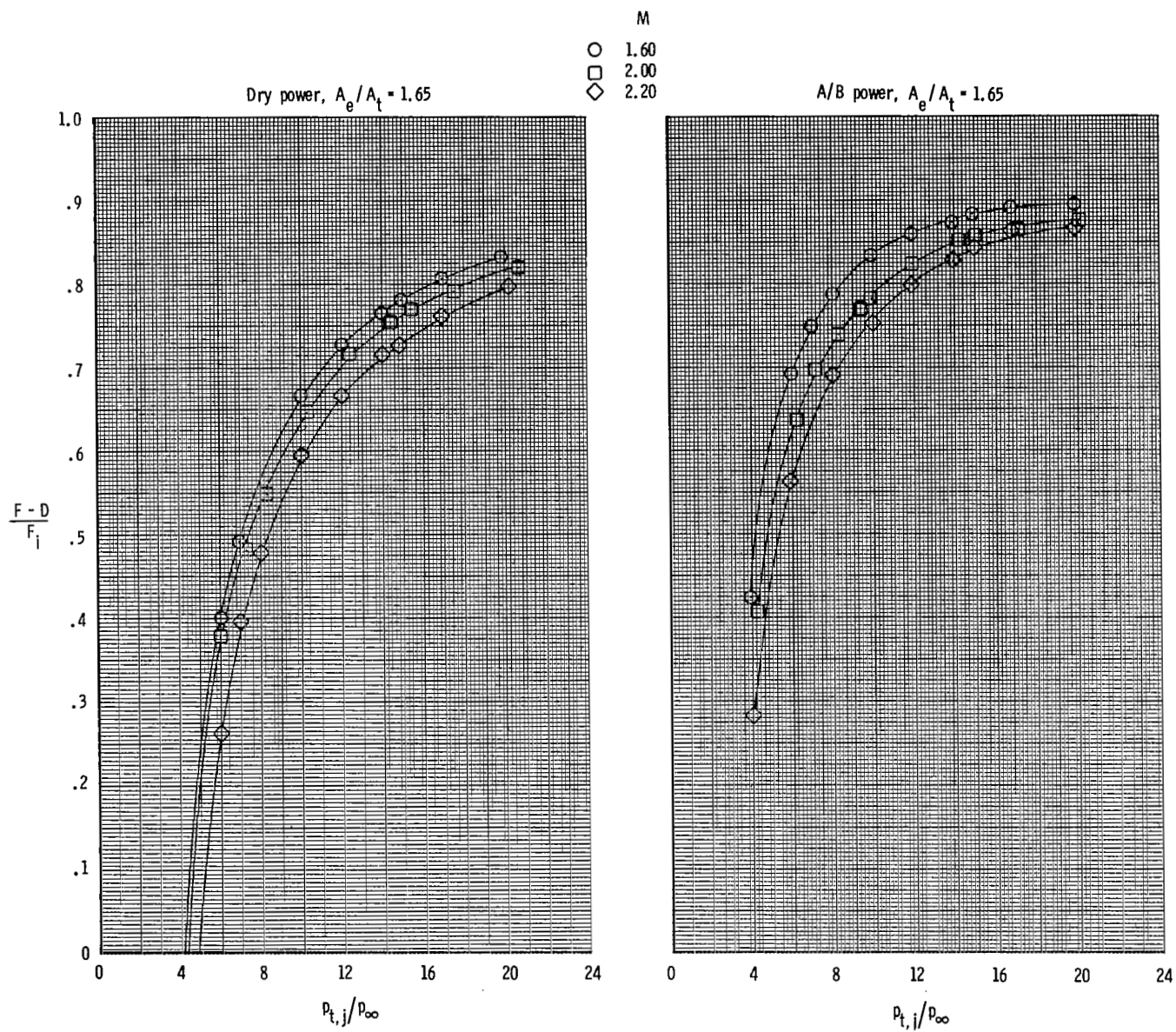


Figure 16.- Continued.



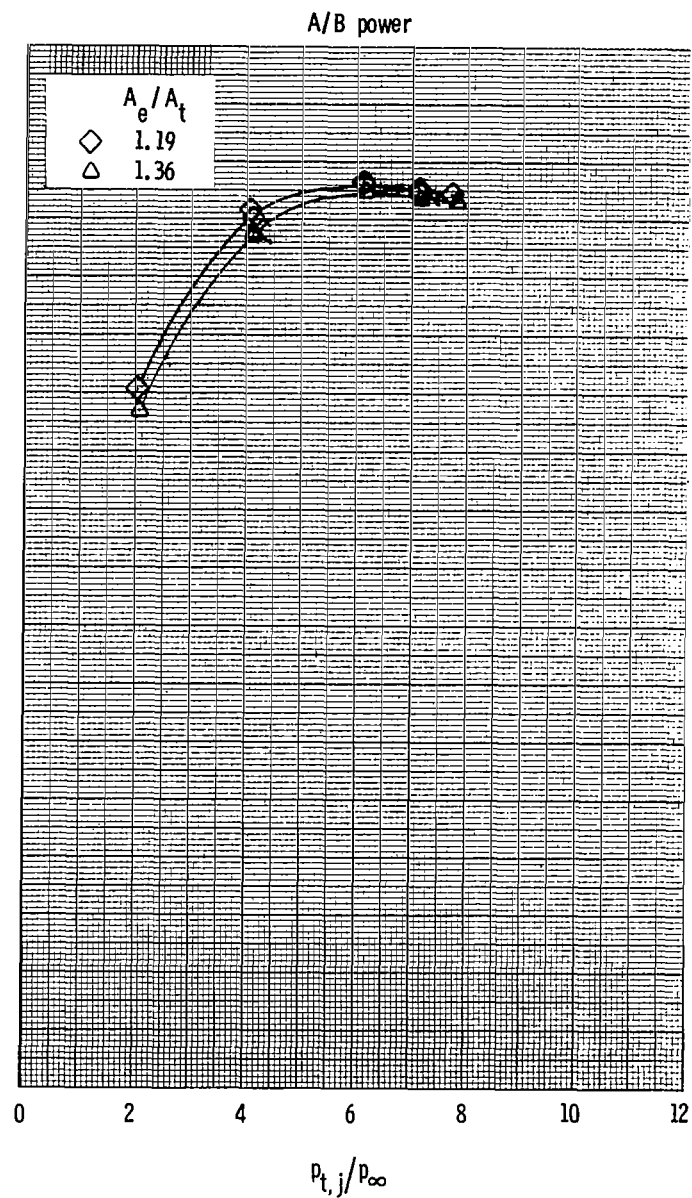
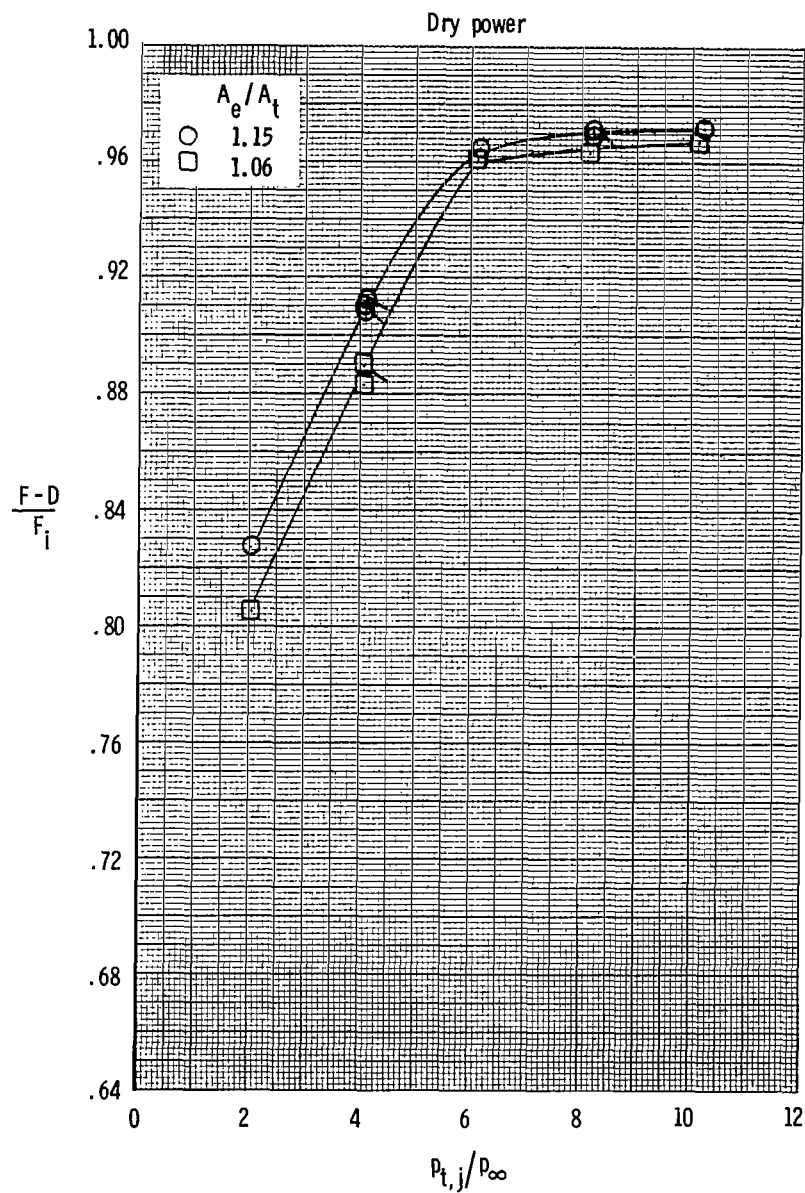
(d) $M = 1.20$.

Figure 16.- Continued.



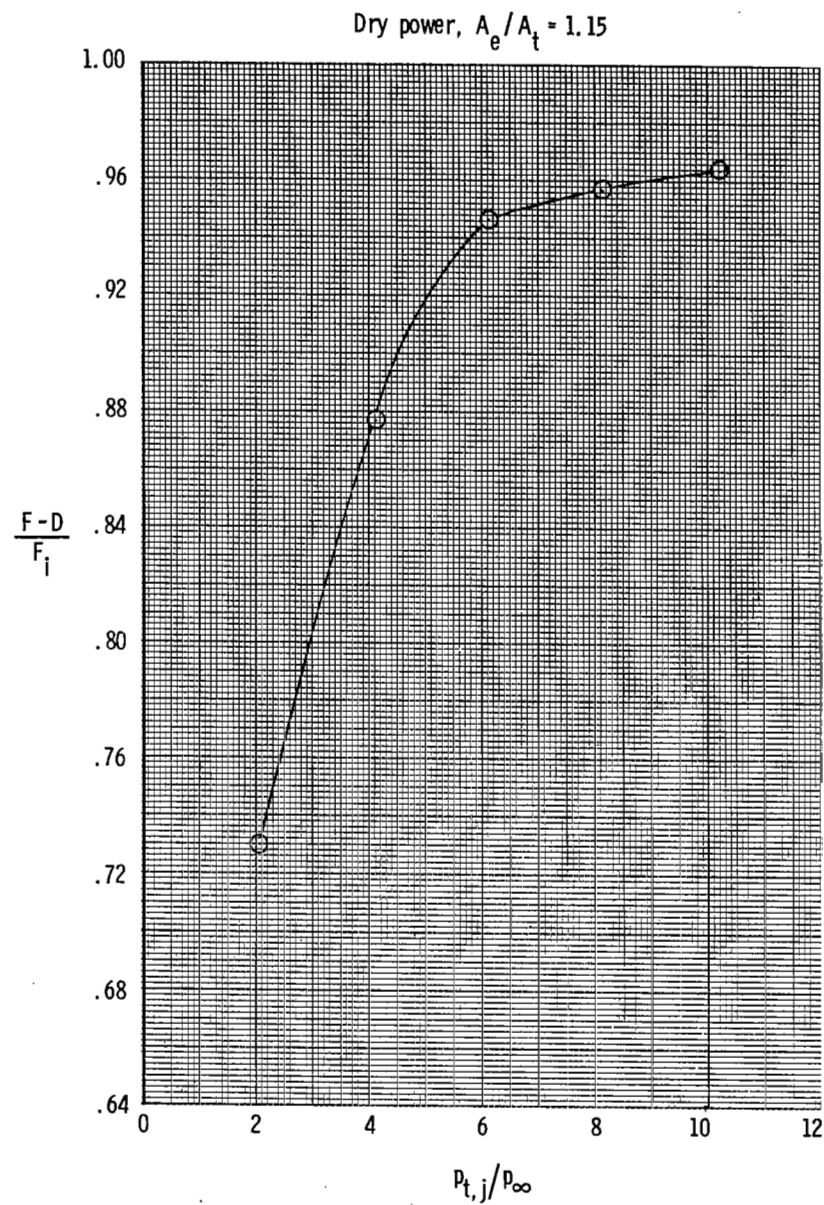
(e) $M = 1.60$ to 2.20 .

Figure 16.- Concluded.



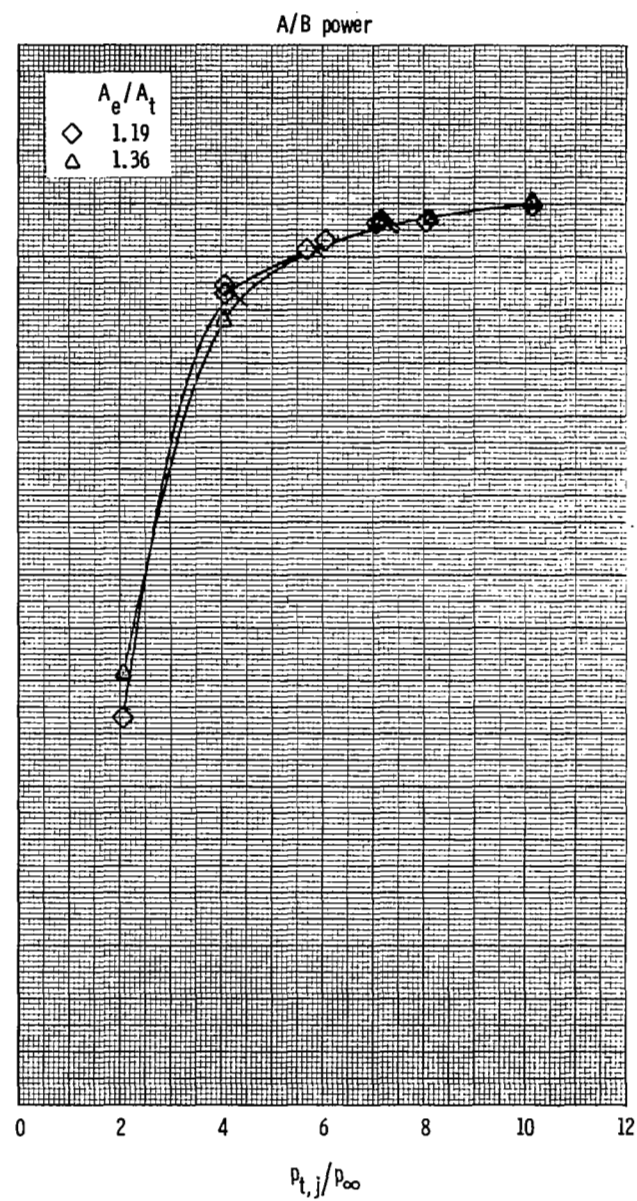
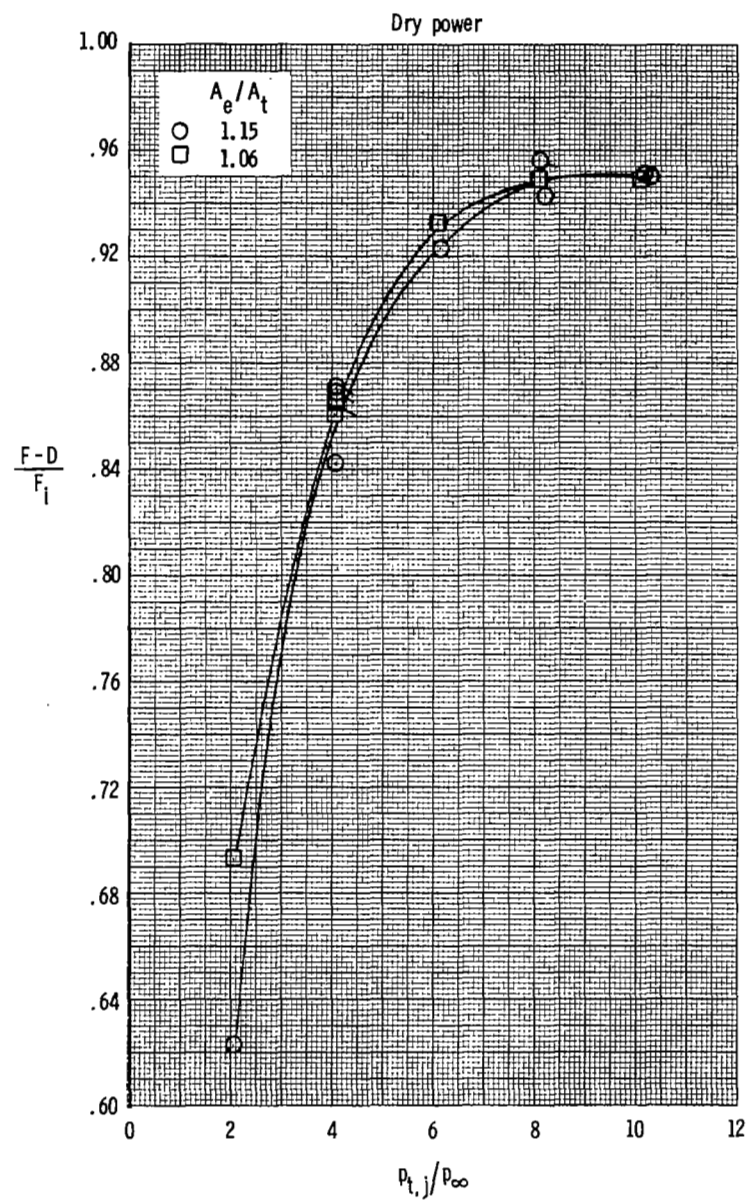
(a) $M = 0.60$.

Figure 17.- Effect of expansion ratio and Mach number on afterbody performance for SERN. Symbols with ticks indicate repeat points.



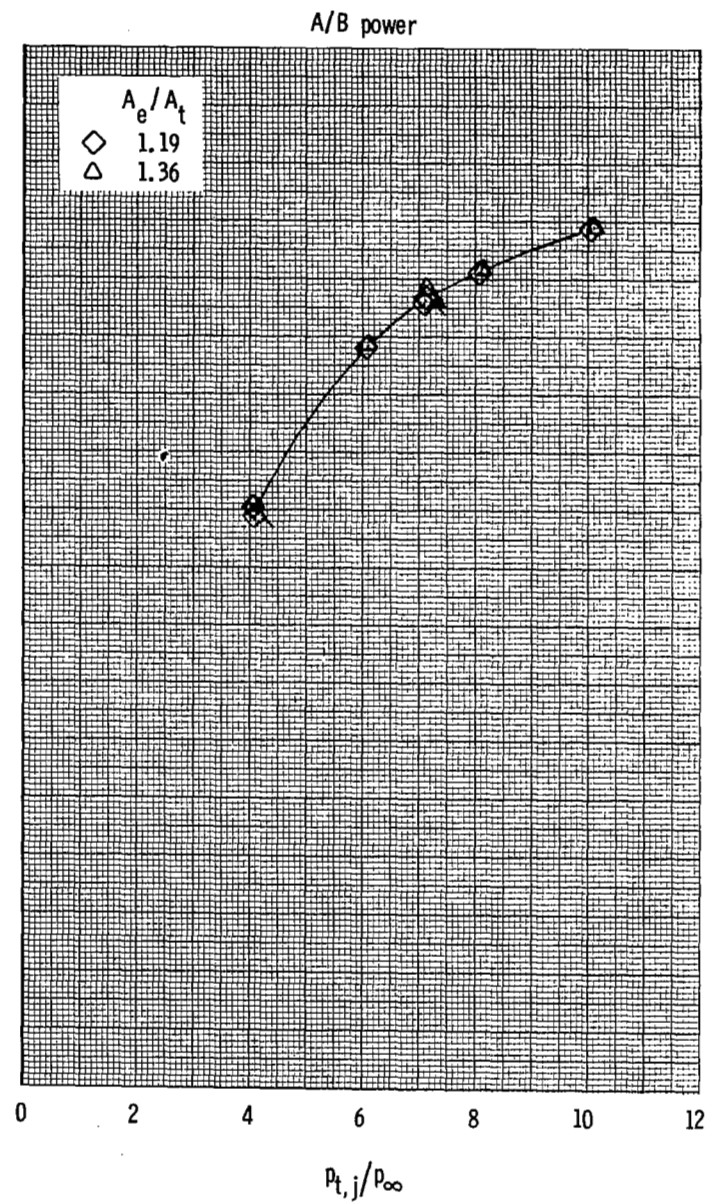
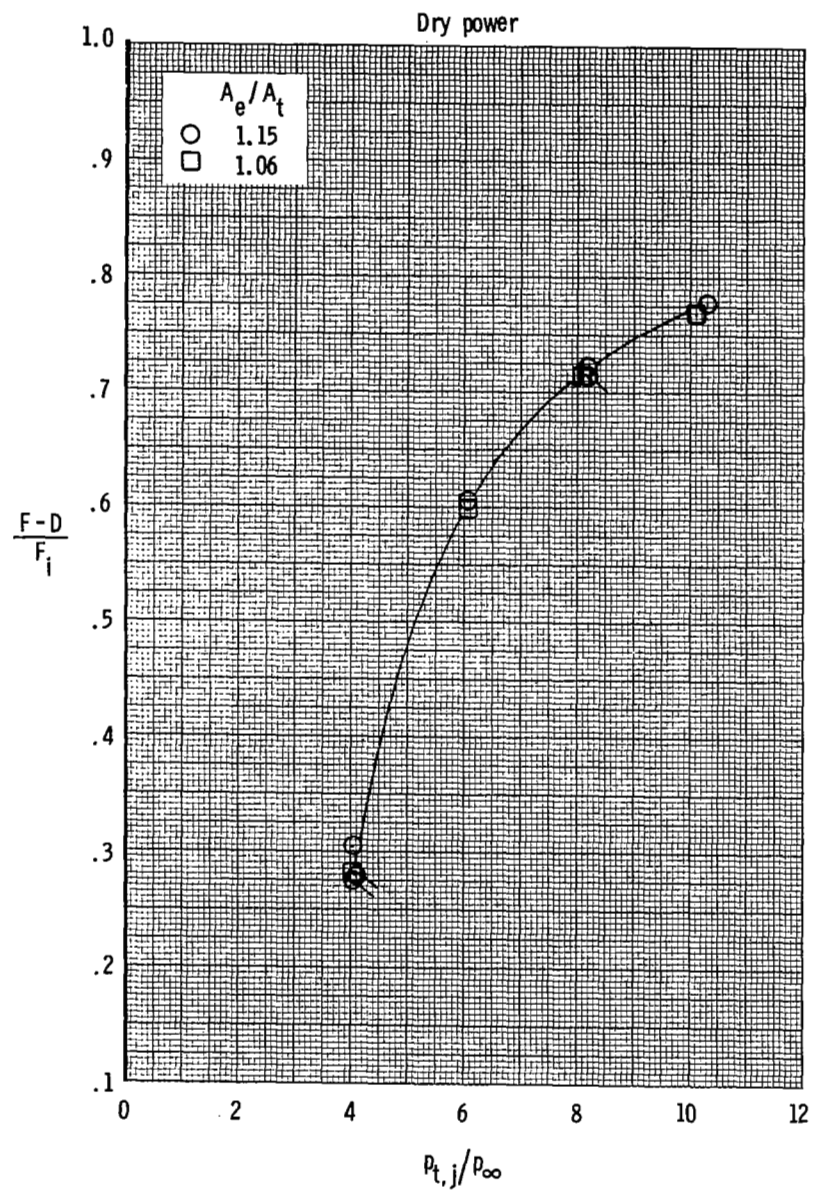
(b) $M = 0.80$.

Figure 17.- Continued.



(c) $M = 0.90$.

Figure 17.- Continued.



(d) $M = 1.20$.

Figure 17.- Continued.

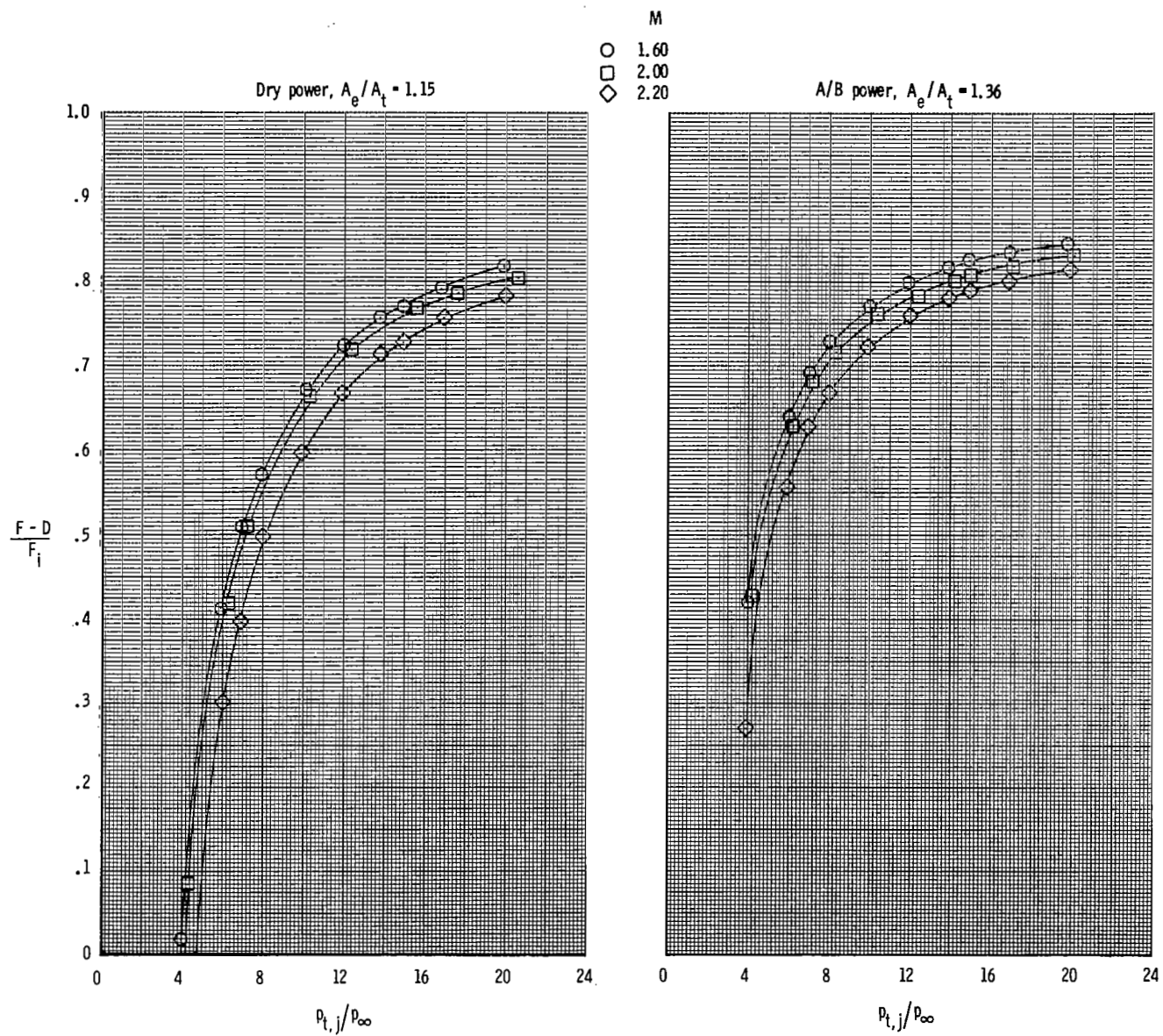
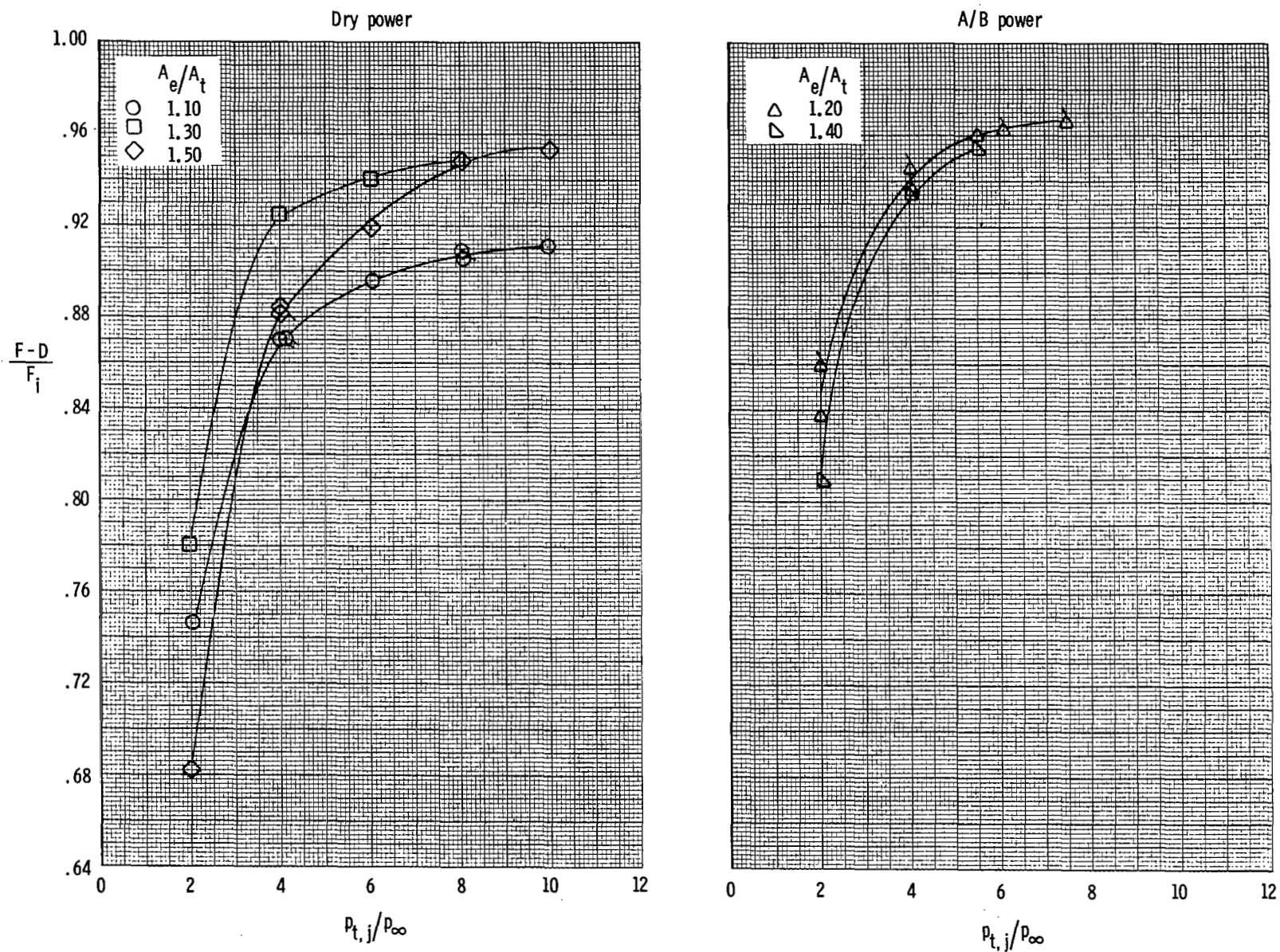
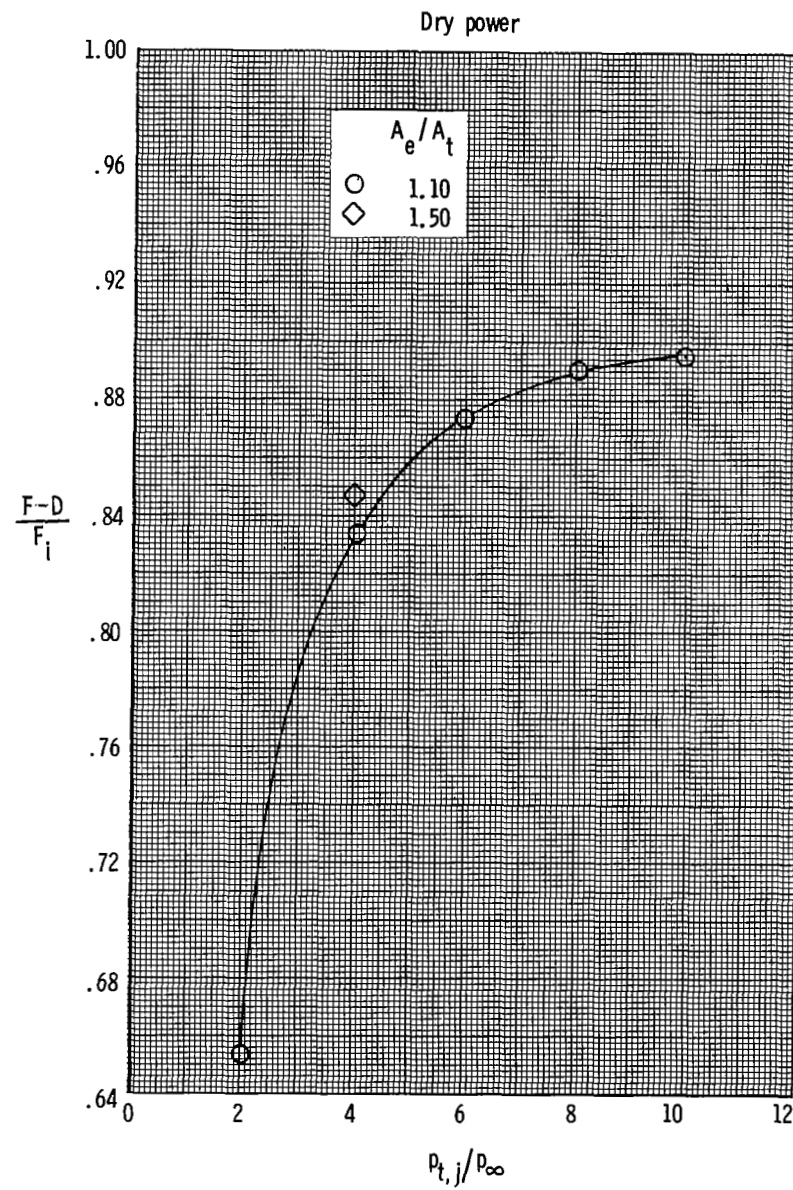


Figure 17.- Concluded.



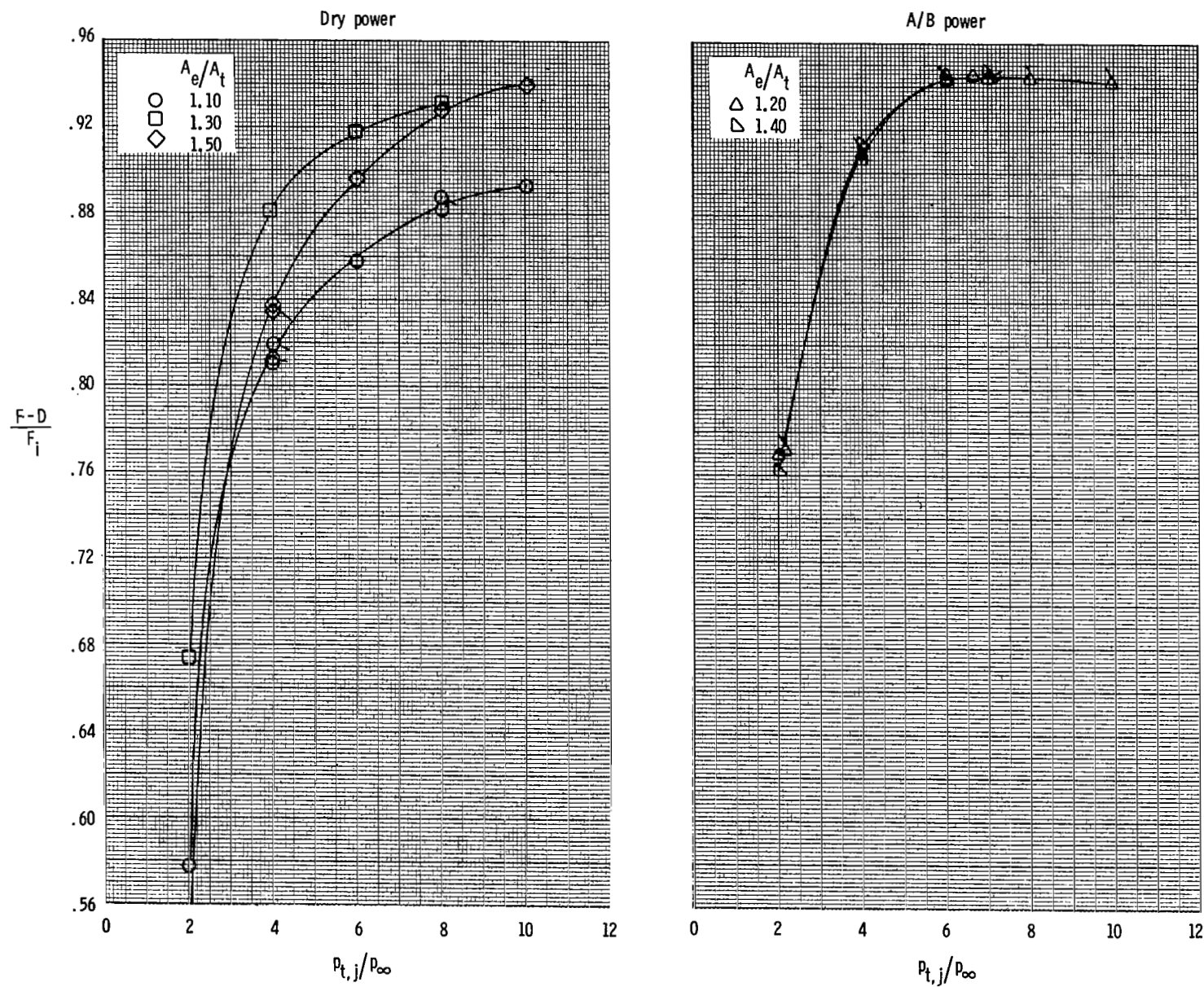
(a) $M = 0.60$.

Figure 18.- Effect of expansion ratio and Mach number on afterbody performance for wedge nozzle. Symbols with ticks indicate repeat points.



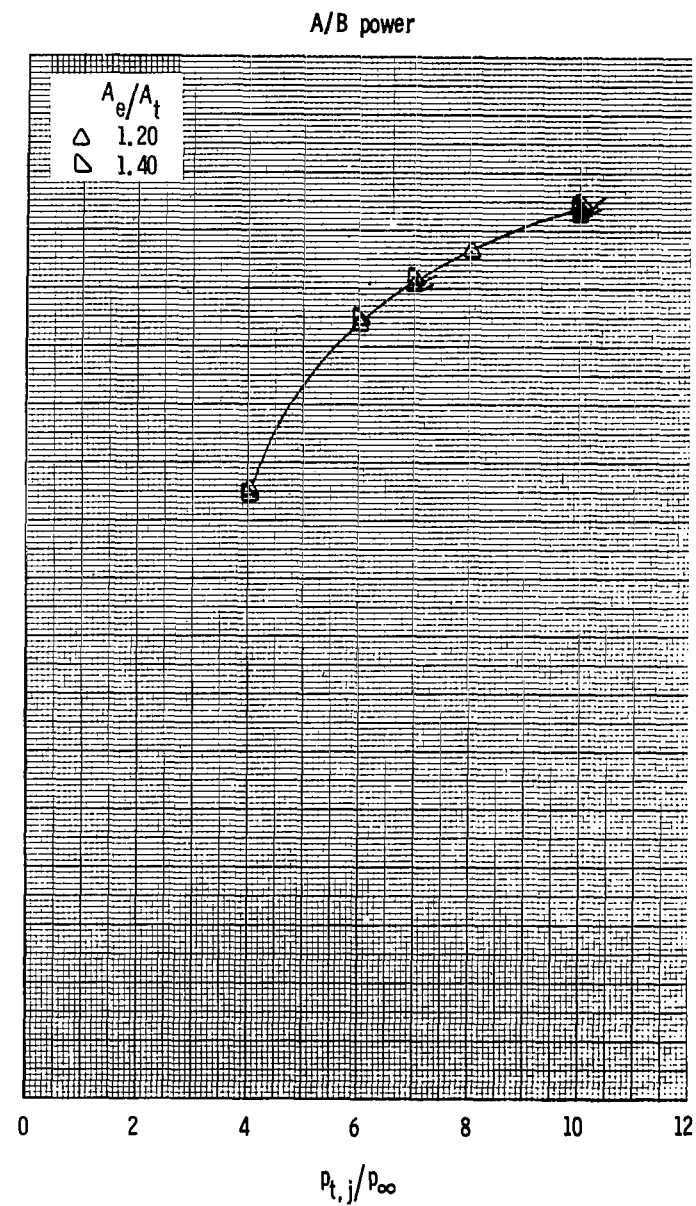
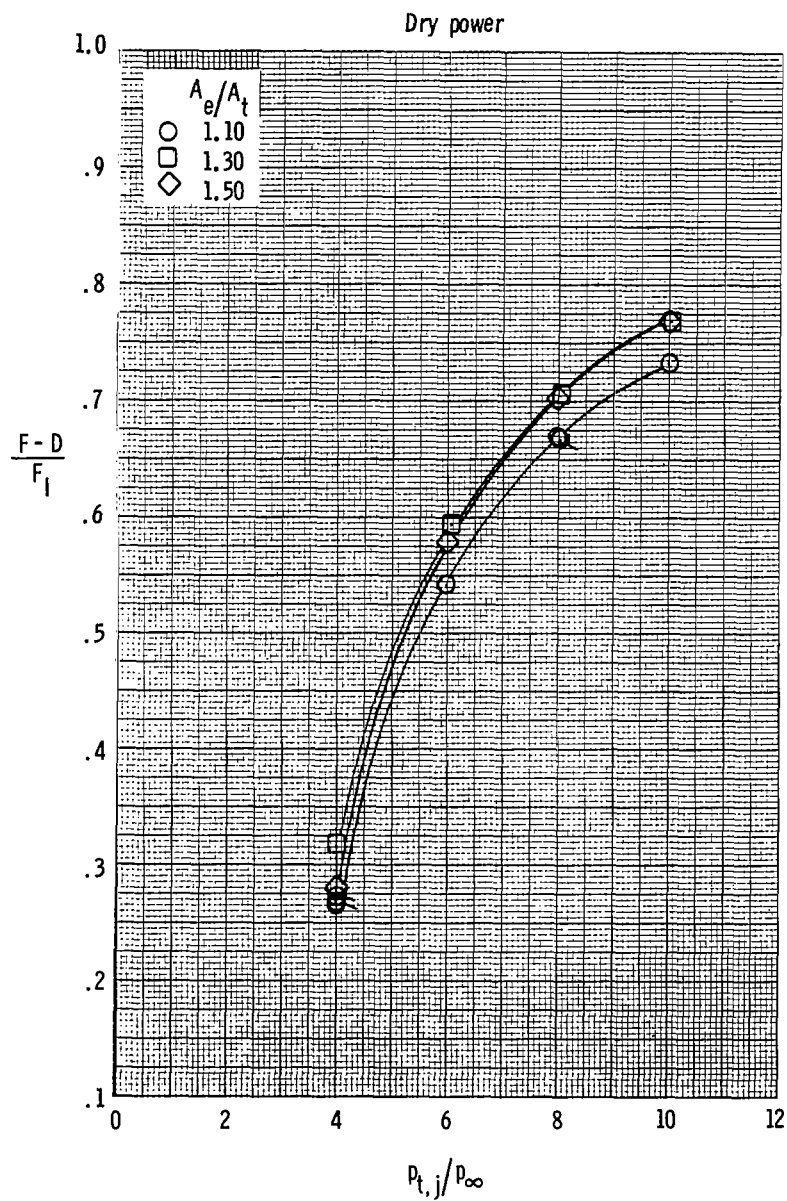
(b) $M = 0.80$.

Figure 18.- Continued.



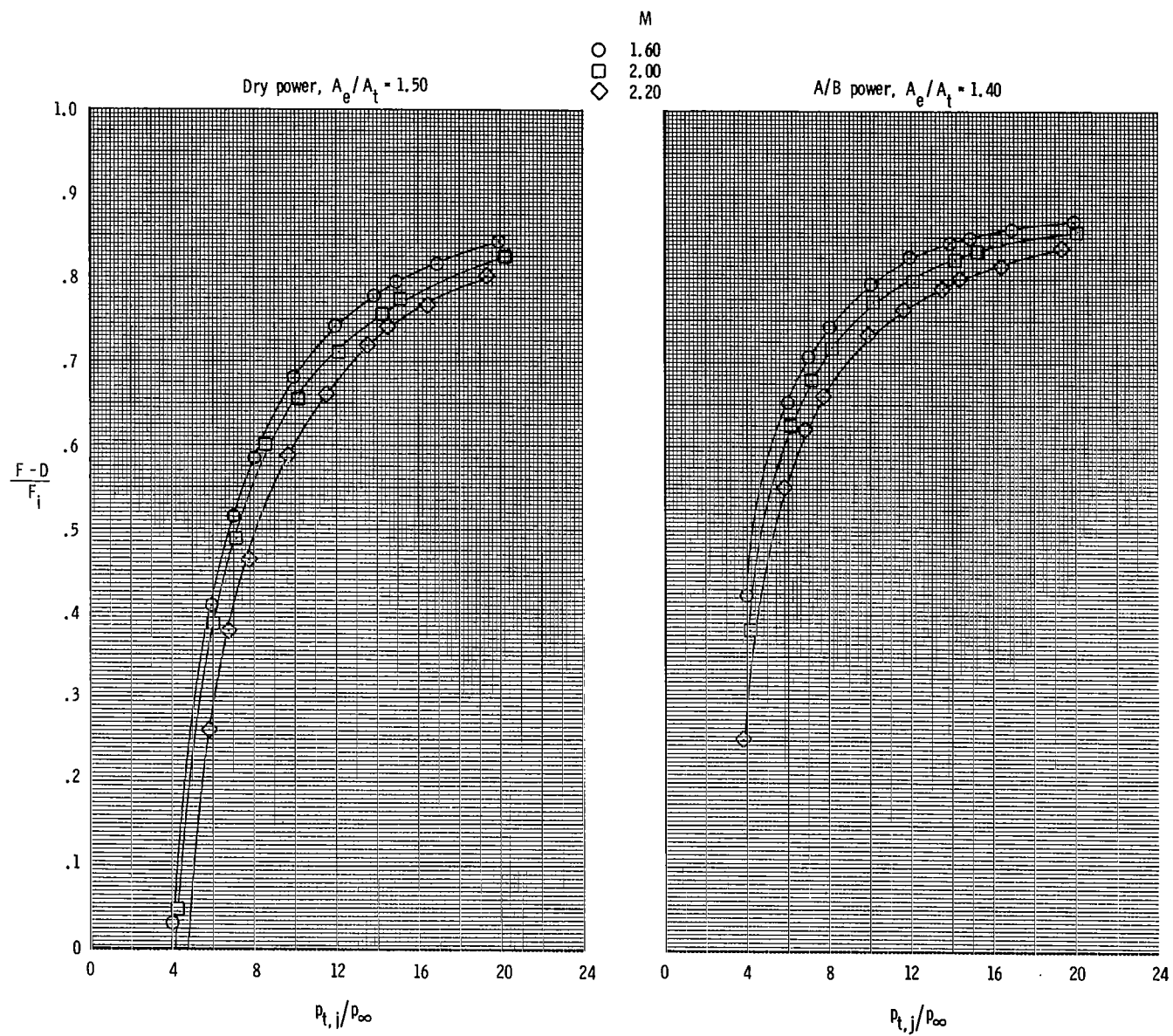
(c) $M = 0.90$.

Figure 18.- Continued.



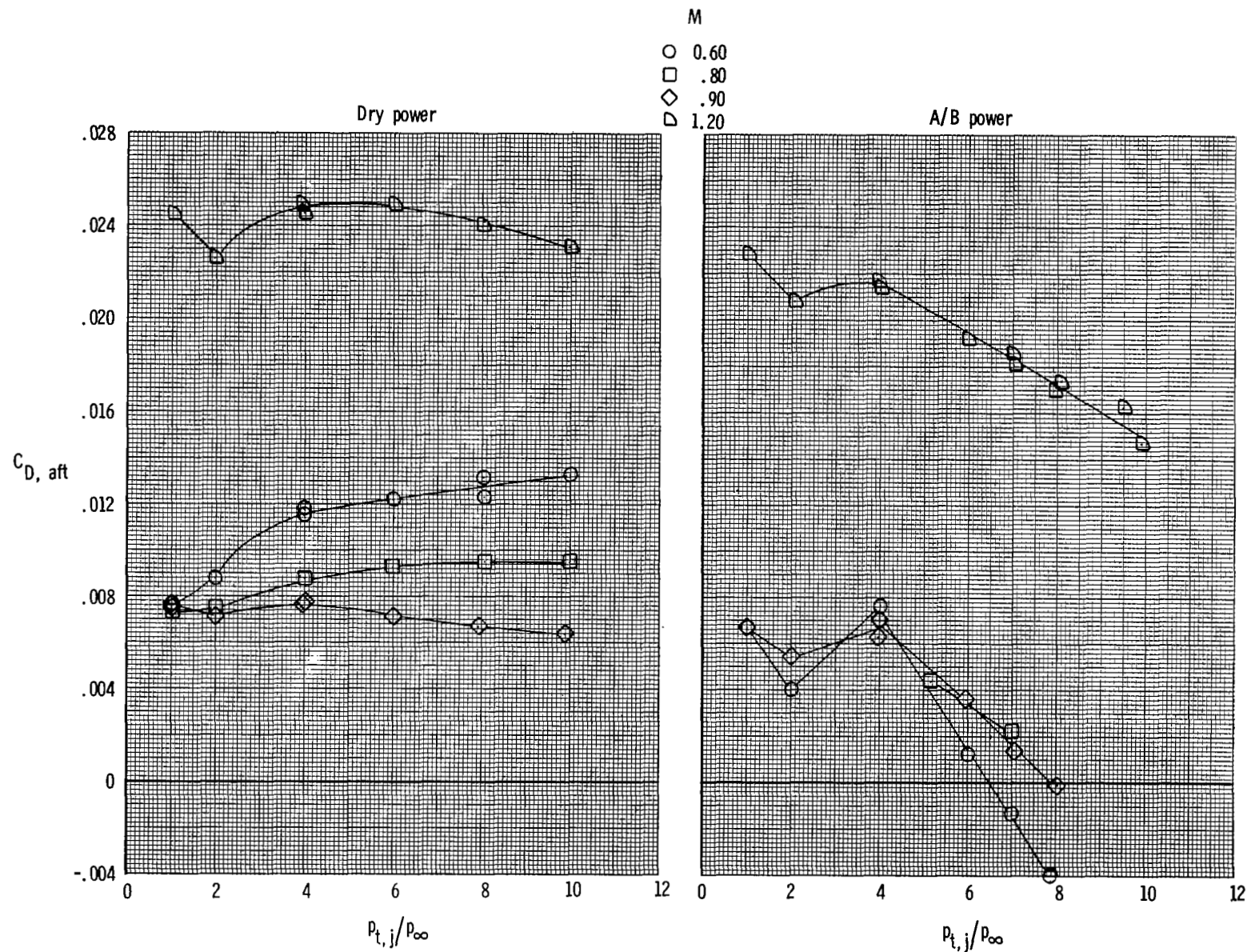
(d) $M = 1.20$.

Figure 18.- Continued.



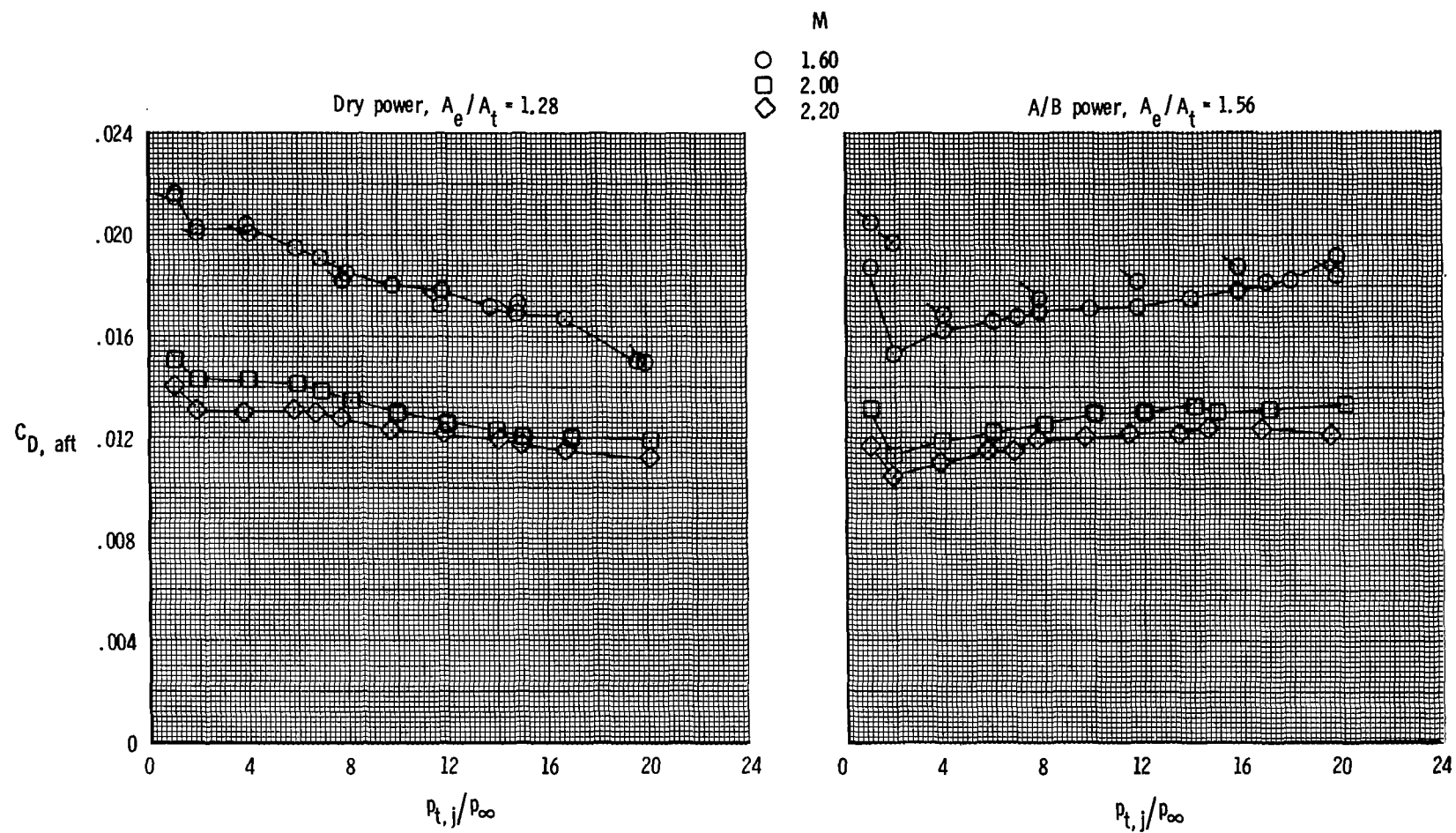
(e) $M = 1.60$ to 2.20 .

Figure 18.- Concluded.



(a) $M = 0.60$ to 1.20 .

Figure 19.- Effect of Mach number on afterbody drag coefficient for axisymmetric nozzle.



(b) $M = 1.60$ to 2.20 .

Figure 19.- Concluded.

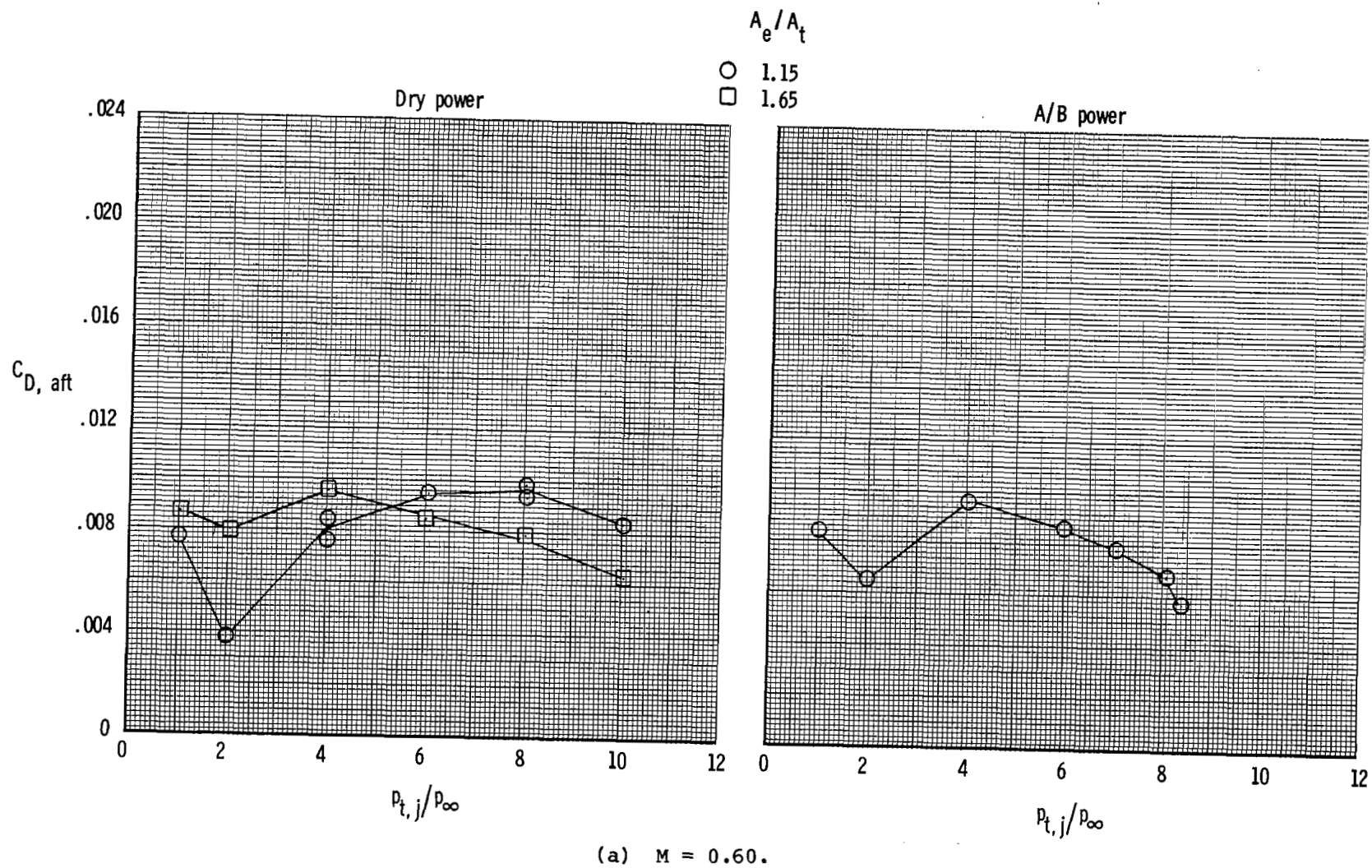
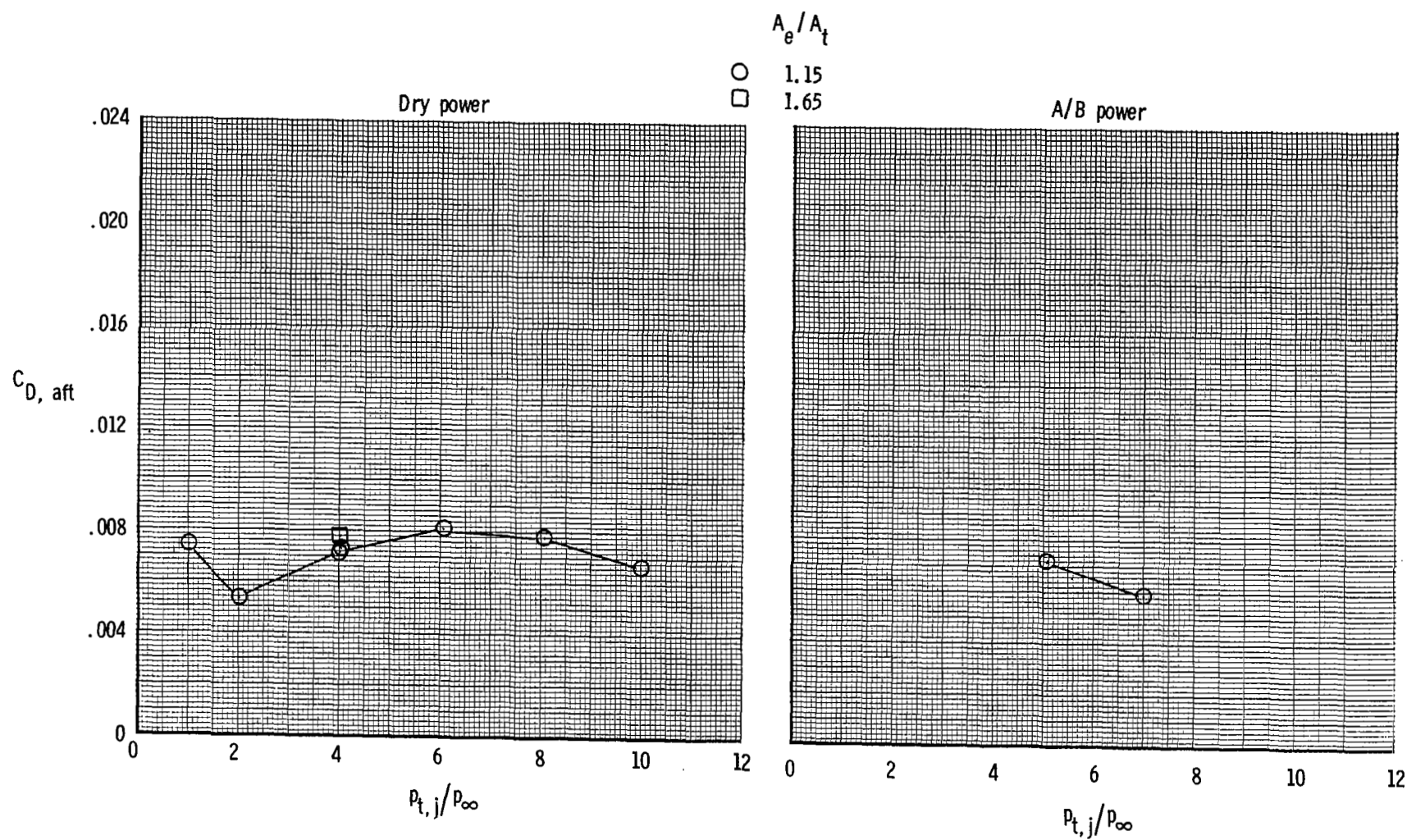
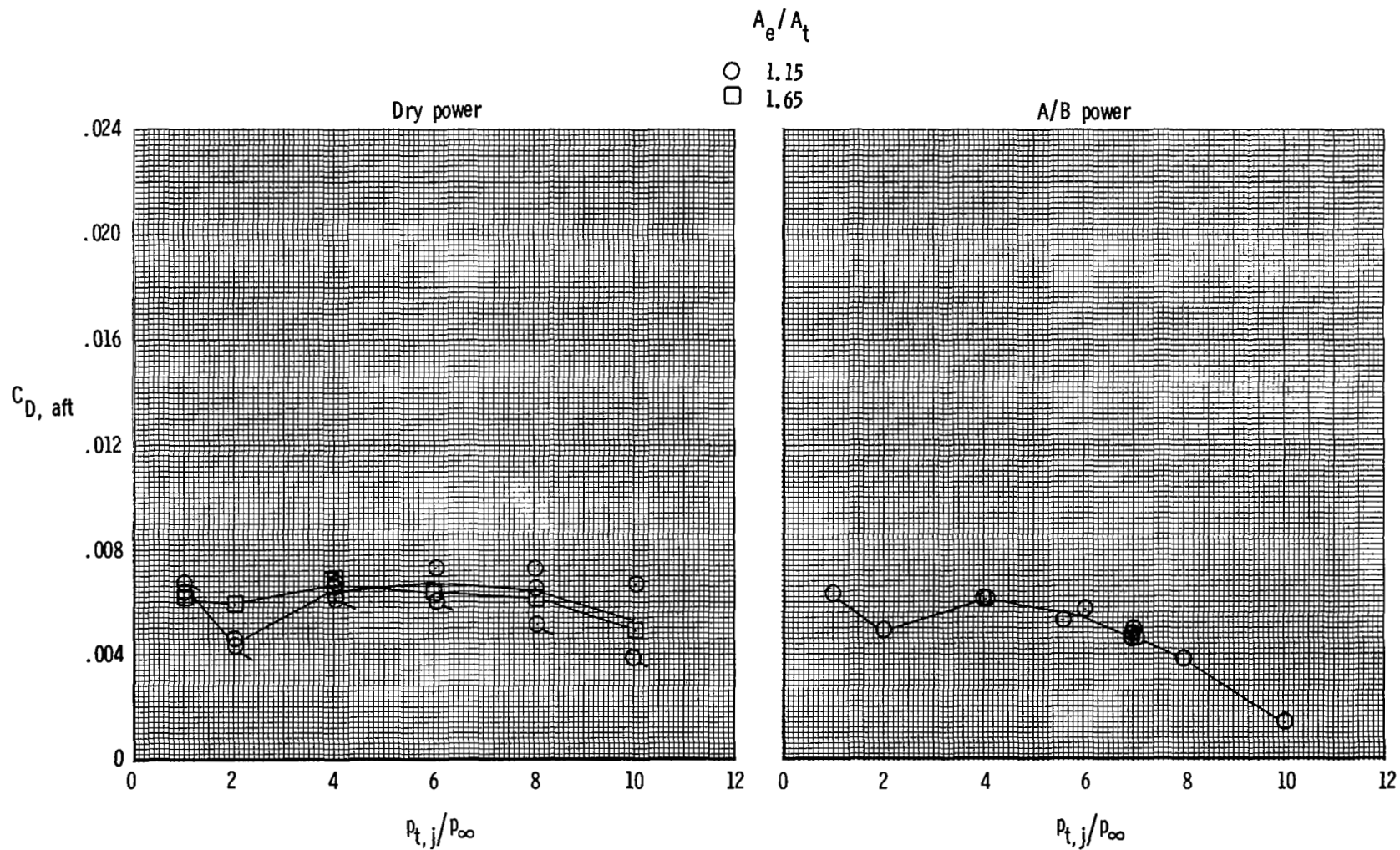


Figure 20.- Effect of Mach number and expansion ratio on afterbody drag coefficient for 2-D C-D nozzle.



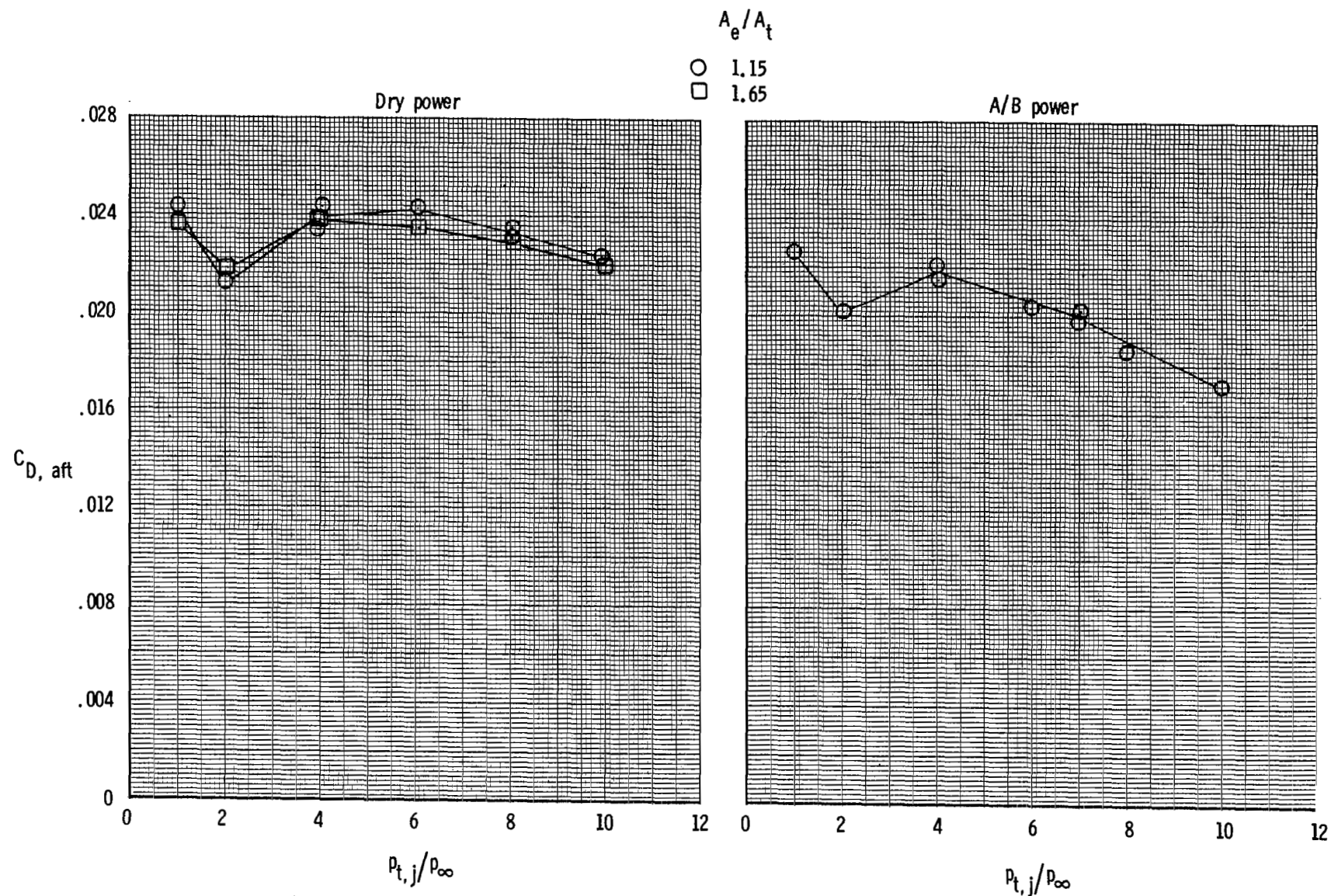
(b) $M = 0.80$.

Figure 20.- Continued.



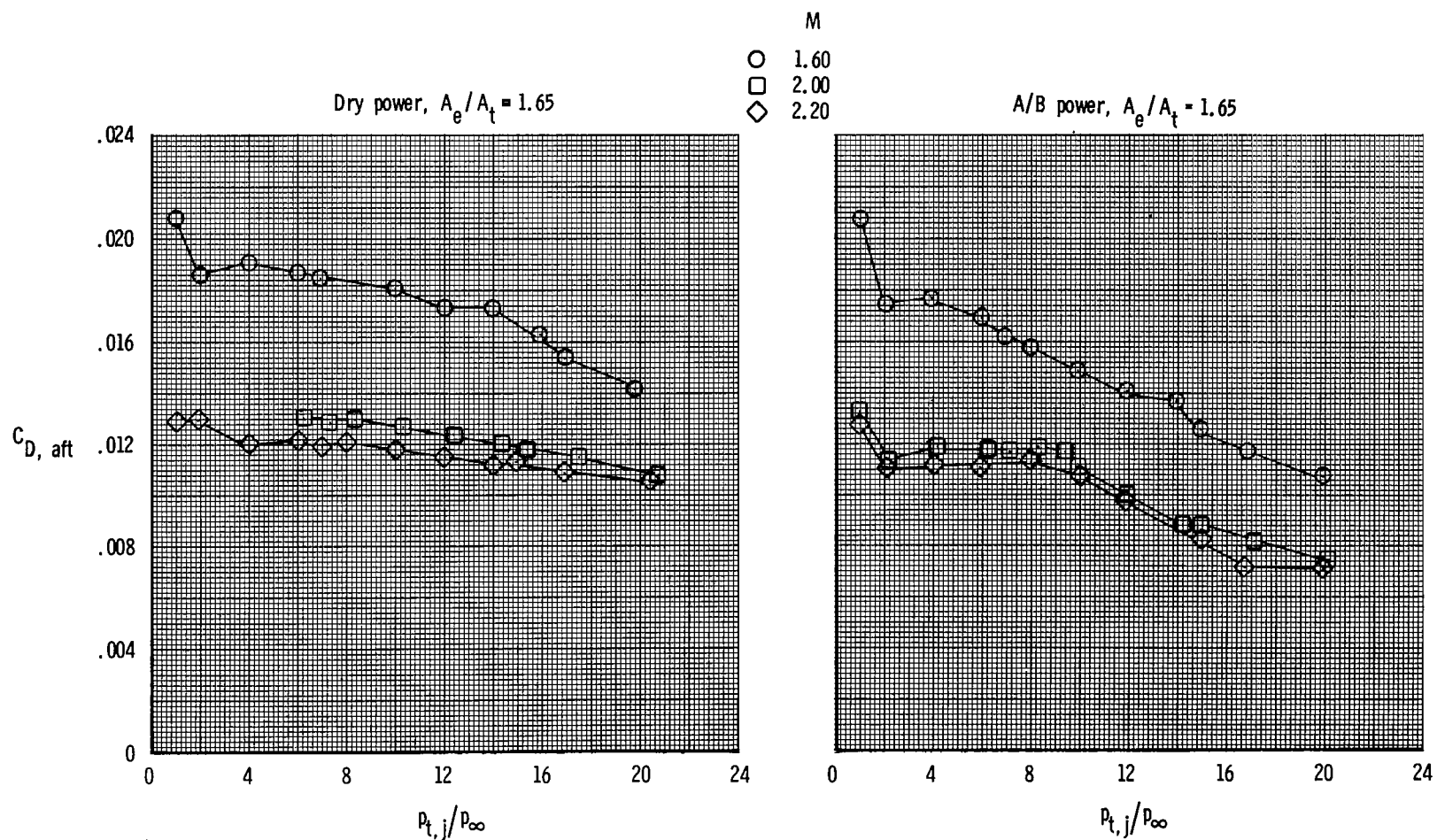
(c) $M = 0.90$.

Figure 20.- Continued.



(d) $M = 1.20$.

Figure 20.- Continued.



(e) $M = 1.60$ to 2.20 .

Figure 20.- Concluded.

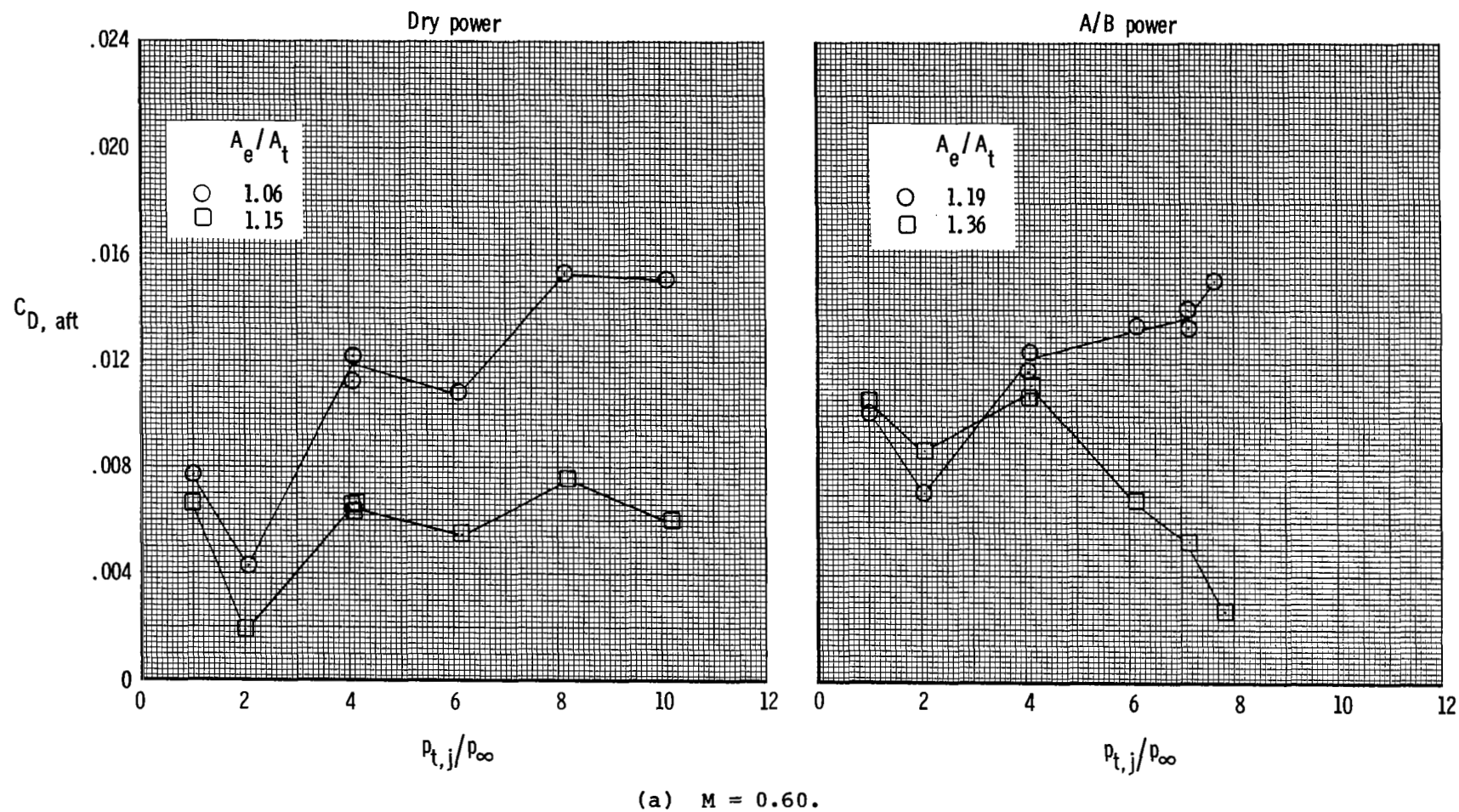
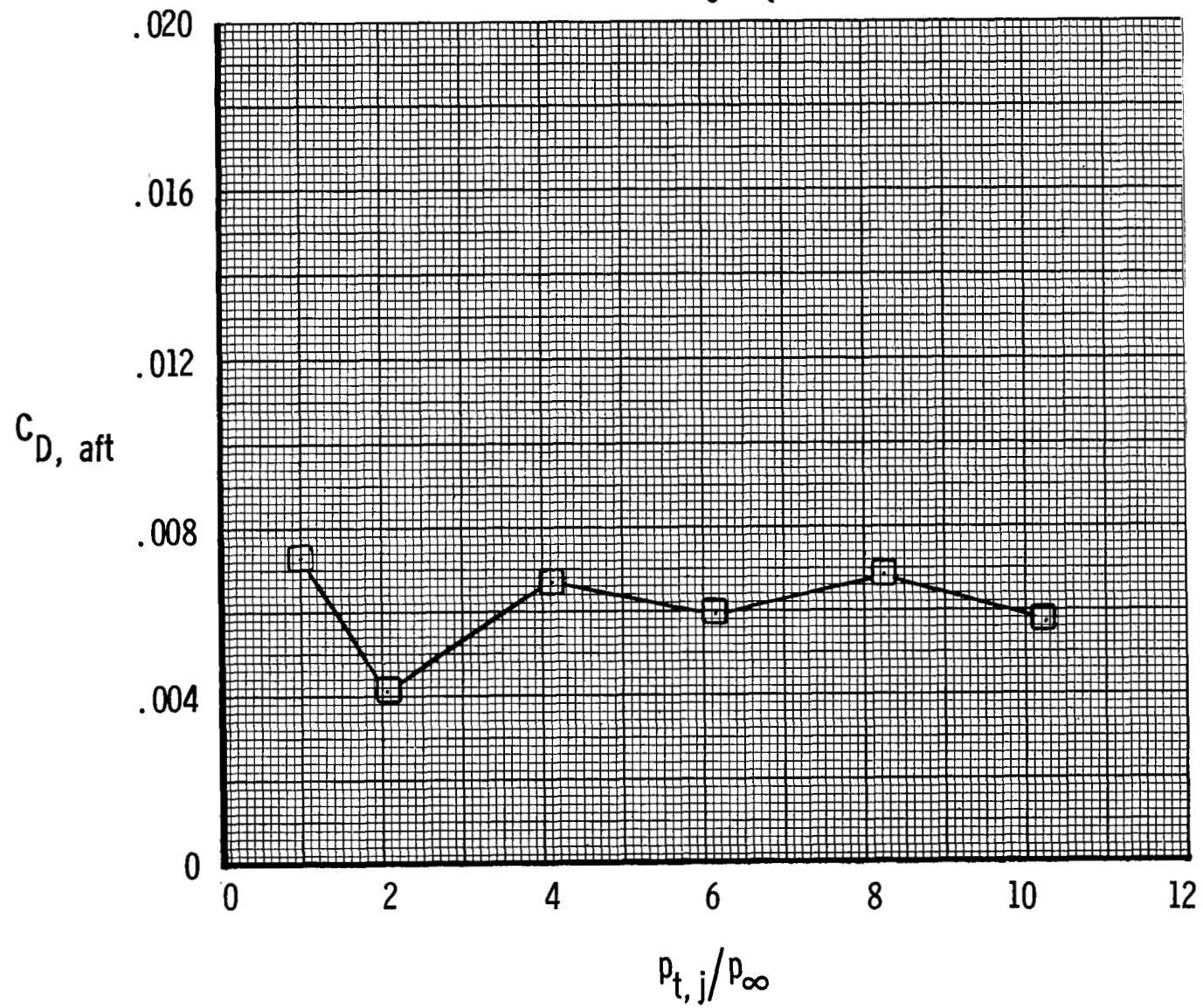


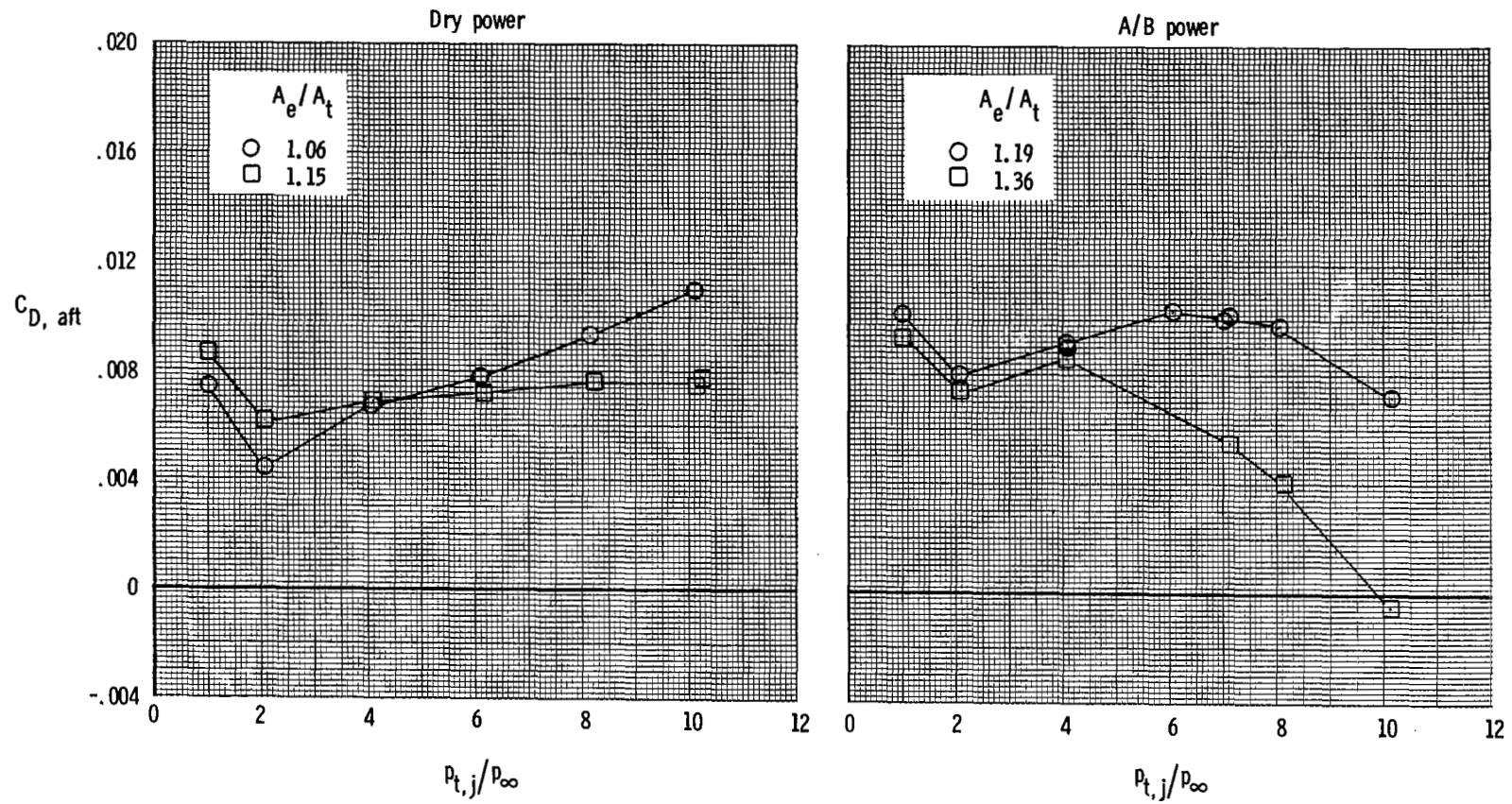
Figure 21.- Effect of Mach number and expansion ratio on afterbody drag coefficient for SERN.

Dry power, $A_e/A_t = 1.15$



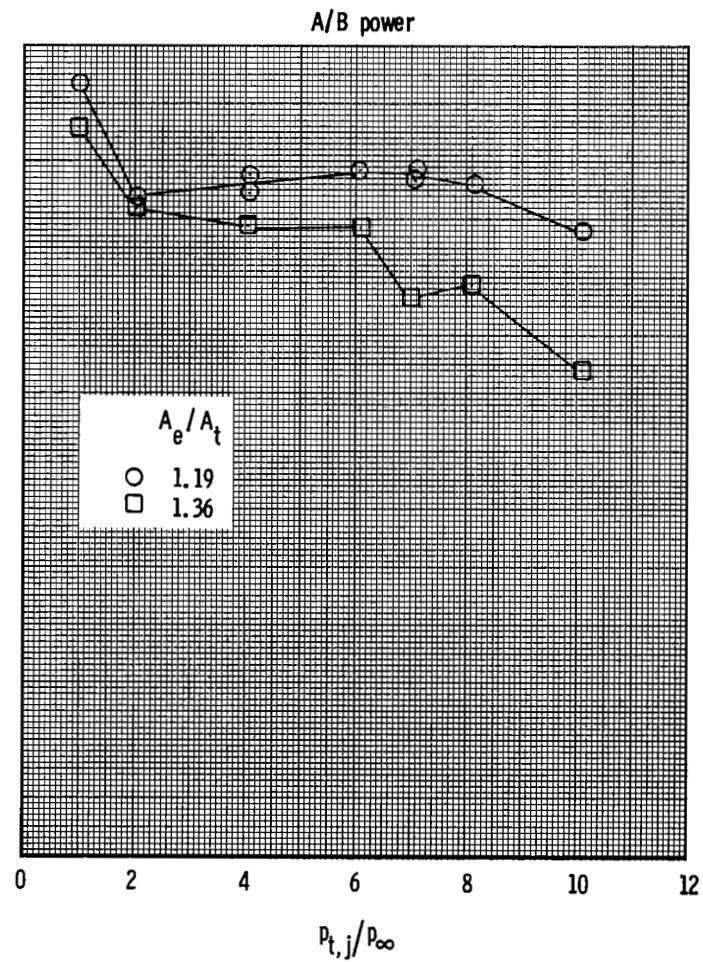
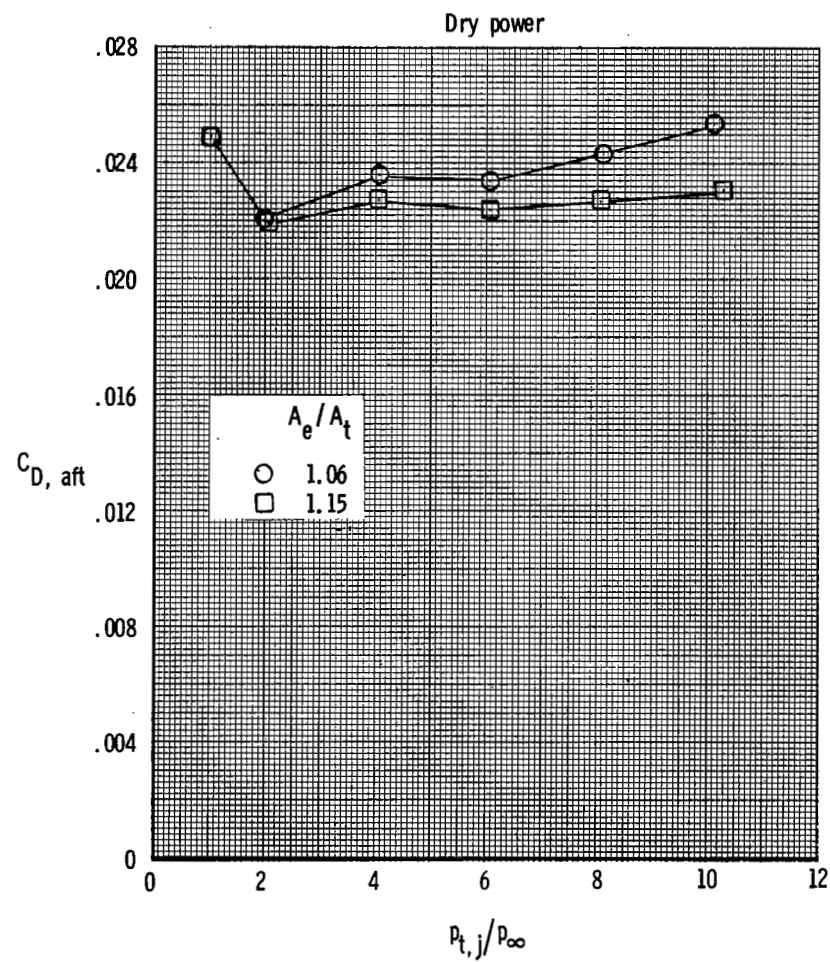
(b) $M = 0.80$.

Figure 21.- Continued.



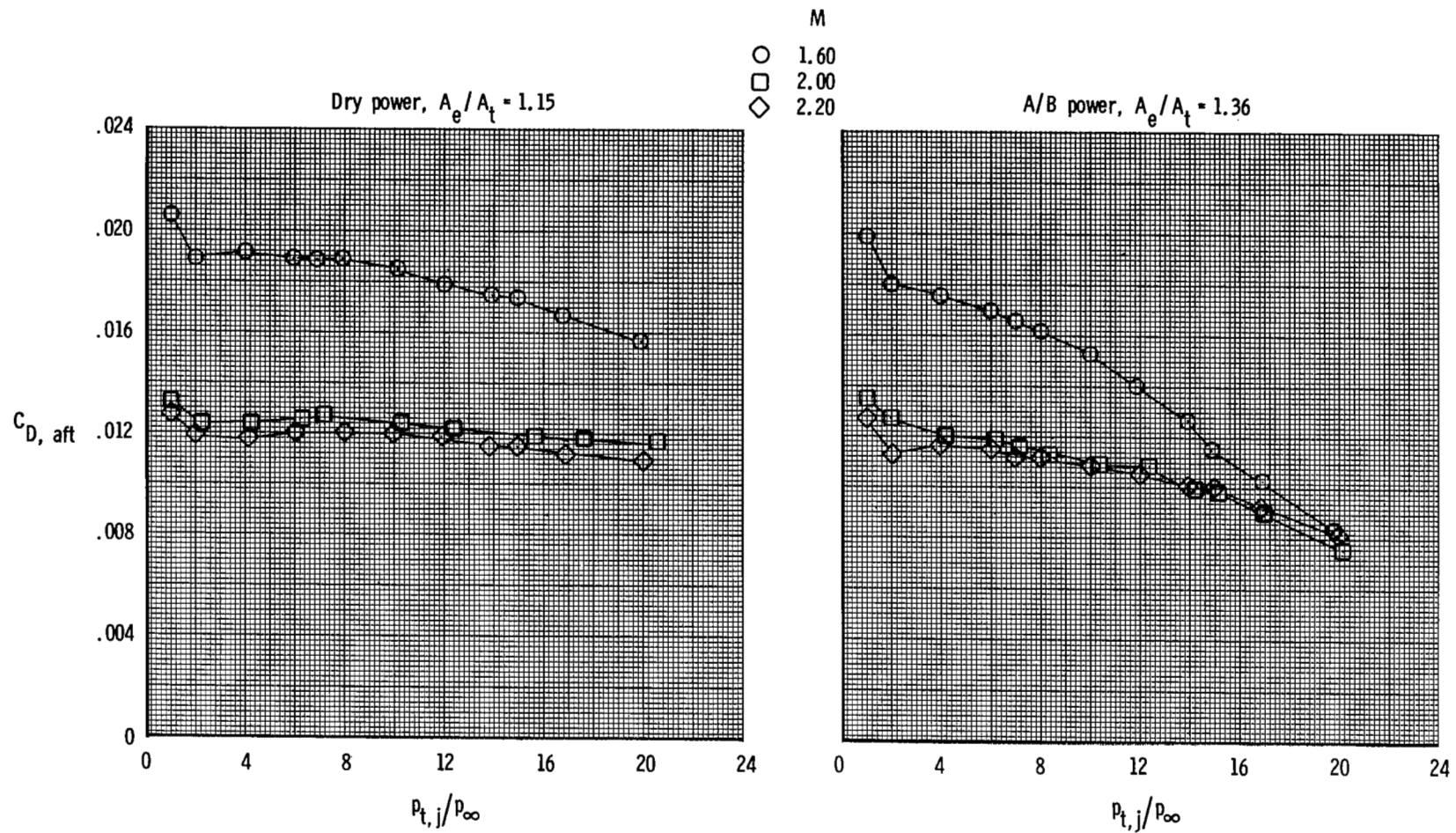
(c) $M = 0.90$.

Figure 21.- Continued.



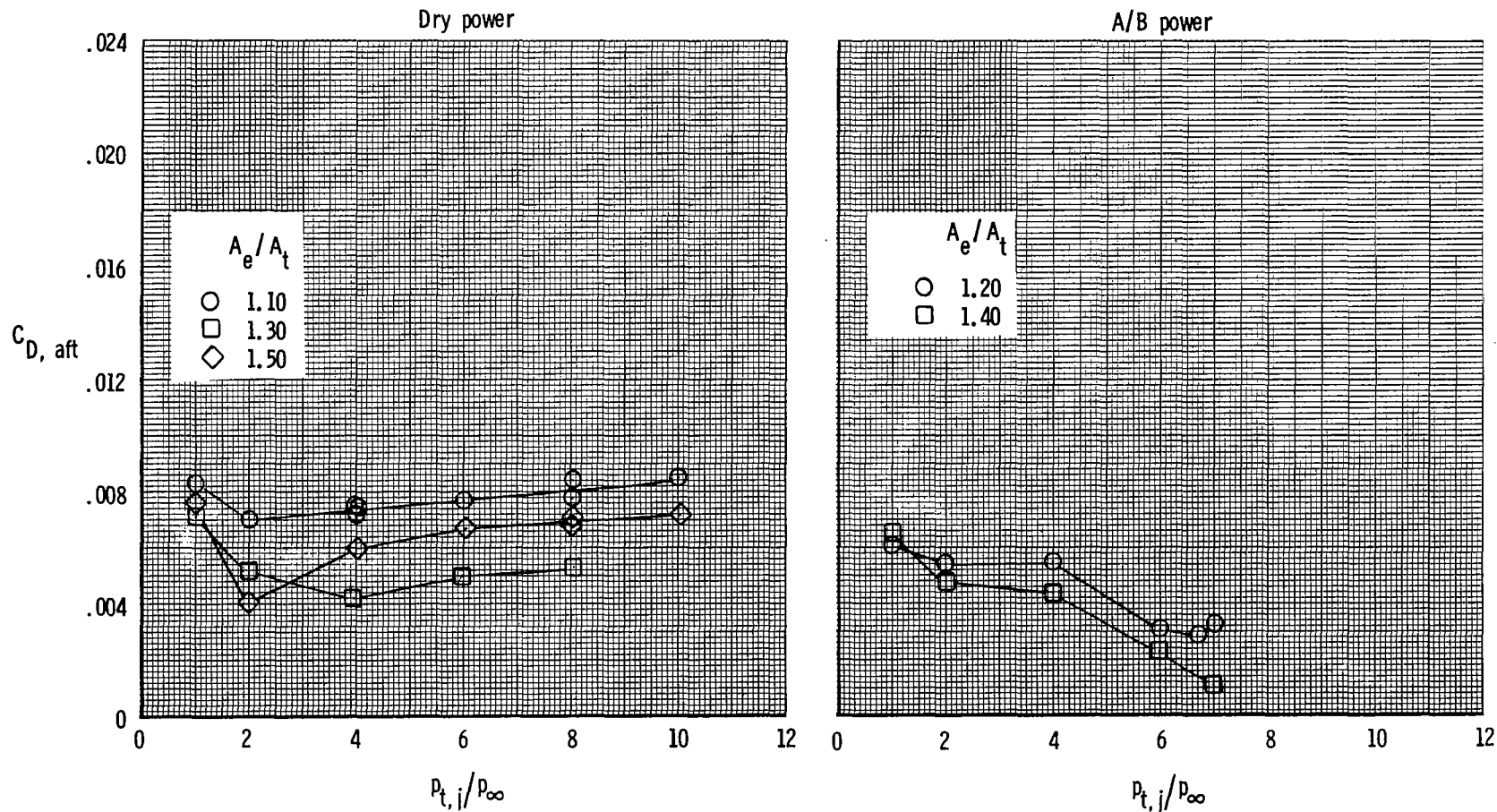
(d) $M = 1.20$.

Figure 21.- Continued.



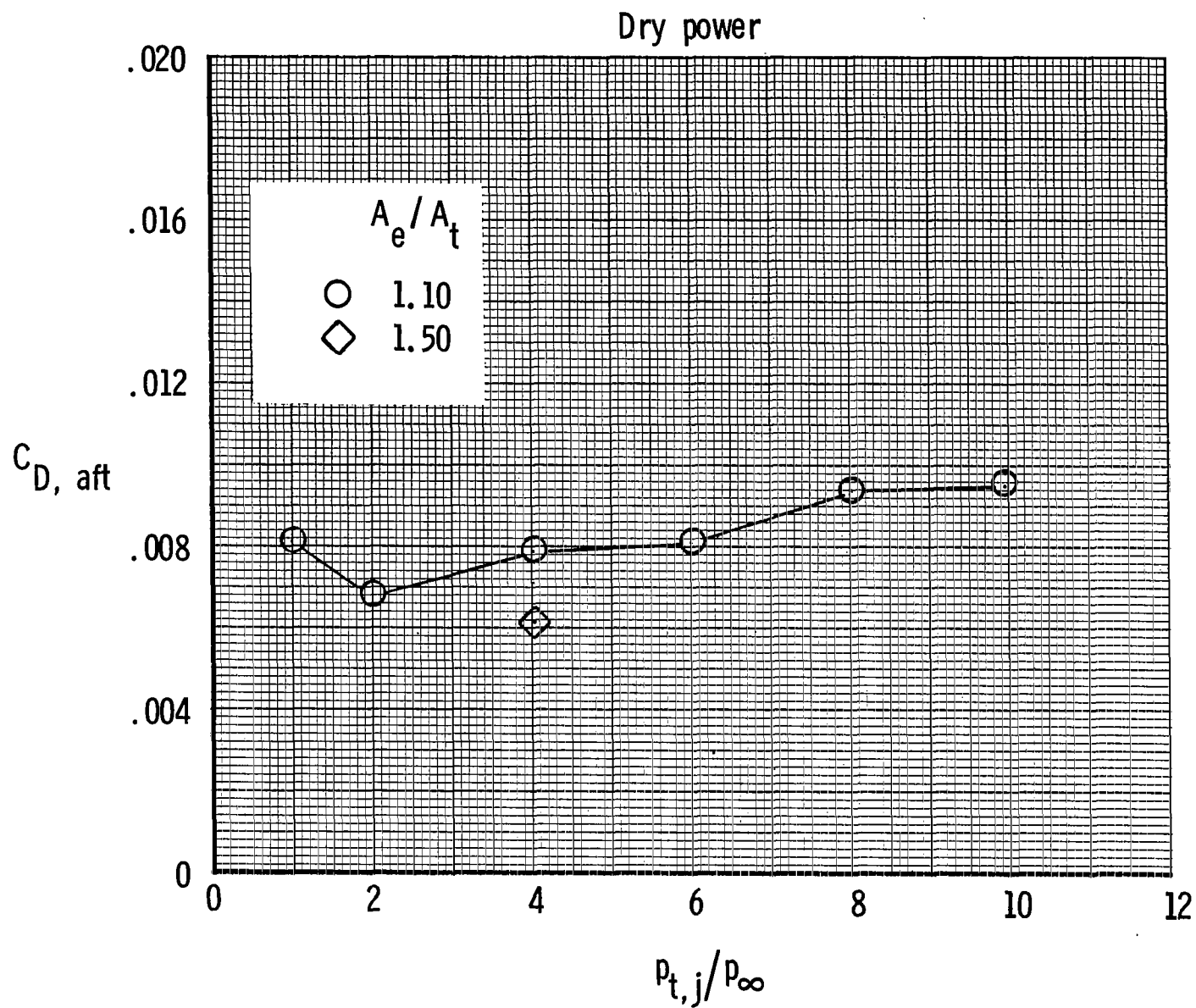
(e) $M = 1.60$ to 2.20 .

Figure 21.- Concluded.



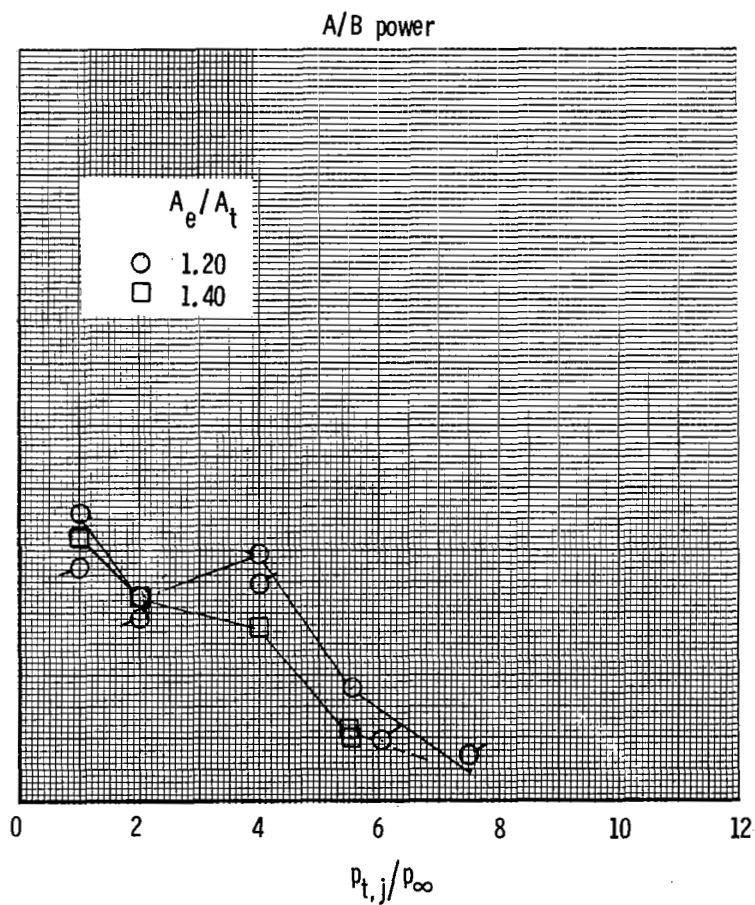
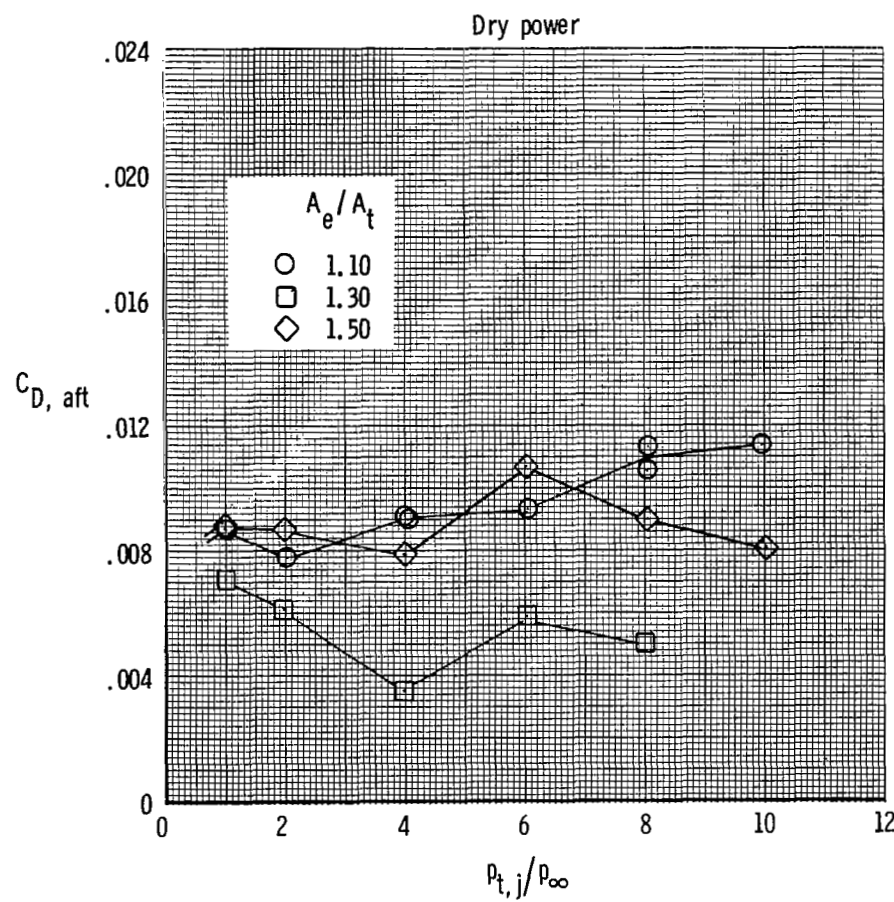
(a) $M = 0.60$.

Figure 22.- Effect of Mach number and expansion ratio on afterbody drag coefficient for wedge nozzle.



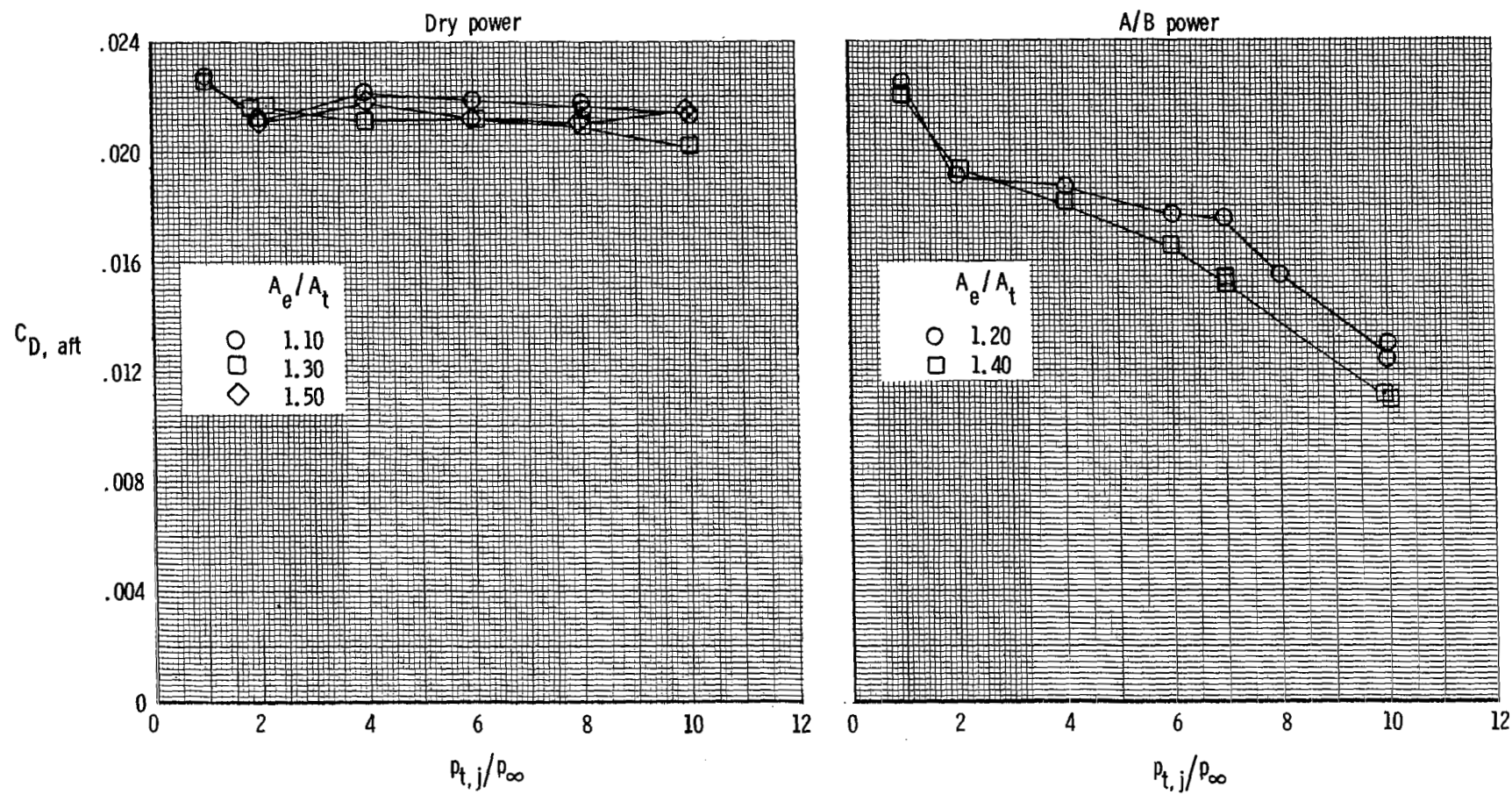
(b) $M = 0.80$.

Figure 22.- Continued.



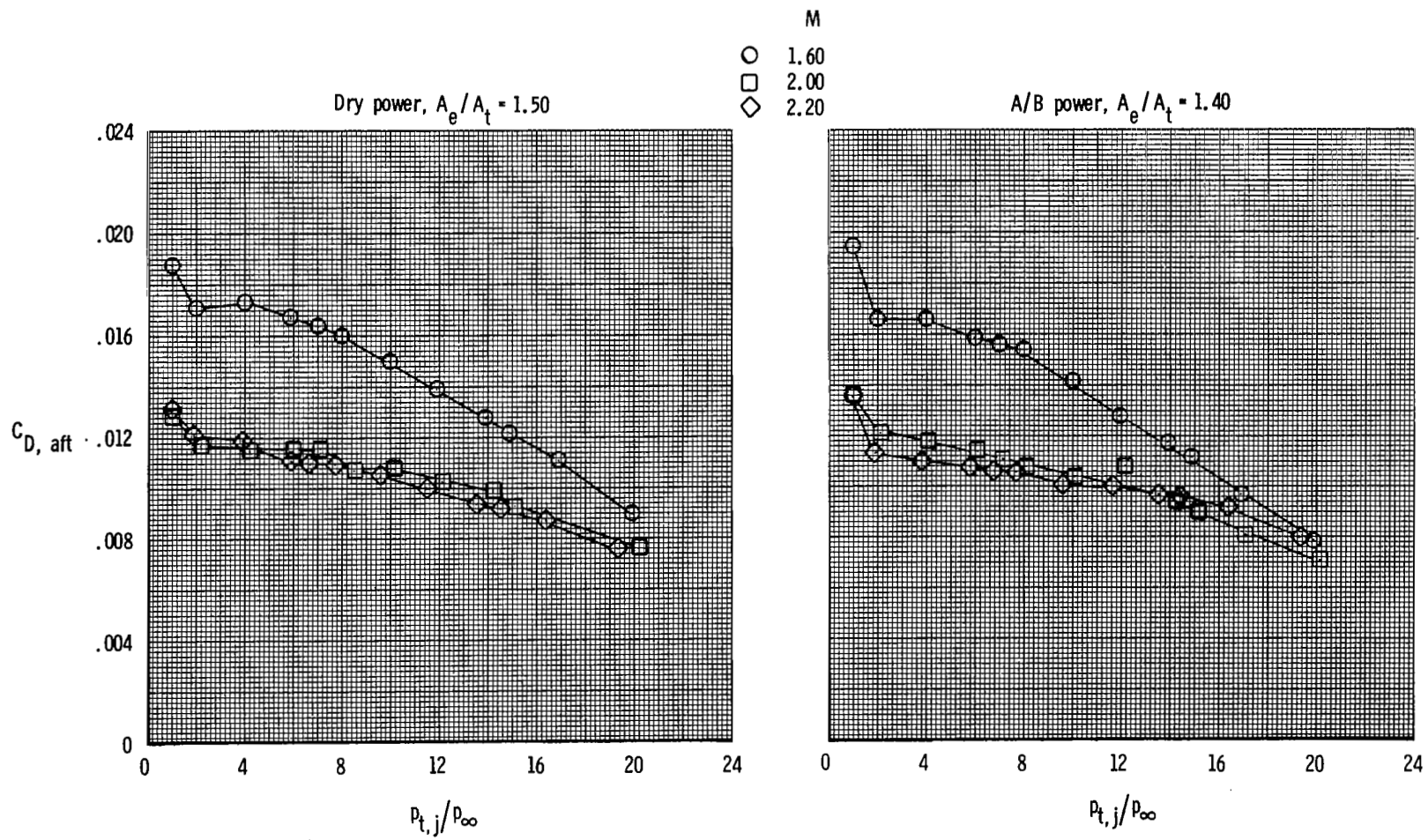
(c) $M = 0.90$.

Figure 22.- Continued.



(d) $M = 1.20$.

Figure 22.- Continued.



(e) $M = 1.60$ to 2.20 .

Figure 22.- Concluded.

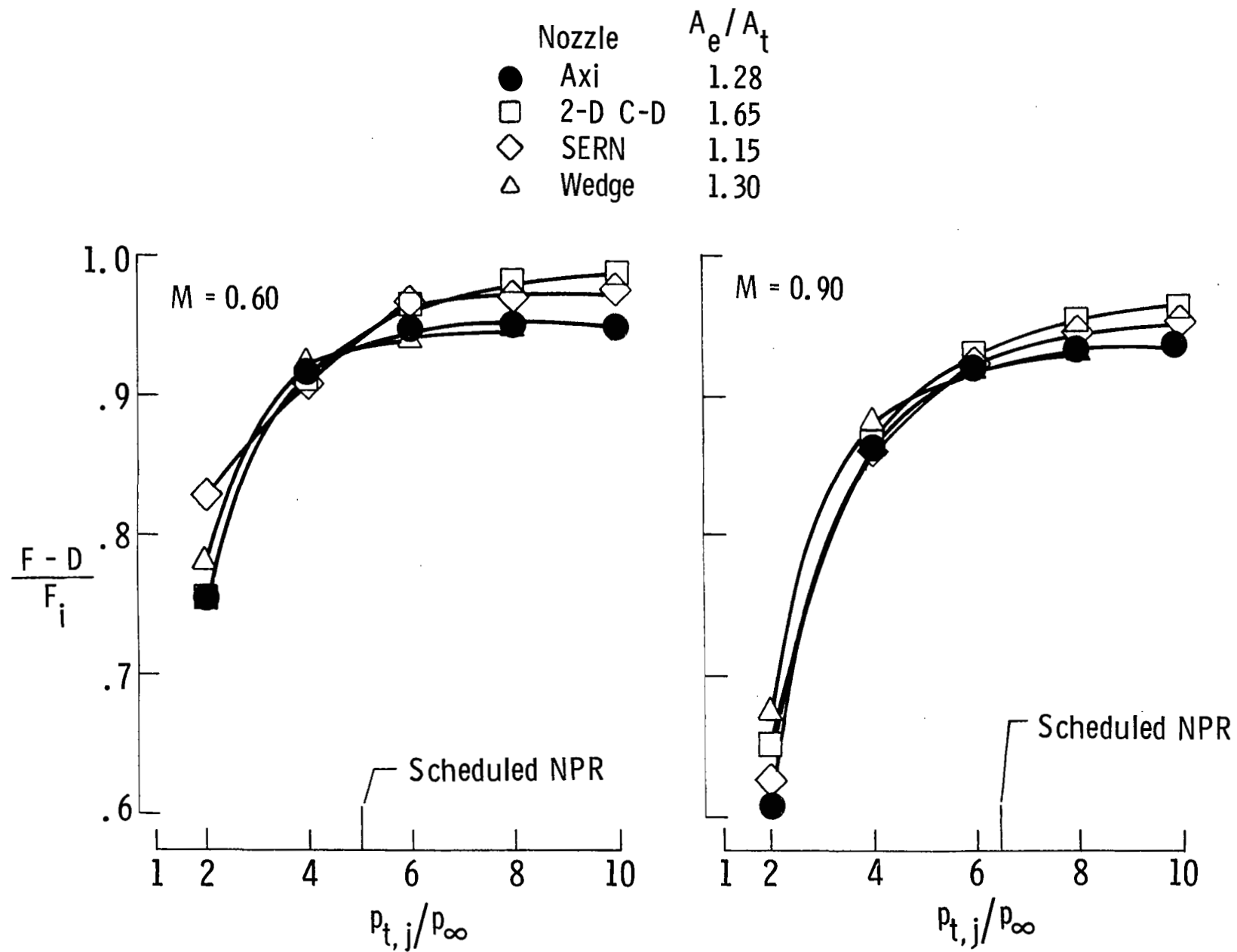


Figure 23.- Subsonic afterbody aeropropulsive performance comparisons for dry power.

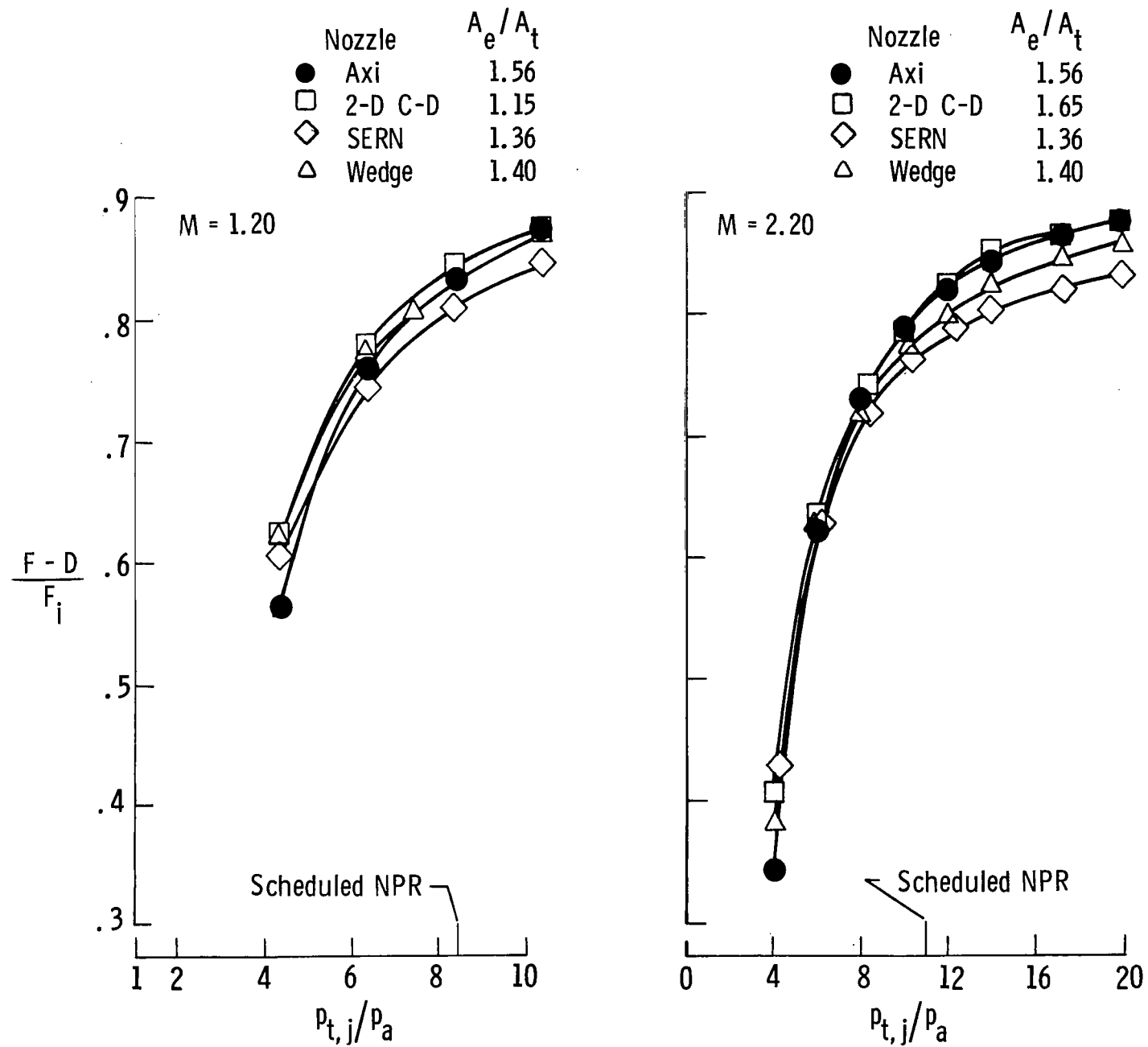


Figure 24.- Supersonic afterbody aeropropulsive performance comparisons for A/B power.

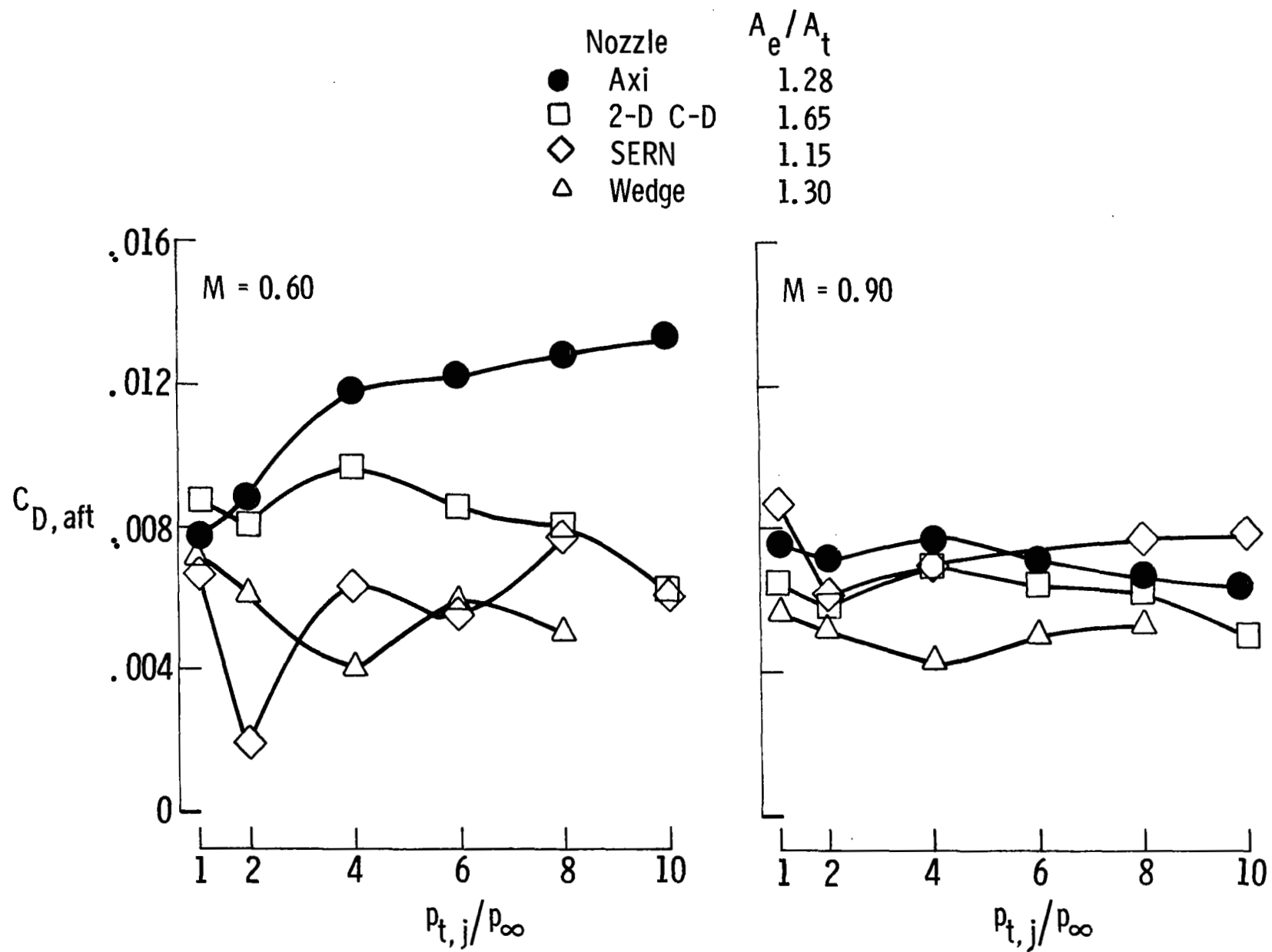


Figure 25.- Subsonic afterbody drag comparisons for dry power.

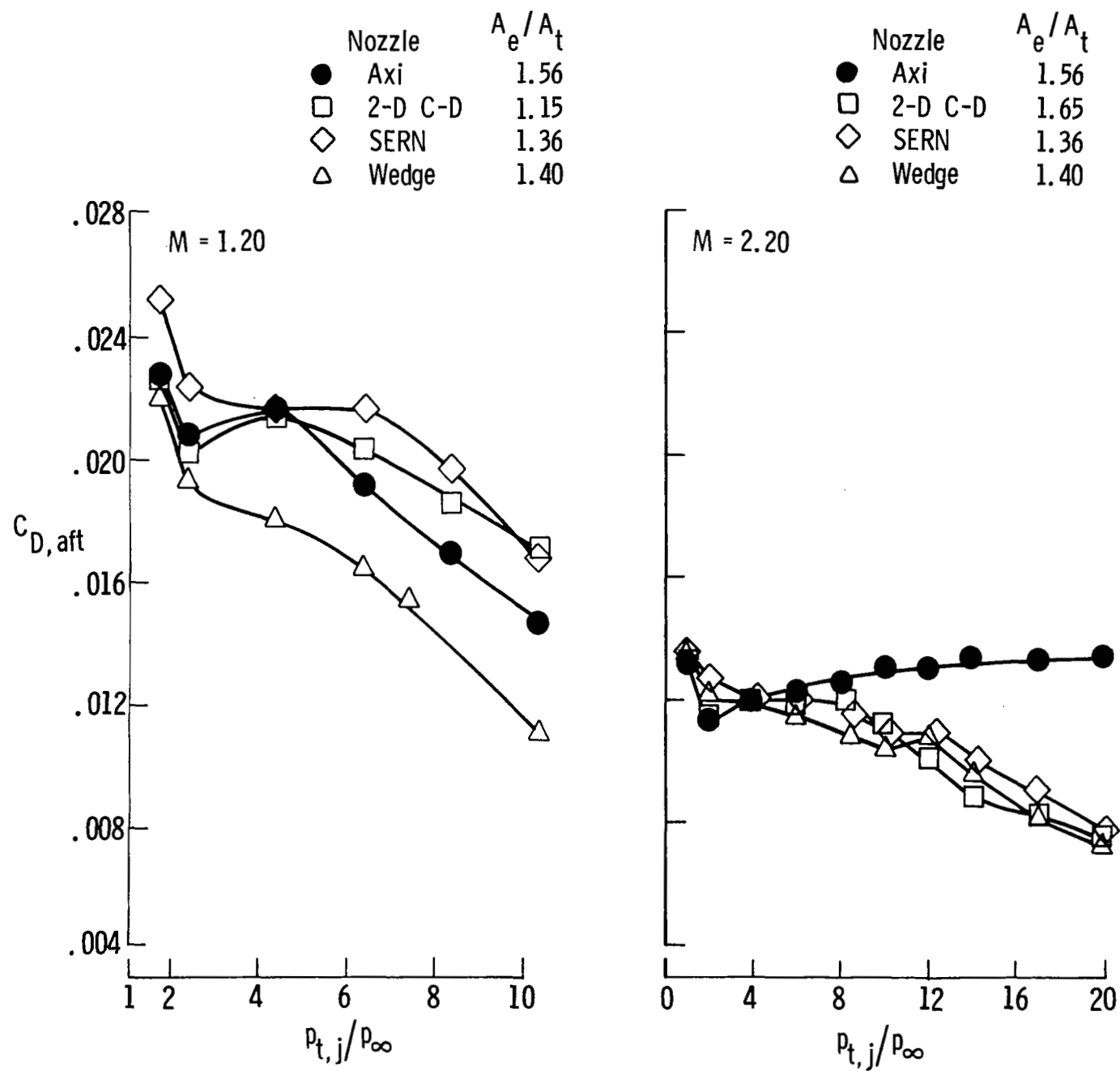


Figure 26.- Supersonic afterbody drag comparisons for A/B power.

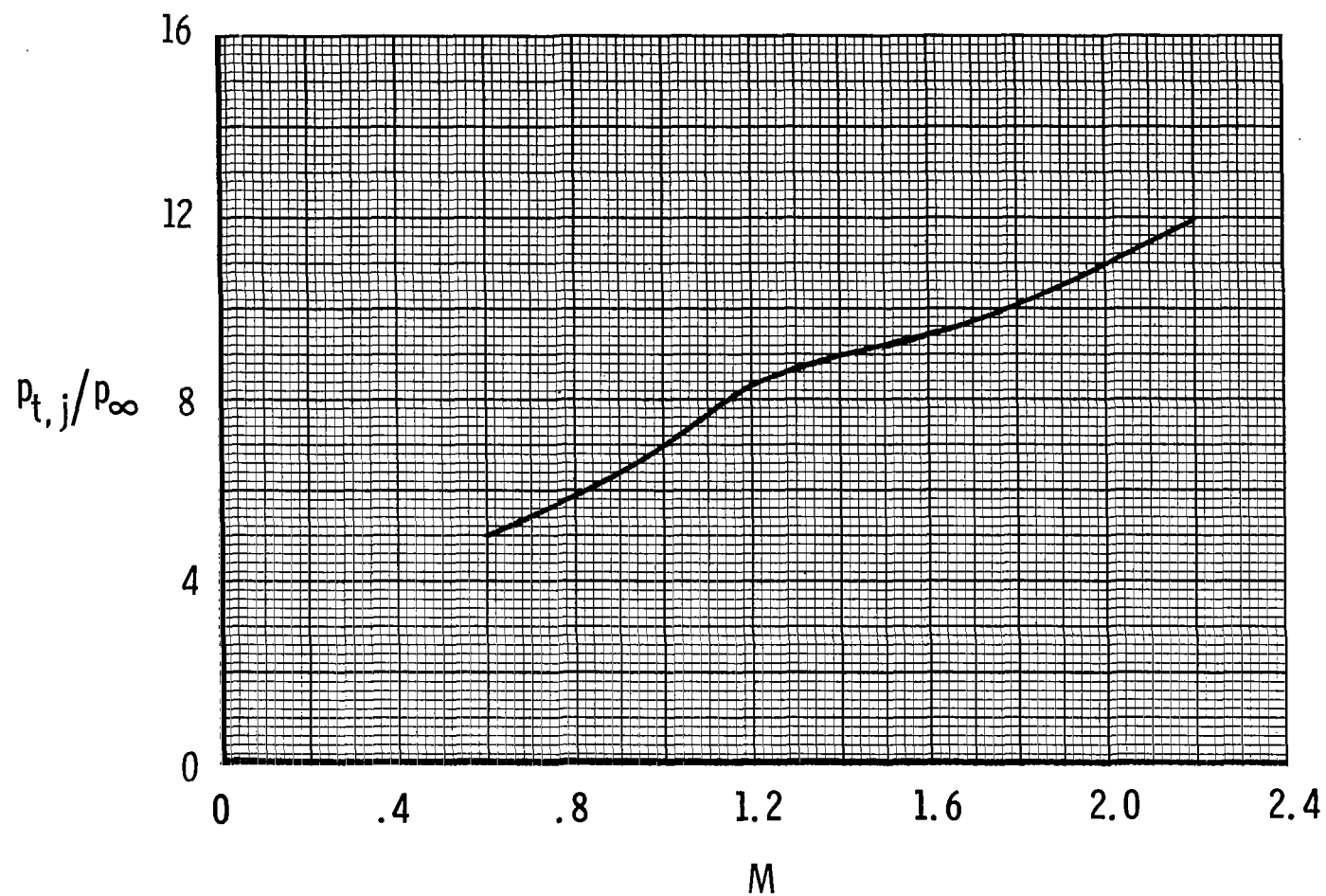


Figure 27.- Typical schedule of nozzle pressure ratio with Mach number for F-18 airplane.

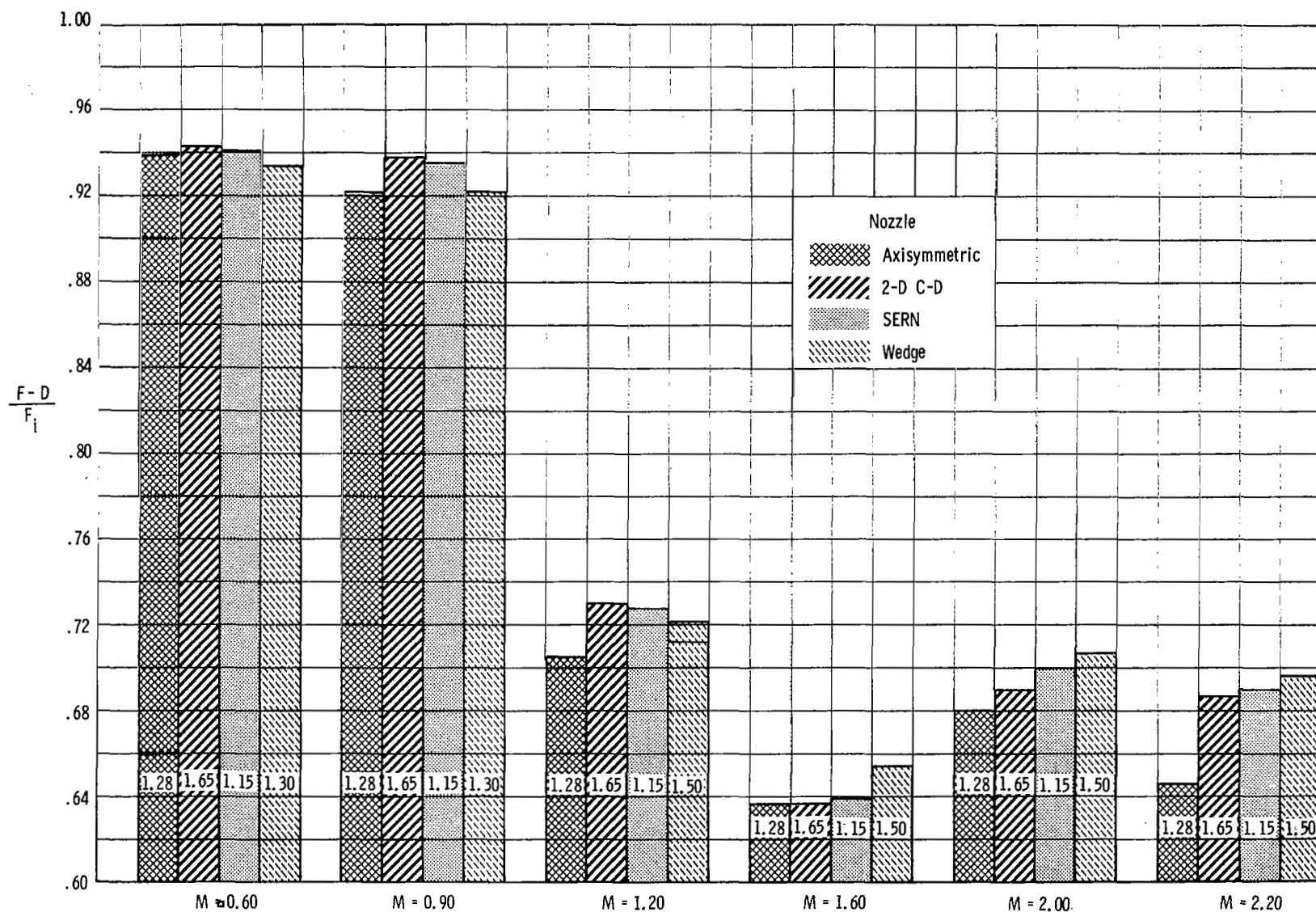


Figure 28.- Comparison of afterbody aeropropulsive characteristics at scheduled NPR for various configurations at dry power. Number on bars indicates nozzle expansion ratio.

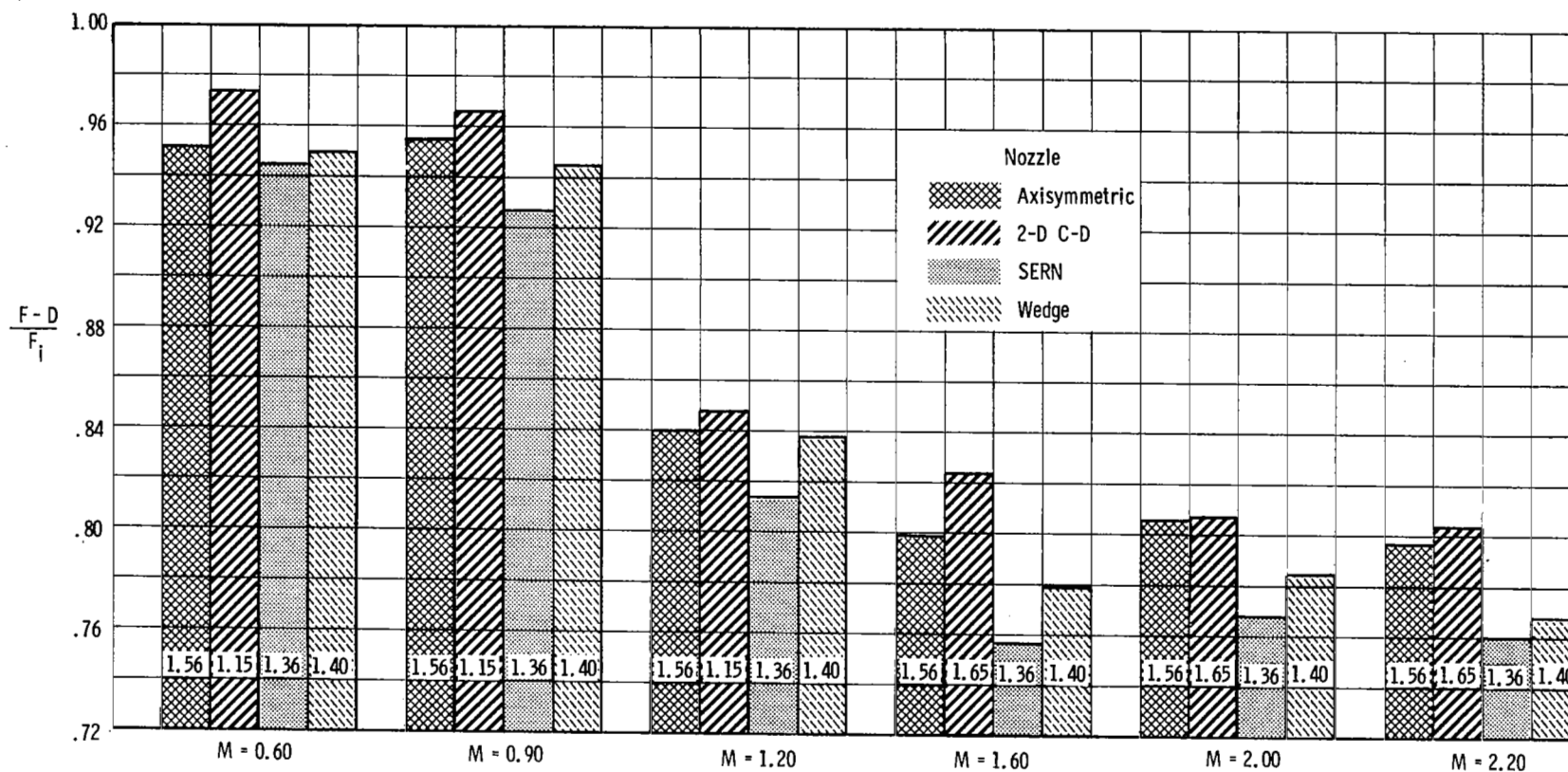


Figure 29.- Comparison of afterbody aeropropulsive characteristics at scheduled NPR for various configurations at A/B power. Number on bars indicate nozzle expansion ratio.

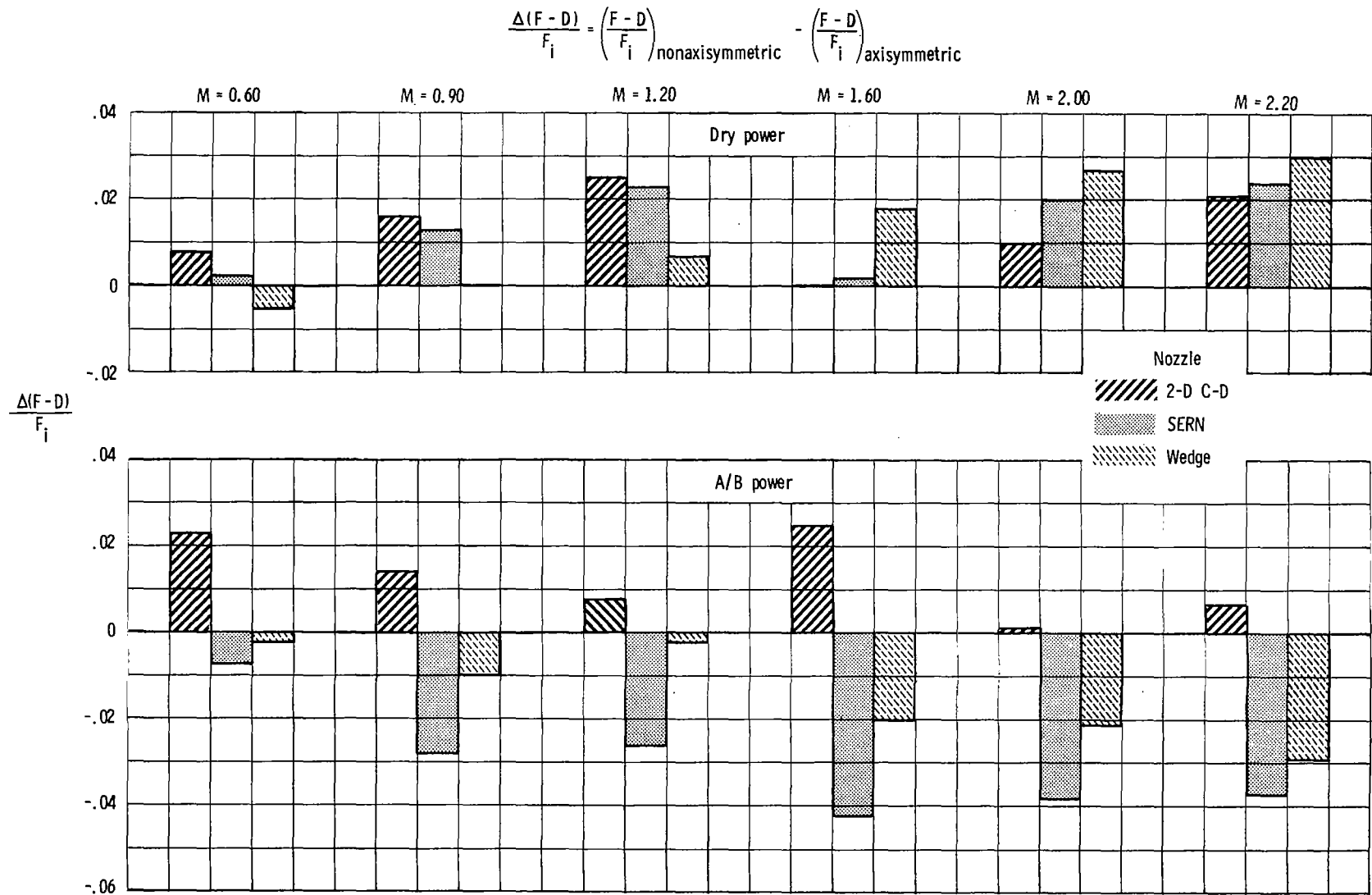


Figure 30.- Incremental afterbody aeropropulsive characteristics at scheduled NPR for the various configurations. Nozzle expansion ratios are those indicated in figures 28 and 29.

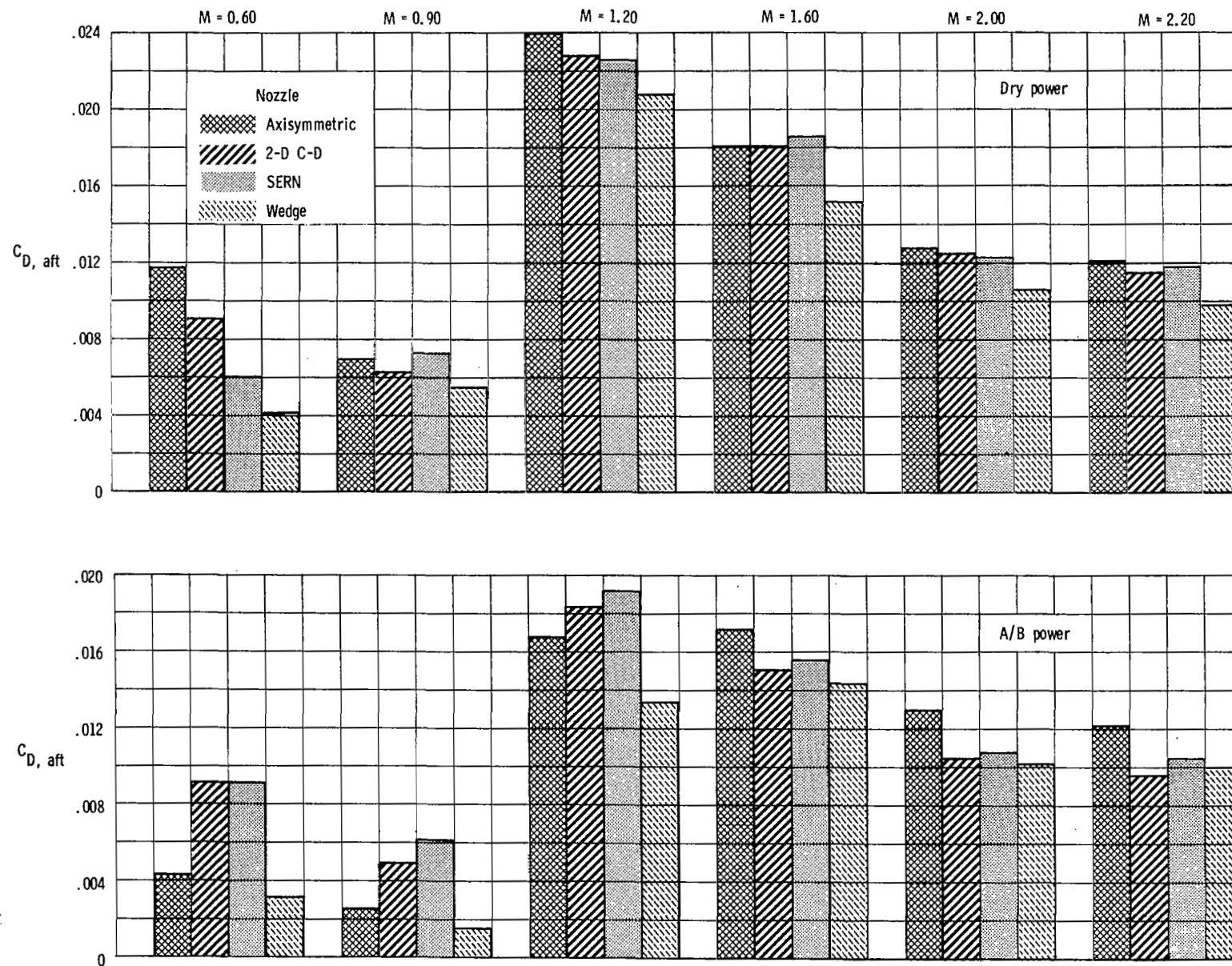


Figure 31.- Comparison of afterbody drag characteristics at scheduled NPR for various configurations. Nozzle expansion ratios are those indicated in figures 28 and 29.

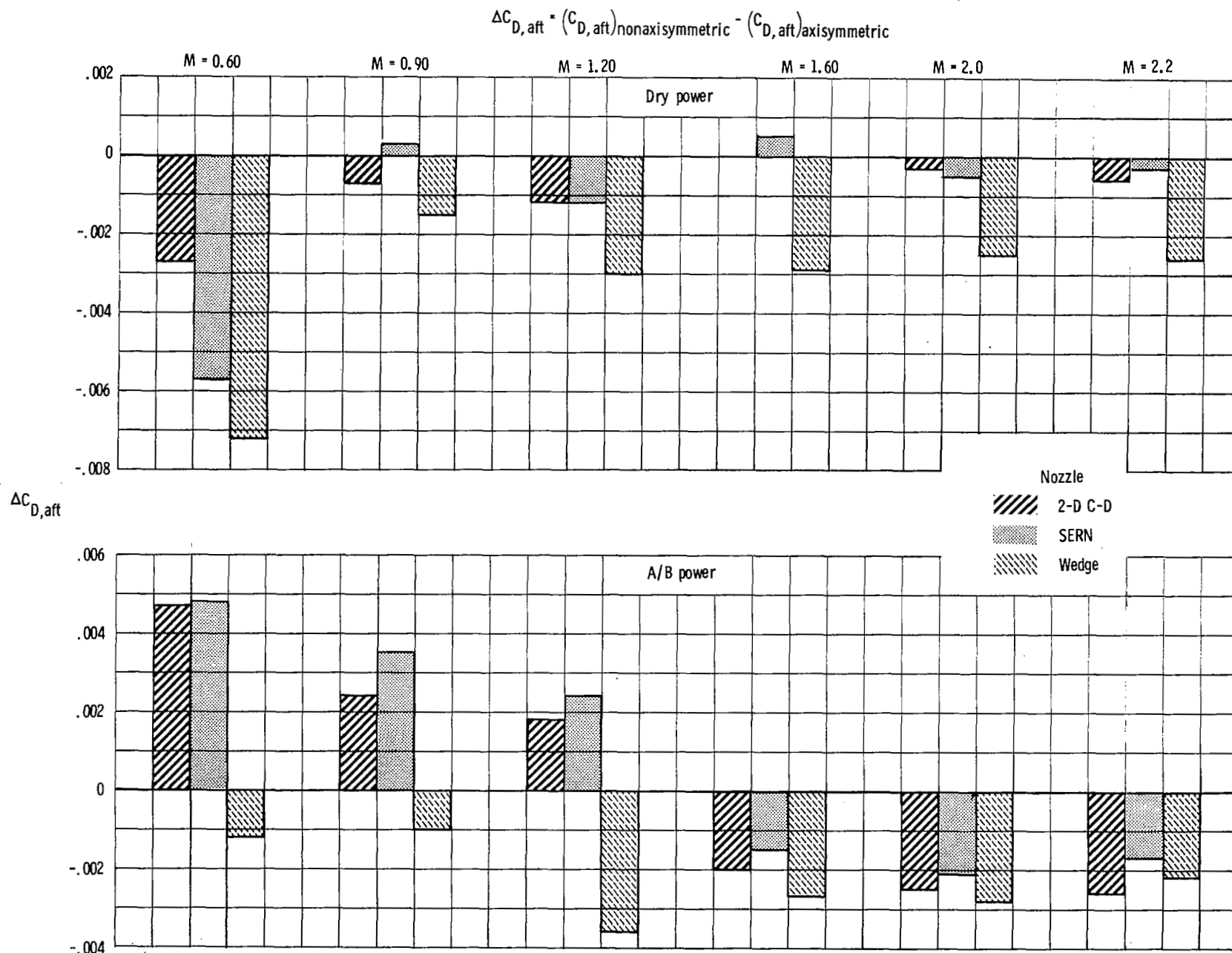


Figure 32.- Incremental afterbody drag characteristics at scheduled NPR for various configurations. Nozzle expansion ratios are those indicated in figures 28 and 29.

1. Report No. NASA TP-2044	2. Government Accession No.	3. Recipient's Catalog No.	
4. Title and Subtitle AEROPROPULSIVE CHARACTERISTICS AT MACH NUMBERS UP TO 2.2 OF AXISYMMETRIC AND NONAXISYMMETRIC NOZZLES INSTALLED ON AN F-18 MODEL		5. Report Date August 1982	
		6. Performing Organization Code 505-43-23-01	
7. Author(s) Francis J. Capone		8. Performing Organization Report No. L-15208	
		10. Work Unit No.	
9. Performing Organization Name and Address NASA Langley Research Center Hampton, VA 23665		11. Contract or Grant No.	
		13. Type of Report and Period Covered Technical Paper	
12. Sponsoring Agency Name and Address National Aeronautics and Space Administration Washington, DC 20546		14. Sponsoring Agency Code	
15. Supplementary Notes			
16. Abstract An investigation to determine the aeropropulsive characteristics of nonaxisymmetric nozzles on an F-18 jet effects model has been conducted in the Langley 16-Foot Transonic Tunnel and the AEDC 16-Foot Supersonic Wind Tunnel. The performance of a two-dimensional convergent-divergent nozzle, a single expansion ramp nozzle, and a wedge nozzle was compared with that of the baseline axisymmetric nozzle. Test data were obtained at static conditions and at Mach numbers from 0.60 to 2.20 at an angle of attack of 0°. Nozzle pressure ratio was varied from jet-off to about 20.			
17. Key Words (Suggested by Author(s)) Nonaxisymmetric nozzles Two-dimensional nozzles		18. Distribution Statement Unclassified - Unlimited	
		Subject Category 02	
19. Security Classif. (of this report) Unclassified	20. Security Classif. (of this page) Unclassified	21. No. of Pages 78	22. Price A05

National Aeronautics and
Space Administration

Washington, D.C.
20546

Official Business

Penalty for Private Use, \$300

THIRD-CLASS BULK RATE

Postage and Fees Paid
National Aeronautics and
Space Administration
NASA-451



5 1 1U,A, 820720 S00903DS
DEPT OF THE AIR FORCE
AF WEAPONS LABORATORY
ATTN: TECHNICAL LIBRARY (SUL)
KIRTLAND AFB NM 87117

S

NASA

POSTMASTER: If Undeliverable (Section 158
Postal Manual) Do Not Return